

**Investigation of the intra-cellular localisation of
Retinoblastoma Binding Protein 6 using
immunofluorescence microscopy**

Anna Victoria Szmyd-Potapczuk

A thesis submitted in fulfilment of the requirement for the degree of
Doctor Philosophiae in the Faculty of Natural Science,
University of the Western Cape



Supervisor: Prof David JR Pugh

UNIVERSITY
WESTERN CAPE

September 2017

ABSTRACT

Investigation of the intra-cellular localisation of Retinoblastoma Binding Protein 6 using immunofluorescence microscopy

AV Szmyd-Potapczuk

PhD thesis, Department of Biotechnology, Faculty of Natural Science, University of the Western Cape

Human Retinoblastoma Binding Protein 6 (RBBP6) is a 200 kDa protein that has been implicated in a number of crucial cellular processes. It forms part of the mRNA 3'-end processing complex in both humans and yeast, and it contains an RS-like domain and interacts with core splicing proteins, suggesting multiple roles in mRNA processing. Through its RING finger domain it has been implicated in catalysing ubiquitination of the tumour suppressor p53, the oncogene Y-Box Binding Protein 1 (YB-1) and the DNA replication-associated protein zBTB38. It is one of only a few proteins known to bind to both p53 and pRb. At the N-terminus of the protein is the DWNN domain, an ubiquitin-like domain which is found only in this protein family. Four protein isoforms of RBBP6 have been identified in humans, all of which contain the DWNN domain: isoform 1 contains 1972 residues, isoform 2 contains 1758 residues and isoform 4 contains 952 residues. Isoform 3, which contains the first 101 residues of the full length protein (isoform 1), including the DWNN domain, followed by an unique 17-amino acid tail, is reported to be expressed independently of the other isoforms and to be down-regulated in a number of cancers.

RBBP6 has recently been reported to regulate expression of approximately 4000 genes through regulation of the process of 3'-polyadenylation. The DWNN domain has been shown to bind directly to the 64-kDa subunit of the polyadenylation-associated factor CstF (CstF-64); since the DWNN domain is common to all isoforms of RBBP6, this has led to the proposal of a model in which isoform 3 completes with isoform 1 (and possibly other isoforms), through their DWNN domains, for binding to CstF-64.

In light of the above model, the localisation of the various isoforms of RBBP6 becomes of interest. Although RBBP6 is widely reported as localising to nuclear speckles, this has not been

verified by co-localisation with known speckle-resident proteins, and no studies have investigated the localisation of isoform 3.

The current study uses immunofluorescence microscopy to investigate the intra-cellular localisation of the various isoforms of RBBP6. Our findings support previous reports that endogenous isoform 1 localises to punctate bodies within the nucleus and provided strong evidence that these bodies are indeed nuclear speckles. On the other hand, we have found that endogenous isoform 3 localises predominantly to the cytoplasm, but also weakly to nuclear speckles. Following administration of a number of different cellular stresses - heat shock, DNA damage induced by UV and DNA damage induced by cisplatin - isoform 3 translocates to nuclear speckles within 30 minutes and remains there for up to 24 hours. These results were replicated using exogenous HA-tagged proteins, supporting the conclusion that the results do, in fact, reflect the localisation of RBBP6, and are not the result of *de novo* gene expression. The same effect was found in a number of independent human cell lines, indicating that the effect is not confined to one particular cell type.

Although it is induced by DNA damage, isoform 3 was not found to localise to sites of DNA damage. Whereas standard conditions were used to induce DNA damage by UV and cisplatin, the conditions used to induce heat shock were significantly less severe than those typically reported in the literature. Nevertheless the effect was found to be robust under small variations in the conditions.

In conclusion, our results provide the first evidence of stress-dependent localisation of the isoforms of RBBP6, which may provide a mechanism linking cell stress to gene expression through modulation of 3'-end processing. The rapidity of the response, the low level of heat shock necessary to induce it, the fact that it is induced by very different forms of stress and, potentially, in all cell types, suggests that this may represent a very fundamental part of the cell's response to stress.

Keywords: Retinoblastoma binding protein 6, nuclear speckles, DWNN, colocalisation, 3'-end mRNA processing

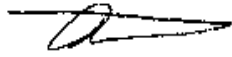
DECLARATION

I declare that “**Investigation of the intra-cellular localisation of Retinoblastoma Binding Protein 6 using immunofluorescence microscopy**” is my own work that has not been submitted for any degree or examination in any other university and that all the sources I have used or quoted have been indicated and acknowledged by references.

Anna Victoria Szmyd-Potapczuk

September 2017

Signed: _____



CONTENTS

ABSTRACT	ii
DECLARATION.....	iv
LIST OF FIGURES	viii
LIST OF TABLES	x
LIST OF ABBREVIATIONS	xi
ACKNOWLEDGEMENTS.....	xiii
CHAPTER 1 LITERATURE REVIEW	1
1.1 INTRODUCTION	1
1.2 RETINOBLASTOMA BINDING PROTEIN 6	2
1.2.1 THE GENERAL ORGANISATION OF RBBP6 AND ITS FUNCTIONS IN CELLS	2
1.2.2 THE DWNN DOMAIN.....	4
1.2.3 THE RING FINGER DOMAIN	4
1.2.4 THE RS DOMAIN	6
1.2.5 THE RB-BINDING DOMAIN.....	7
1.2.6 THE p53-BINDING DOMAIN	7
1.2.7 ISOFORMS OF RBBP6.....	8
1.2.8 THE ROLE OF RBBP6 IN CANCER.....	9
1.3 CELL RESPONSE TO STRESS.....	9
1.3.1 INTRODUCTION	9
1.3.3 CELLULAR RESPONSE TO DNA DAMAGE.....	14
1.4 UBIQUITINATION.....	19
1.4.1 INTRODUCTION	19
1.4.2 THE UBIQUITINATION PATHWAY	19
1.4.3. UBIQUITIN AND UBIQUITIN-LIKE MOLECULES.....	20
1.4.4 UBIQUITIN-ACTIVATING ENZYME.....	21
1.4.5 UBIQUITIN-CONJUGATING ENZYMES.....	21
1.5 NUCLEAR SPECKLES.....	23
1.5.1 INTRODUCTION	23
1.5.2 THE STRUCTURE AND FUNCTION OF NUCLEAR SPECKLES	24
1.5.3 THE COMPOSITION OF NUCLEAR SPECKLES.....	25
1.5.4 THE DYNAMICS OF NUCLEAR SPECKLES	26
1.6 THE PRINCIPLES OF COLOCALISATION.....	27

1.6.1	INTRODUCTION	27
1.6.2	ACQUIRING IMAGES FOR COLOCALISATION.....	27
1.7	RATIONALE FOR THE STUDY	31
1.8	AIMS AND OBJECTIVES OF THE STUDY	32
CHAPTER 2	MATERIALS AND METHODS.....	33
2.1	CELL CULTURE.....	33
2.2	ADMINISTRATION OF CELL STRESS.....	33
2.3	IMMUNOFLUORESCENCE MICROSCOPY.....	34
2.4	ANTIBODIES USED	35
2.4.1	PRIMARY ANTIBODIES	35
2.4.2	SECONDARY ANTIBODIES.....	37
2.5	WESTERN BLOTTING.....	37
2.5.1	PREPARATION OF CRUDE LYSATE.....	37
2.5.2	SDS-PAGE AND IMMUNODETECTION OF PROTEINS.....	38
2.6	TRANSFECTIONS.....	39
2.6.1	THE PRINCIPLE OF LIPID-BASED TRANSFECTION	39
2.6.2	METHODS USED IN TRANSFECTION.....	39
2.7	QUANTITATIVE ANALYSIS OF IMAGES	40
2.8	COLOCALISATION ANALYSIS.....	41
2.9	STATISTICAL ANALYSIS.....	42
CHAPTER 3	ISOFORM 3 OF RBBP6 TRANSLOCATES TO NUCLEAR SPECKLES FOLLOWING CELL STRESS	43
3.1	INTRODUCTION.....	43
3.2	SPECIFICITY OF THE ANTIBODIES GENERATED AGAINST THE DWNN DOMAIN OF RBBP644	
3.3	LOCALISATION OF RBBP6 AND ITS ISOFORMS IN UNSTRESSED CELLS.....	46
3.4	ISOFORMS OF RBBP6 FORM SPECKLES IN THE NUCLEUS THAT BECOME MORE PRONOUNCED AFTER CELL STRESS.....	50
3.5	INCREASE IN NUCLEAR INTENSITY IS CAUSED BY ISOFORM 3 ALONE.....	59
3.6	STRESS-INDUCED INCREASE IN NUCLEAR INTENSITY IS NOT DUE TO <i>DE NOVO</i> PROTEIN SYNTHESIS.....	62
3.7	TRANSLOCATION OF ISOFORM 3 OCCURS IN A VARIETY OF CELL LINES	64
3.8	CONFIRMATION OF ENDOGENOUS FINDINGS USING OVEREXPRESSED CONSTRUCTS.....	69

3.9	RBBP6 LOCALISES TO NUCLEAR SPECKLES	77
3.10	ISOFORM 3 DOES NOT LOCALISE TO SITES OF DNA DAMAGE REPAIR	81
CHAPTER 4	DISCUSSION	85
4.1	ISOFORM 3 OF RBBP6 TRANSLOCATES TO NUCLEAR SPECKLES FOLLOWING STRESS... 85	
4.1.1	LOCALISATION OF RBBP6 ISOFORMS IN THE CELL, AND THE EFFECT OF CELL STRESS ON THE LOCALISATION OF THESE PROTEINS	85
4.1.2	CHARACTERIZATION OF THE STRESS EFFECT	87
4.1.3	ISOFORM 3 LOCALISES TO NUCLEAR SPECKLES FOLLOWING CELL STRESS.....	87
4.2	RBBP6 ISOFORMS DO NOT LOCALISE TO SITES OF DNA DAMAGE	88
4.3	IMPLICATIONS FOR THE FUNCTION OF RBBP6.....	88
4.4	OUTLOOK.....	90
CHAPTER 5	REFERENCES	93
CHAPTER 6	APPENDIX.....	109



UNIVERSITY *of the*
WESTERN CAPE

LIST OF FIGURES

Figure 1.1: Schematic representation of the domains of full-length RBBP6.....	3
Figure 1.2: Schematic representation of the various isoforms of RBBP6.....	8
Figure 1.3 Schematic illustrating the transcriptional regulation of heat shock by HSF1.....	14
Figure 1.4: An overview of the DNA damage response.....	15
Figure 1.5: Schematic representation of the various homologous repair mechanisms to repair double-stranded breaks.....	18
Figure 1.6: The ubiquitin-proteasome system illustrating the various forms of ubiquitination possible.....	20
Figure 3.1: Western blot analysis of the specificity of the mouse monoclonal anti-DWNN antibody.....	45
Figure 3.2: Western blot analysis of the specificity of the rabbit polyclonal anti-DWNN antibody.....	46
Figure 3.3 HeLa cells stained with mouse monoclonal anti-DWNN.....	47
Figure 3.4: HeLa cells stained with rabbit polyclonal anti-DWNN.....	48
Figure 3.5 HeLa cells stained with C133084.....	49
Figure 3.6: Localisation of the DWNN domain following heat shock.....	51
Figure 3.7: Localisation of the DWNN domain following UV shock.....	51
Figure 3.8 Localisation of the DWNN domain following exposure to cisplatin.....	52
Figure 3.9: Nuclear and cytoplasmic intensity values of cells stressed by three different stressors.....	54
Figure 3.10 Nuclear/cytoplasmic ratios in cells subjected to various forms of cell stress.....	55
Figure 3.11: Nuclear and cytoplasmic intensity values following heat shock.....	56
Figure 3.12: Nuclear and cytoplasmic intensity values following DNA damage induced by UV..	57
Figure 3.13: Measured nuclear intensity as a function of heat shock exposure time, which is a measure of the amount of shock applied.....	59
Figure 3.14 Antibody C133084, which is expected to target isoforms 1, 2 and 4 but not 3, is found exclusively in the nucleus in speckle-like bodies in the absence of stress.....	60
Figure 3.15 Antibody C133084 is found exclusively in the nucleus in speckle-like bodies following heat shock.....	61
Figure 3.16: Antibody C133084 is found exclusively in the nucleus in speckle-like bodies following UV-treatment.....	61

Figure 3.17 Nuclear intensity values corresponding to isoforms 1, 2 and 4, following heat shock and DNA damage caused by UV.....	62
Figure 3.18: Cycloheximide has no effect on changes of nuclear intensity induced by cisplatin.	64
Figure 3.19: H157 cells stained with mouse monoclonal anti-DWNN antibody before (left) and after (right) DNA damage inflicted using UV.....	66
Figure 3.20: KMST cells stained with mouse monoclonal anti-DWNN antibody, before (left) and after (right) DNA damage inflicted using UV.....	66
Figure 3.21: HepG2 cells stained with mouse monoclonal anti-DWNN antibody, before (left) and after (right) DNA damage inflicted using UV.....	67
Figure 3.22: A549 cells stained with mouse monoclonal anti-DWNN antibody, before (left) and after (right) DNA damage inflicted using UV.....	67
Figure 3.23: HeLa cells stained with mouse monoclonal anti-DWNN antibody before (left) and after (right) DNA damage inflicted using UV.....	68
Figure 3.24: Translocation of isoforms 3 to nuclear speckle-like bodies in a number of cell lines.	69
Figure 3.25: Unstressed HeLa cells transfected with HA-isoform 1 and detected using an anti-HA antibody.....	71
Figure 3.26 Heat-shocked HeLa cells transfected with HA-isoform 1 and detected using an anti-HA antibody	72
Figure 3.27: Unstressed HeLa cells transfected with HA-isoform 3.....	74
Figure 3.28 Stressed HeLa cells transfected with HA-isoform 3.....	75
Figure 3.29: The ratio of nuclear to cytoplasmic intensity in stressed and unstressed cells.....	76
Figure 3.30: Bleed through and non-specific secondary antibody control.....	78
Figure 3.31: A549 cells co-stained showing that the DWNN domain localises to the same nuclear speckles as SC35 following stress induced by heat shock.....	80
Figure 3.32: Colocalisation analysis of A549 cells stained with rabbit polyclonal anti-DWNN and mouse monoclonal anti-SC35.....	80
Figure 3.33: Stain showing that γ H2AX localises to the nucleus and only appears after DNA damage.....	82
Figure 3.34 Bleed-through controls and non-specific secondary antibody controls	83
Figure 3.35 Stressed A549 co-stained with anti- γ H2AX and anti-DWNN showing the lack of colocalisation between the two.	84

LIST OF TABLES

Table 2:1: Cell lines used in the study	33
Table 2:2: List of commercially obtained primary antibodies used in the study	36
Table 2:3 List of anti-RBBP6 antibodies used in the study and which isoforms of RBBP6 they are expected to detect	37
Table 2:4: Secondary antibodies used during the study.....	37
Table 3:1: The effect of heat shock and DNA damage (UV and cisplatin) on nuclear and cytoplasmic signal from stressed and unstressed cells	53
Table 3:2 Quantitative analysis of nuclear/cytoplasmic intensity ratios of cells after being subjected to various forms of cell stress.....	55
Table 3:3: Nuclear intensity values corresponding to isoforms 1, 2 and 4, before and after heat shock treatment	62
Table 3:4: Nuclear intensities measured using the mouse monoclonal anti-DWNN antibody in cells treated with cycloheximide and subjected to DNA damage.	63
Table 3:5: Cell lines used in DWNN translocation experiment.....	65
Table 3:6: Nuclear intensity values for a number of cell lines, before and after UV-induced stress.....	65
Table 3:7: The ratio of nuclear to cytoplasmic intensity in stressed and unstressed cells.....	77

UNIVERSITY of the
WESTERN CAPE

LIST OF ABBREVIATIONS

Bcl-2	B-cell lymphoma 2 protein
BSA	Bovine serum albumin
cDNA	Complimentary deoxyribonucleic acid
CRS	Cytoplasmic retention signal
CSD	Cold shock domain
CstF-64	Cleavage stimulation factor 64
DMBA	7,12-dimethylbenz[α]anthracene
DMEM	Dulbecco's modified eagle medium
DNA	Deoxyribonucleic acid
EDTA	Ethylenediaminetetraacetic acid
EGFR	Epidermal growth factor receptor
eIF4E	Eukaryotic translation initiation factor 4E
EMT	Epithelial-mesenchymal transition
FBI-1	Factor binding IST protein 1
FRAP	Fluorescence recovery after photobleaching
GBM	Glioblastoma multiforme
GFP	Green fluorescent protein
HDM2	Human double minute 2
HECT	Homologous to the E6-AP carboxyl terminus
HER2	Human epidermal growth factor receptor 2
HMG-17	High mobility group protein 17
hnRNP	Heterogeneous ribonucleoprotein particle
Hsp70	Heat shock protein 70
IGC	Interchromatin granule cluster
IGF	Insulin-like growth factor
Kb	Kilobase pair
kDa	Kilo Dalton
LS	Large subunit
MAb	Monoclonal antibody
MALAT1	Metastasis associated lung adenocarcinoma transcript 1
MDM2	Murine double minute 2
MDMX	Murine double minute X

MDR-1	Multi-drug resistance protein 1
MEF	Mouse embryonic fibroblast
MMP-2	Matrix metalloproteinase 2
mRNA	Messenger ribonucleic acid
MRP-1	Multi-drug resistance associated protein 1
MSH-2	MutS protein homolog 2
NaCl	Sodium chloride
NEDD	Neural precursor cell expressed developmentally down-regulated protein
NLS	Nuclear localisation signal
NMR	Nuclear magnetic resonance spectroscopy
P2P-R	Proliferation potential protein related
PAb	Polyclonal antibody
PACT	p53-associated cellular protein testis derived
PBS	Phosphate buffered saline
PCNA	Proliferating cell nuclear antigen
Pidd	p53-induced death domain protein
PIK3CA	Phosphatidylinositol-4,5-bisphosphate 3-kinase, catalytic subunit alpha
pRb	Retinoblastoma protein
PSKH1	Serine/threonine-protein kinase H1
PTP1B	Protein-tyrosine phosphatase 1B
Puma	p53 up-regulated mediator of apoptosis
RBBP6	Retinoblastoma binding protein 6
RBQ-1	Retinoblastoma binding Q protein 1
RING	Really interesting new gene
RNA	Ribonucleic acid
RNAi	Ribonucleic acid interference
Ser	Serine
snRNA	Small nuclear ribonucleic acid
snRNP	Small nuclear ribonucleic particle
SR	Serine rich
SUMO	Small ubiquitin-like modifier
TLS	Translocation liposarcoma protein
tRNA	Transfer ribonucleic acid
UV	Ultraviolet
YB-1	Y-box binding protein 1
zBTB38	Zinc finger and BTB binding protein 38

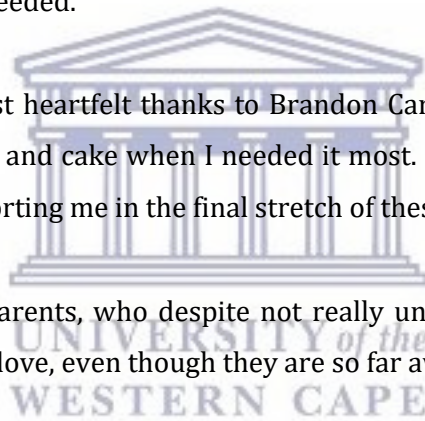
ACKNOWLEDGEMENTS

I would like to thank my supervisor Prof David JR Pugh for his invaluable advice and assistance in structuring the project and accepting my ideas when I decided to change direction. I would also like to express my deepest gratitude to Dr Dirk Lang and Ms. Susan Cooper at the UCT Confocal and Light Microscopy Imaging Facility for their invaluable advice on confocal microscopy and colocalisation analysis. Thanks also to Prof Sharon Prince for generously sharing lab space and her group's expertise when I needed it.

I would also like to thank Andrew Faro for listening to my ideas while providing insightful and wise feedback and Faqeer Hasseem for making sure that the lab ran smoothly and I always had the equipment and supplies I needed.

I would like to convey my most heartfelt thanks to Brandon Carter who provided unwavering support, general awesomeness and cake when I needed it most. I owe him and all my friends a giant debt of gratitude in supporting me in the final stretch of these studies.

My deepest love goes to my parents, who despite not really understanding what I was doing provided me with support and love, even though they are so far away.



CHAPTER 1 LITERATURE REVIEW

1.1 INTRODUCTION

Retinoblastoma Binding Protein 6 (RBBP6) is a 200 kDa multi-domain protein reported to play a role in a diverse set of cellular processes through interactions with a number of different proteins. Such roles include regulation of the cell cycle via the interaction with the Retinoblastoma protein (pRb) (Simons *et al.* 1997; Sakai *et al.* 1995; Witte and Scott 1997), regulation of tumorigenesis via interactions with Y-box protein 1 (YB-1) (Chibi *et al.* 2008) and p53 (Simons *et al.* 1997; Witte and Scott 1997, Li *et al.* 2007), mRNA processing via interactions with splicing associated Sm proteins (Witte & Scott 1997, Kappo *et al.* 2012) as well as 3'-end processing proteins (Shi *et al.* 2009, Di Giammartino *et al.* 2014), DNA repair and embryonic development via interaction with zBTB38 (Miotto *et al.* 2014). Whether these functions are all independent activities of RBBP6 or whether they are part of a unified mechanism is yet unknown and further studies are needed to determine the answer. However, since RBBP6 is essential to eukaryotic development and is present in all eukaryotic species investigated (Frigerio *et al.* 1995; Pugh *et al.* 2006; Yoshitake *et al.* 2004), it is without a doubt a vital component of the cell.

Many of the interactions between RBBP6 and other proteins are due to the function of RBBP6 as an E3 ubiquitin ligase, where it catalyses the ubiquitination and suppression of protein levels in the cell. This function is mediated by the RING domain of RBBP6 (Chibi *et al.* 2008). Proteins ubiquitinated by RBBP6 include YB-1, zBTB38 and p53. The N-terminal DWNN domain of RBBP6 is a ubiquitin-like domain that may potentially act as a ubiquitin-like modifier, suggesting that other domains of RBBP6 may also play different roles in the ubiquitination pathway (Pugh *et al.* 2006). This DWNN domain is also independently expressed as a 13 kDa protein, referred to as isoform 3 of RBBP6, and is down-regulated in a number of cancers (Mbita *et al.* 2012). This would suggest a synergy between the various domains of the RBBP6 protein in the regulation of a number of important cellular mechanisms.

The cellular localisation of RBBP6 is essential for understanding its function, as it has to be in the right place at the right time to carry out its regulatory functions. Most of the processes RBBP6 is involved, including mRNA processing, cell cycle regulation and splicing, occur in the

nucleus, and initial localisation findings placed RBBP6 in the nucleus, particularly associated with nuclear bodies known as nuclear speckles (Gao, Witte, and Scott 2002). This would suggest that RBBP6 is involved in mRNA processing taking place in these nuclear bodies. However, other proteins with which RBBP6 is reported to interact, such as Hsp70 (Kappo *et al.* 2012), are primarily cytoplasmic, suggesting that the localisation of RBBP6 may be more complex than initially anticipated.

The following study was carried out with the aim of answering some of these questions, focusing primarily on the localisation of different isoforms of the RBBP6 protein, particularly following various forms of genotoxic stress. While our results confirm that RBBP6 is largely confined to nuclear speckles, we also find compelling evidence that isoform 3 translocates rapidly to nuclear speckles following genotoxic stress. This is of interest in view of recent reports suggesting that isoforms 1 and 3 or RBBP6 compete with each other for binding to components of the 3'-end processing machinery, thereby regulating the expression of around 4000 cancer-associated genes. Our results may therefore provide a mechanism for shifting the relative concentrations of isoforms 1 and 3 in the nucleus, thereby altering gene expression in response to cell stress.

1.2 RETINOBLASTOMA BINDING PROTEIN 6

1.2.1 THE GENERAL ORGANISATION OF RBBP6 AND ITS FUNCTIONS IN CELLS

RBBP6 is a 200 kDa protein that is present in potentially all eukaryotic organisms, but not in prokaryotes (Pugh *et al.* 2006). While the precise function of RBBP6 in cells is unknown, there is evidence implicating it in a number of cellular processes, including mRNA processing and metabolism (Mandel *et al.* 2008; Shi *et al.* 2009; Di Giammartino *et al.* 2014), regulation of the cell cycle (Scott *et al.* 2003; Gao, Witte, and Scott 2002; Gao and Scott 2002), as well as tumorigenesis (Simons *et al.* 1997; Witte & Scott 1997, Yoshitake *et al.*, 2004). The full-length protein contains a number of functional domains, including the DWNN domain, a zinc knuckle, a RING finger domain, a serine-arginine-rich domain, a retinoblastoma binding domain, a p53 binding domain and a C-terminal nuclear localisation signal. These domains are illustrated in Figure 1.1 below. The domains will be discussed in detail later in this review.



Figure 1.1: Schematic representation of the domains of full-length RBBP6, isoform 1, adapted from Pugh *et al.* 2006

RBBP6 was originally cloned and sequenced as three partial cDNAs in three different studies, namely Retinoblastoma Binding Q protein 1 (RBQ-1) (Sakai *et al.* 1995), p53 associated cellular protein testis derived (PACT) (Simons *et al.* 1997) and the proliferation potential protein related (P2P-R)(Witte and Scott 1997). Both RBQ-1 and PACT were cloned due to their ability to bind Rb and p53 respectively, while P2P-R was cloned due to its recognition by two antibodies specific for heterogeneous nuclear ribonucleoproteins.

RBBP6 has been strongly implicated in tumorigenesis, due to its ability to interfere with the binding of p53 to DNA (Simons *et al.* 1997) and its ability to block the binding of Rb to adenovirus E1a (Witte and Scott 1997). This hypothesis is supported by reports that high levels of expression of RBBP6 correlate with increased proliferation rate of oesophageal cancer cells, and that cytotoxic T-cells directed against RBBP6-derived peptides were able to produce regression in oesophageal tumours in mice xenograft models (Yoshitake *et al.* 2004). Recent studies have shown that overexpression of RBBP6 is associated with poor prognosis in colon cancer patients, regardless of whether p53 is mutated or not. Patients with mutant p53 and overexpressed RBBP6 displayed the highest relapse and death rates, indicating the prognostic value of RBBP6 levels in colon cancers, regardless of their p53 status (Chen *et al.* 2013).

RBBP6 has been associated with mRNA maturation through several observations: it associates with heterogeneous nuclear ribonucleoproteins (Witte and Scott 1997), it contains an SR-like domain at residues 477-570 (Simons *et al.* 1997), it localises to the periphery of chromosomes during mitosis (Gao and Scott 2003), it also localises to nuclear speckles which are believed to be the main sites of activity for pre-mRNA splicing and processing during interphase (Li *et al.* 2007; Simons *et al.* 1997) and it forms part of the mRNA 3'-processing complex in both yeast and humans (Vo *et al.* 2001; Shi *et al.* 2009; Di Giammartino *et al.* 2014).

At least two of the domains of RBBP6, namely the DWNN and RING domains, have functions related to ubiquitination. The structure of the DWNN domain is highly similar to that of ubiquitin (Pugh *et al.* 2006), and the RING domain has been shown to function as an E3 ligase with the ability to ubiquitinate YB-1 (Chibi *et al.* 2008) and zBTB38 (Miotto *et al.* 2014).

1.2.2 THE DWNN DOMAIN

The DWNN domain of RBBP6 is found at the N-terminus of all isoforms of the protein (Figure 1.1). An alignment of DWNN orthologues from a variety of eukaryotes shows very little similarity with any other sequences, which suggests that the DWNN domain is a novel motif that was present in the earliest eukaryotes (Pugh *et al.* 2006). Isoform 3 of RBBP6 consists of the DWNN domain followed by a 37 residue C-terminal tail, of which the last 18 amino acids do not form part of the full length protein. Isoform 3 is expressed from an alternative promoter to the full length protein and appears to be independently expressed in all vertebrates, but not in invertebrates (Pugh *et al.* 2006).

Isoform 3 has also been shown to mediate binding of isoform 1 to CstF-64, an element of the 3'-end RNA processing machinery involved in poly(A) processing (et al. 2014). Isoform 3 was also shown to compete for binding to CstF-64 with isoform 1 and inhibited cleavage when overexpressed in cells. This provides another potential role for RBBP6 and its isoforms in the mediation of proliferation through the regulation of 3'-end processing.

Ubiquitin-like proteins are a class of proteins that have an ubiquitin-like structure and, like ubiquitin, become covalently attached to other proteins. They include proteins such as Small Ubiquitin-Related Modifier (SUMO), Neural Precursor Cell-Expressed Developmentally Downregulated-8 (Nedd8) and Interferon-Stimulated Gene 15 (ISG15) (Schwartz and Hochstrasser 2003). These proteins typically share a C-terminal GG motif which plays a critical role in formation of the isopeptide bond with the substrate lysine. This motif is present at the equivalent position in the DWNN domain, suggesting that it may become covalently linked to other proteins in a process which could be termed "DWNNylation".

1.2.3 THE RING FINGER DOMAIN

E3 ligases form the last part of a three-enzyme chain that is responsible for catalysis of isopeptide bonds between ϵ -amino groups of target lysines on the substrate and the C-terminus of ubiquitin or ubiquitin-like proteins. This leads to a variety of different outcomes, including degradation of the substrate in the 26S proteasome complex (Joazeiro and Weissman 2000; Xie and Varshavsky 1999; Deshaies 1999). E3 ligases can be divided into two categories based upon whether they take part directly in the reaction or whether they act as a bridge between the ubiquitin-conjugated E2 and the substrate. E3 ligases that take part directly in the reaction have a HECT domain with a catalytic cysteine to which ubiquitin is transferred before being transferred to a lysine on the substrate. E3 ligases that act as adaptor proteins contain either a

RING finger domain or the similarly-structured U-box domain (Christensen and Klevit 2009). The presence of a RING finger domain suggests that RBBP6 acts as an adaptor E3 ubiquitin ligase.

Li and co-workers reported that knockdown of RBBP6 in a mouse model results in up-regulation of p53 and embryonic lethality due to widespread ectopic apoptosis. They showed further that RBBP6 was required for poly-ubiquitination of p53, but that Human Double Minute 2 (Hdm2), the human homologue of Murine Double Minute 2 (MDM2), was also required (Li *et al.* 2007). This finding was confirmed by generating a mutant RBBP6 that lacked the RING finger domain, which resulted in a lack of ubiquitination and degradation of p53, despite the presence of over-expressed Hdm2.

In addition to being necessary for the ubiquitination of p53 *in vivo*, RBBP6 has been shown to catalyse the ubiquitination and degradation of YB-1 and zBTB38 *in vivo* (Chibi *et al.* 2008; Miotto *et al.* 2014). Overexpression of RBBP6 led to a decrease of YB-1 levels in cultured mammalian cells in a proteasome-dependent manner, suggesting that RBBP6 catalysed the attachment of poly-ubiquitin chains responsible for tagging the substrate for degradation in the proteasome (Chibi *et al.* 2008). *In vitro* ubiquitination studies have shown that, unlike in the mouse model of Li and co-workers, RBBP6 was able to poly-ubiquitinate YB-1 without the assistance of MDM2 (A Faro and DJR Pugh, unpublished data).

This direct interaction between YB-1 and the RING finger of RBBP6 is surprising as it suggests that the RING finger interacts with both the substrate and the ubiquitin-charged E2. This is in contrast to the standard model in which the RING finger interacts with the E2 while the substrate interaction is handled by a dedicated substrate-binding domain. Since the isolated RING finger domain of RBBP6 has been shown to catalyse ubiquitination of YB-1 independently *in vitro* (Chibi *et al.* 2008), it is possible that the RING finger can perform more than one function simultaneously.

NMR analysis shows that the RING finger domain forms a homodimer in solution along an interface similar to many other RING finger and U-box domains. The structure closely resembles that of the U-box from the C-terminus of Hsp70 interacting protein, with many residues in the homodimer interface being conserved between the two domains (Kappo *et al.* 2012). An important characteristic of U-box ligases is that they have a tendency to operate in complex with target chaperone proteins such as Hsp70, Hsp90 and Hsp40, ubiquitinating unfolded proteins sequestered by these chaperones. As the RING finger domain of RBBP6 interacts

directly with Hsp70 (Kappo *et al.* 2012), and RBBP6 interacts with Hsp90 *in vivo* (Simons *et al.* 1997), it is possible that RBBP6 has a role to play in chaperone-mediated ubiquitination of unfolded proteins.

1.2.4 THE RS DOMAIN

Serine-arginine rich (SR) proteins are a class of proteins involved in pre-mRNA processing and alternative splicing (Zahler *et al.* 1992). In addition, some SR proteins shuttle between the nucleus and the cytoplasm, allowing them to associate with translating ribosomes and stimulate translation of reporter mRNAs in the cytoplasm (Sanford *et al.* 2004), suggesting that SR proteins play a central role in coupling splicing and translation.

SR proteins are divided into two broad categories: classical SR proteins that are all structurally similar and can be purified using magnesium chloride (Zahler *et al.* 1992); and SR-related proteins that contain a serine/arginine-rich domain but do not have the defined RNA-recognition motif of classical SR proteins (Lin and Xiang-Dong 2007). In addition, SR proteins have one or two copies of RNA-recognition motifs that interact with pre-mRNA in the early stages of spliceosome assembly and stimulate the binding of the U1 snRNP to the 5' splice site (Eperon *et al.* 1993) as well as the binding of the U2AF snRNP to the 3' splice site of the pre-mRNA (Zuo and Manley 1993). The serine/arginine-rich domain of SR proteins is responsible for the localisation of these proteins to sites of splicing in the nucleus, namely nuclear speckles. Deletion of the serine/arginine-rich domain of an SR proteins results in the protein being unable to localise correctly and instead diffuses freely throughout the cell (Cáceres *et al.* 1997). As SR proteins are phosphoproteins, phosphorylation of the serine residues in the serine/arginine-rich domain is required to efficiently recruit SR proteins to the site of active transcription and hence is responsible for the localisation of these proteins to nuclear speckles (T Misteli and Spector 1997).

The interaction of RBBP6 with YB-1 (Chibi *et al.* 2008), whose strong association with mRNA has led to it being described as an mRNA chaperone (Okamoto *et al.* 2000), supports the notion that RBBP6 plays a role in mRNA splicing and processing. This is supported by the fact that RBBP6 localises strongly to nuclear speckles which are the prime sites of pre-mRNA processing (Scott *et al.* 2003) as well as localising to chromosomes during mitosis (Gao, Witte, and Scott 2002). RBBP6 contains an RS-like domain and is precipitated by magnesium chloride (Simons *et al.* 1997), suggesting that it may be involved with mRNA processing and splicing. Since RS

domains are thought to target RS-containing proteins to nuclear speckles, it is possible that this explains the localisation of full length RBBP6 to nuclear speckles.

1.2.5 THE RB-BINDING DOMAIN

Along with p53, the retinoblastoma protein (pRb) is one of the best characterized tumour suppressors. This is due to the frequent mutations in the retinoblastoma gene (*RB-1*) that occur during the development of cancers such as osteosarcoma and retinoblastoma (Friend *et al.* 1986), which have been found in all retinoblastomas studied to date, as well as a number of other tumours, including small-cell lung, bladder, prostate and breast carcinomas (Sellers and Kaelin 1997).

Since pRb is such an important protein in cancer prognosis, a wide variety of studies have focused on finding potential interaction partners for pRb. Using purified Rb as a probe, screening of a cDNA expression library identified RBBP6 (named RBQ-1 by the authors) as an interaction partner of pRb (Sakai *et al.* 1995). Additional experiments confirmed that RBBP6 bound to hypo-phosphorylated pRb, which is the active tumour-suppressive form, and that this was most likely physiologically relevant. The study identified the pRb-binding domain of RBBP6 as the primary domain involved in the interaction. The pRb-binding domain of RBBP6 is found only in higher eukaryotes, in particular humans and mice, and is not present in plants, fungi or invertebrates (Pugh *et al.* 2006)



1.2.6 THE p53-BINDING DOMAIN

p53 is a transcription factor co-ordinating responses to a multitude of insults to the cell, including DNA damage, reactive oxygen species and heat shock (reviewed in Prives and Hall 1999). Clinical data has shown that p53 mutations are some of the most common abnormalities found in human cancers, with missense mutations in the DNA binding domain or loss of heterozygosity of the p53 locus being the most common of these abnormalities (Greenblatt *et al.* 1994; Hainaut *et al.* 1998).

In a manner similar to that used to identify its interaction with pRb, Simons and co-workers identified RBBP6 as an interaction partner to p53 using a screen of a cDNA expression library (Simons *et al.* 1997). Recombinant forms of RBBP6, designated as PACT by the authors, were able to bind to wild-type p53, but not to mutant p53 found in human tumours, suggesting that RBBP6 binding is dependent on p53 conformation. RBBP6 also interfered with the ability of p53 to bind to DNA, which suggests that overexpression of RBBP6 would interfere with p53

transcriptional activity, which is essential for its ability to initiate apoptosis and cell cycle arrest. As with the pRb binding domain, the p53 binding domain of RBBP6 is found only in higher eukaryotes (Pugh *et al.* 2006).

1.2.7 ISOFORMS OF RBBP6

RBBP6 is expressed as four major isoforms, as shown in Figure 1.2: the full length transcript of 6.1 kb, known as isoform 1, as well as shorter transcripts of 6.0 kb and 2.8 kb known as isoforms 2 and 4 respectively. These result in proteins of 1792, 1758 and 952 amino acids respectively (UniProt 2017). A 1.1 kB transcript, known as isoform 3, is expressed from an alternative promoter. The translated protein consists of the first 101 residues of isoform 1, followed by 17 residues unique to isoform 3.

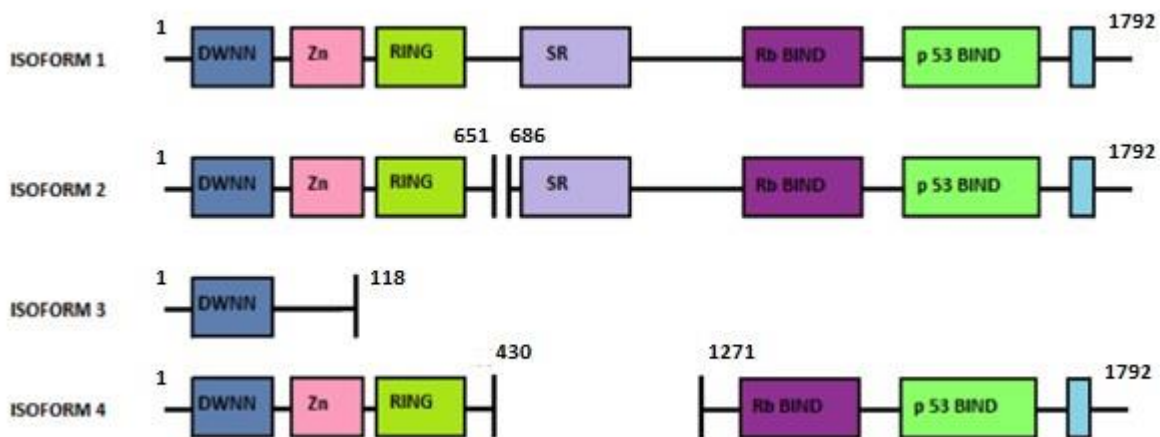


Figure 1.2: Schematic representation of the various isoforms of RBBP6. Isoform 1 is the longest and contains all the domains, while isoform 2 is slightly shorter, missing an exon before the SR binding domain. Isoform 3 consists of the DWNN domain and a unique C-terminal sequence, while isoform 4 is missing the SR domain.

Isoform 1 contains a number of well-characterised domains, shown schematically in Figure 1.2. Isoform 2 contains the same domains as isoform 1, but is missing residues 652 – 685 (Pugh *et al.* 2006). Isoform 3, which is made up primarily of the N-terminal ubiquitin-like domain, known as the DWNN domain, is independently expressed in human cells (Pugh *et al.* 2006; Mbita *et al.* 2012) and contains a unique C-terminal tail (VCKNTISHFFYTLPL) not expressed in other isoforms. Isoform 4 has only been identified *in silico* and is missing residues 431-1270. It thus contains all of the domains found in isoform 1, with the exception of the SR domain (UniProt 2009).

While a number of studies have been performed characterizing the localisation and potential function of isoform 1 (S Gao and Scott 2003; Simons *et al.* 1997; L. Li *et al.* 2007; Kappo *et al.*

2012; Chibi *et al.* 2008; Miotto *et al.* 2014) and several on isoform 3 (Pugh *et al.* 2006; Mbita *et al.* 2012), to date no studies have been conducted specifically on isoforms 2 or 4. Thus their localisation and function in the cell are unknown.

1.2.8 THE ROLE OF RBBP6 IN CANCER

RBBP6 interacts and potentially regulates a number of proteins that are involved in the regulation of cancer, including pRb, p53 and YB-1 (Sakai *et al.* 1995; Simons *et al.* 1997; Chibi *et al.* 2008), which suggests that RBBP6 may itself play a similar role. Reports show that RBBP6 is heavily up-regulated in oesophageal cancer, and this up-regulation is correlated strongly with higher rates of proliferation and poor prognosis for patients with oesophageal cancer (Yoshitake *et al.* 2004). RBBP6 has been shown to also be up-regulated in small lung adenocarcinoma cell as well as liver carcinoma cell lines (Mbita and Dlamini 2006; Motadi, Bhoola, and Dlamini 2011) and overexpression of RBBP6 has been associated with poor prognosis in colon cancer, irrespective of the p53 status of the cancer (Chen *et al.* 2013).

However, contradictory evidence shows that overexpression of RBBP6 results in apoptosis (Gao and Scott 2002; Gao and Scott 2003), suggesting that RBBP6 has a role in both anti-apoptotic and pro-apoptotic pathways. The effect of RBBP6 on cancer may therefore be highly complex and further studies will be required before the full picture is apparent.

1.3 CELL RESPONSE TO STRESS

1.3.1 INTRODUCTION

Cells and organisms are constantly exposed to detrimental environmental conditions that threaten their survival. These include increases or decreases in temperature that affect the folding of proteins, and DNA damaging agents such as ionising radiation and intercalating agents. The danger posed by these factors has prompted organisms to develop strategies to rapidly protect themselves against environmental changes. These stress responses are seen in all organisms, from bacteria to higher vertebrates, indicating their necessity for cell survival (Yahara 2013). The response to increased temperature, the so-called heat shock response, typically features the production of proteins which protect functional proteins from irreversible damage as well as assisting with renaturation. DNA damage repair mechanisms help to protect DNA from a number of insults, including irradiation and replication errors (Yahara 2013). Together, these two stress responses protect cells from minor environmental changes, and if the damage is too great induce apoptosis and controlled cell death.

1.3.2 CELLULAR RESPONSE TO HEAT SHOCK

1.3.2.1 Introduction

An observation made by in the 1960s regarding the induction of puffs in polygene chromosomes in the salivary glands of *Drosophila melanogaster* larvae (Ritossa 1962) led to the search and eventual identification of what were named “heat shock proteins” (Peterson, Moller, and Mitchell 1979). The heat shock response is a mechanism found across eukaryotes ranging from yeast to higher vertebrates, and is induced not only by changes in temperature, but also other factors leading to destabilisation of proteins, so called “proteotoxic” insults, including oxidative stress, the presence of heavy metals, bacterial infections and toxins (Akerfelt, Morimoto, and Sistonen 2010). Two main areas of focus in the heat shock field are the analysis of the function of heat shock proteins (S Lindquist and Craig 1988) and the regulation of the stress response (Morimoto 1996).

1.3.2.2 What happens to a cell during heat shock?

The heat shock response is highly sensitive to changes in temperature, with changes of a few degrees being sufficient to trigger it, even in organisms living at extreme temperatures (D’Amico *et al.* 2006; Takai *et al.* 1998). The reason for this is that proteins are only stable at a very specific temperature and any change in this temperature can cause unfolding, entanglement or aggregation, all of which are severely disruptive to cellular activities. In fact the heat shock response does not monitor temperature directly, or any other other source of stress, but rather is triggered by the presence of unfolded proteins (Richter, Haslbeck, and Buchner 2010).

In addition to causing individual proteins to unfold, heat shock has severe effects on the internal organization of the cell (Welch 1985; Toivola *et al.* 2010). Mild heat shock leads to re-organization of actin filaments into stress fibres (Welch 1985), while severe heat shock leads to the collapse of actin and tubulin networks in the cell (Welch 1986). As the cytoskeleton breaks down, organelles in the cell lose their correct localisation and the breakdown of intracellular transport occurs (Welch 1985), including the fragmentation of the Golgi system and endoplasmic reticulum. The number of mitochondria and lysosomes in the cell also decreases, leading to a dramatic drop in ATP levels in the cell during heat stress (Lambowitz *et al.* 1983; Patriarca and Maresca 1990). Heat shock results in an immediate cessation of both splicing and translation? Cessation of translation causes large RNA-protein structures known as stress granules to form in the cytosol, which contain non-translating mRNA and translation components (Nover, Scharf, and Neumann 1989, Asburner and Bonner 1979).

Together, these disrupted cellular processes lead to cell-cycle arrest (Zeuthen 1971) and the stagnation of growth and proliferation (Susan Lindquist 1980) which, depending on the severity of the stress, may lead to cell death. However, if the cell is able to survive the stress, it leads to tolerance of more severe stresses due to the increase of heat shock protein levels in the cell (S Lindquist 1986).

The heat shock response is therefore a rapid and transient programme of gene expression (Richter, Haslbeck, and Buchner 2010), with the kinetic profiles for the different genes involved being quite diverse, with some genes being expressed faster than others. The most well characterized model for heat shock gene expression is in baker's yeast, *Saccharomyces cerevisiae*, where an increase from 25 °C to heat shock conditions of 37 °C results in the expression of heat shock proteins peaking within 10 – 15 minutes (Eisen *et al.* 1998). Some genes peak later than this, with some taking as long as 2 hours to become active (Eisen *et al.* 1998). It is likely that the first phase correlates to the production of proteins that can counter the consequences of heat shock while later phases represent adaptation and recovery processes (Richter, Haslbeck, and Buchner 2010).

1.3.2.3 The heat shock proteins

The largest class of heat shock proteins are the molecular chaperones, which can be subdivided into five major conserved families, namely Hsp100, Hsp90, Hsp70, Hsp60 and the small heat shock proteins (Richter, Haslbeck, and Buchner 2010). While essential for heat shock response, these molecular chaperones also play a vital role in *de novo* protein folding and the refolding of non-native polypeptide chains (Gragerov *et al.* 1991; Bukau, Hesterkamp, and Luirink 1996). Molecular chaperones tend to recognise hydrophobic amino acids (Viitanen, Gatenby, and Lorimer 1992), and assist protein folding through the prevention of unwanted inter-molecular interactions (Richter, Haslbeck, and Buchner 2010).

Chaperonins are ring-shaped molecular complexes that encapsulate non-native proteins in an ATP-dependent manner (Richter, Haslbeck, and Buchner 2010). The most common bacterial chaperonin, GroEL, is made of 14 Hsp60 subunits that form a cylinder of two heptameric rings (Grallert and Buchner 2001). Non-native proteins up to 60 kDA can enter one of two cavities within the complex (Horwich, Farr, and Fenton 2006) which is then closed by GroES in the presence of ATP (Todd, Viitanen, and Lorimer 1994). The role of this protein in stress response is to sequester misfolded or unfolded proteins, allowing them to refold correctly (Richter, Haslbeck, and Buchner 2010). However, while this protein can bind to up to 50% of *E. coli*

proteins (Viitanen, Gatenby, and Lorimer 1992), the eukaryotic homologue, TRiC, has a much more limited substrate spectrum (Yam *et al.* 2008) and is down-regulated under stress conditions in yeast (Eisen *et al.* 1998), which suggests that it does not act as a heat shock protein in the case of eukaryotes (Richter, Haslbeck, and Buchner 2010).

Hsp70 is one of the most highly conserved chaperones, with DnaK, the prokaryotic homologue, showing 60% sequence homology with eukaryotic Hsp70 (Richter, Haslbeck, and Buchner 2010). Hsp70s are involved in both heat shock response and *de novo* protein folding under normal conditions (Mayer and Bukau 2005). The protein consists of two domains: an ATPase domain and a protein binding domain which can accommodate a stretch of seven mainly hydrophobic amino acids in an extended conformation (Zhu *et al.* 1996). As Hsp70 performs a variety of tasks in the cell, regulation of access to the various substrates is essential and is carried out by a variety of cofactors, the largest class of which is the Hsp40/J-domain containing proteins (Frydman *et al.* 1994; Frydman 1997). These cofactors bind to the non-native protein and deliver it to Hsp70. The J-domains then interact with the ATPase domain of Hsp70 to stimulate the hydrolysis of bound ATP, which assists with the opening and closing of the substrate-binding cavity of Hsp70 (Mayer and Bukau 2005).

Hsp90 is found at very high concentrations in the cytosol of both prokaryotic and eukaryotic organisms (Welch and Feramisco 1982), and is further up-regulated in the event of cell stress. Hsp90 is much less promiscuous in its substrate spectrum than either Hsp70 or GroEL (Pratt and Toft 2003) and does not bind unfolded proteins, but rather targets native-like proteins (Ursula Jakob *et al.* 1995). Hsp90 represents the most sophisticated chaperone machinery of all the chaperone molecules in that it works with a large number of co-chaperones in a defined order during the chaperone cycle (Wandinger, Richter, and Buchner 2008). Only two of these co-chaperones are upregulated in the presence of cell stress, namely Sti1 and prolyl isomerase Crp6 (Eisen *et al.* 1998). Sti1 is a non-competitive inhibitor of the Hsp90 ATPase (Richter *et al.* 2003) which keeps Hsp90 in a conformation that facilitates interaction with substrate proteins but prevents conformational changes required for substrate processing (Hessling, Richter, and Buchner 2009). This might suggest that under heat shock conditions Hsp90 is allowed to perform basic holding functions to prevent protein aggregation, but cannot process the proteins further (Richter, Haslbeck, and Buchner 2010).

Hsp100 proteins are a conserved group of AAA ATPases (ATPases Associated with diverse cellular Activities), which contain AAA domains, responsible for ATP binding and hydrolysis. AAA ATPases are divided into classes based on the number of AAA domains they contain

(Richter, Haslbeck, and Buchner 2010). These proteins are described in prokaryotes as well as in the mitochondria of plants, yeast and mammals (Barends, Werbeck, and Reinstein 2010). Hsp100 proteins are thought to target misfolded proteins, pulling them through the central pore of their hexameric ring structure in an unfolded state, allowing them to refold (Weber-Ban *et al.* 1999). Hsp100 proteins are also able to support protein disaggregation, and their most important function in the response to heat shock is to combine with Hsp70 and Hsp40 to form complexes that can extract substrates from aggregates and refold them into their original form (Goloubinoff *et al.* 1999). However certain higher eukaryotes, including mammals, seem to lack this ability to form a protein complex with disaggregation properties and have no comparable replacement (Richter, Haslbeck, and Buchner 2010), suggesting that this mechanism is not essential to surviving heat shock.

The main role of small heat shock proteins is to protect proteins from irreversible aggregation, which they do by forming soluble complexes with their substrates (Cashikar, Duennwald, and Lindquist 2005). They represent the most diverse family of molecular chaperones, showing high heterogeneity in size and sequence (Kriehuber *et al.* 2010). Despite their heterogeneity, they all contain a conserved α -crystallin domain which confers the chaperone-like function to the proteins (U Jakob *et al.* 1993) and most are large oligomers composed of 24 subunits of α -crystallin domains (van Montfort *et al.* 2001).

1.3.2.4 Regulation of the heat shock response

The heat shock response is governed primarily by heat shock factor 1 (HSF1) (Vergheze *et al.* 2012), a transcription factor which controls the expression of approximately 165 genes (Gasch *et al.* 2000). Many of these genes are not required for heat shock survival, supporting the hypothesis that the induction of the heat shock response is required for the preparation for instances of subsequent stress as well as the survival of the current stress (Giaever *et al.* 2002).

Under normal conditions HSF1 exists as an inert monomer in complex with Hsp70 and Hsp90 (Zou *et al.* 1998). Cell stress increases the amount of denatured proteins in the cytoplasm, which then bind to Hsp70 and Hsp90, resulting in displacement of HSF1. HSF1 then trimerizes and translocates to the nucleus where it undergoes phosphorylation (Baler, Dahl, and Voellmy 1993). The activated HSF1 trimer is able to induce the transcription of a number of heat shock protein genes-

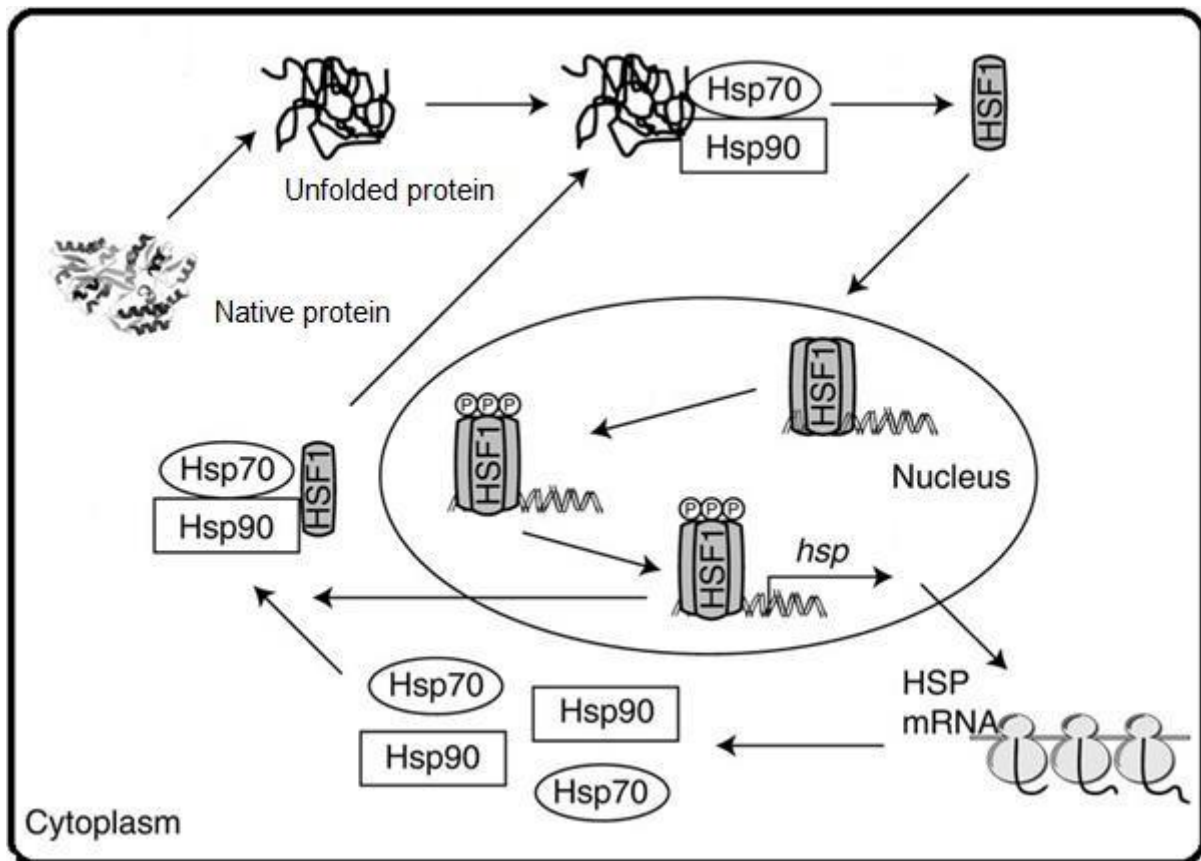


Figure 1.3 Schematic illustrating the transcriptional regulation of heat shock by HSF1, taken from Vabulas *et al.* 2010

In humans, HSF1 localises in punctate bodies within the nucleus following stress (Baler, Dahl, and Voellmy 1993) and the formation of these bodies corresponds to the induction of heat shock gene transcription (Cotto, Fox, and Morimoto 1997; Jolly *et al.* 1997).

1.3.3 CELLULAR RESPONSE TO DNA DAMAGE

1.3.3.1 Introduction

Thousands of DNA lesions occur daily in the human genome (Nakamura *et al.* 1998), with many arising as by-products of cell metabolism or DNA replication (Lindahl and Barnes 2000). DNA damage can also be induced by external factors such as toxic environmental chemicals or by radiation (Goodhead 1989; Dizdaroglu 1992). DNA damage can have negative consequences for the cell as it interferes with DNA replication and transcription and may ultimately result in mutations and chromosomal aberrations (Polo and Jackson 2011). The integrity of the genome is preserved by a number of DNA damage signalling and repair pathways, and defects in these pathways can contribute to various disorders including cancer, developmental defects and neurodegenerative disorders (Jackson and Bartek 2009).

The wide variety of DNA lesions that can occur means that there are multiple DNA repair mechanisms in place to repair specific lesion types. The basic DNA damage response is composed of the generation of a signal by DNA damage sensors which recruit mediators which in turn activate the correct DNA damage repair mechanism which can lead to a variety of cell responses based on the severity of the damage (Polo and Jackson 2011; Jackson and Bartek 2009). An illustration of this process is given below in Figure 1.4.

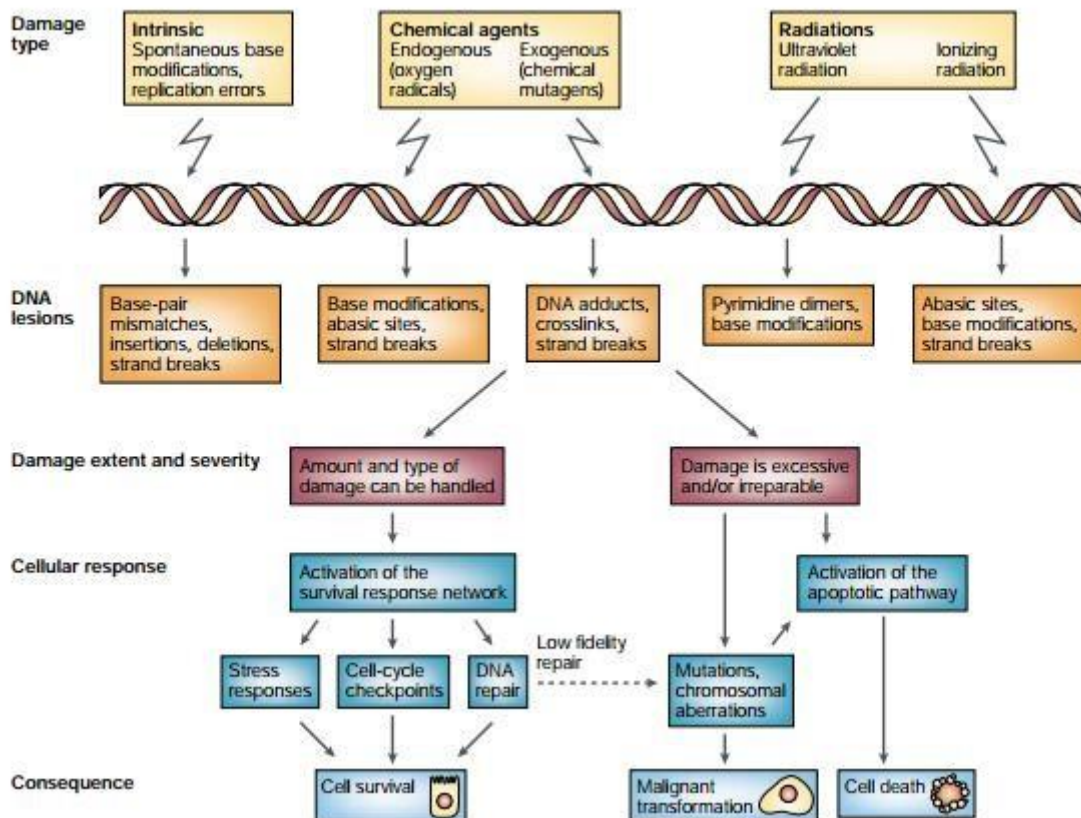


Figure 1.4: An overview of the DNA damage response, showing how the presence of a DNA lesion activates DNA damage sensors that initiate signalling pathways that have an effect on a number of cellular activities, taken from Shiloh, 2003.

1.3.3.2 DNA damage signalling

Like all signal transduction pathways, the DNA damage signalling pathway has three components: sensors, signal transducers and effectors, though there is significant overlap in the functions of various components of the pathway (Sancar *et al.* 2004). The two key signalling components involved in DNA damage repair are protein kinases ATM and ATR. ATM is activated by, and recruited to, the MRN sensor complex that detects double-stranded breaks (Lavin 2007), while ATR responds to replication protein A-coated single stranded DNA (Cimprich and Cortez 2008). In the event of DNA damage, ATM/ATR target protein kinases CHK1 and CHK2

and act in concert with these kinases to inhibit cyclin-dependent kinase (CDK) activity through a number of mechanisms, some of which are p53-dependent (Bartek and Lukas 2007; Riley *et al.* 2008). Inhibition of these CDKs leads to the arrest of the cell cycle at various checkpoints, allowing time for the DNA to be repaired (Bartek and Lukas 2007). At the same time, ATM/ATR signalling induce DNA repair proteins, either transcriptionally or post transcriptionally using mechanisms such as phosphorylation, ubiquitination and SUMOylation (Huen and Chen 2008; Matsuoka *et al.* 2007). If the DNA repair is effective, then inactivation of the repair mechanism commences allowing for the resumption of normal cell activities (Polo and Jackson 2011), and if the damage cannot be repaired, chronic DNA damage repair signalling results in the initiation of programmed cell death via apoptosis (Jackson and Bartek 2009).

Chromatin structure also plays a role in DNA damage repair and can be modulated to respond to DNA damage (Tom Misteli and Soutoglou 2009). The best characterized example of chromatin involvement in DNA damage repair is the ATM/ATR/DNA-PK- mediated phosphorylation of the histone 2A variant H2AX, which flanks sites of double-stranded breaks (Matsuoka *et al.* 2007).

1.3.3.3 Base excision repair

The base excision repair pathway protects cells against small base alterations that do not distort the DNA helix by replacing damaged DNA with new, undamaged DNA (Frosina *et al.* 1996). The main enzymes involved in the pathway are the DNA glycosylases which remove damaged bases by cleaving the *N*-glycosidic bond between the base and the 2-deoxyribose moieties of the nucleotide residue, resulting in an abasic (AP) site on the DNA (Dodson, Michaels, and Lloyd 1994). The AP site is then recognised and removed by an AP endonuclease which nicks the DNA strand 5' of the AP site, or an AP lyase which nicks the 3'-end of the AP site (Dempfle, Herman, and Chen 1991). The deoxyribose phosphate backbone is removed by a phosphodiesterase and the gap filled by a DNA-polymerase. The strand is finally sealed with a DNA ligase and DNA damage repair is completed (Mol *et al.* 1999; Krokan, Standal, and Slupphaug 1997). The specificity of the base excision repair pathway depends on the type of glycosylase involved, as different types of damage are repaired by different glycosylases (Sinha and Häder 2002). For instance, uracil DNA glycosylase will remove uracil lesions in DNA, while AG-mismatch glycosylases will target A-G mismatches (Sinha and Häder 2002).

1.3.3.4 Nucleotide excision repair

Nucleotide excision repair (NER) targets bulky DNA lesions that alter the DNA helix. Such lesions are generally caused by exposure to radiation or DNA damaging chemicals (Sinha and Häder 2002). There are two distinct pathways in nucleotide excision repair: the transcription-

coupled repair pathway and the global genome repair pathway. The transcription-coupled pathway is used when the DNA damage is on a transcribed strand in active genes (Lehmann 1995; Mellon *et al.* 1986) while the global genome repair pathway repairs damage in non-transcribed regions of the genome, as well as non-transcribed strands of active genes (Sinha and Häder 2002). The basic steps for NER are: damage recognition, dual incisions by nucleotides bracketing the lesion to produce a 24 – 32 nucleotide oligomer, release of the oligomer, repair synthesis to fill in the gap and ligation (Sancar *et al.* 2004).

In humans, global genome nucleotide excision repair is carried out by six repair factors, namely RPA, XPA, XPC, TFIIH, XPG and XPF-ERCC1, acting in concert with each other (Mu *et al.* 1997). The excision follows a well characterized path, namely an ATP-independent recognition of damaged DNA, followed by ATP-dependent unwinding of the DNA and the formation of a DNA-protein complex with some of the excision nuclease factors and, finally, dual incisions by the endonucleases (Wakasugi and Sancar 1999). Damage recognition factors for the nucleases are DNA-binding proteins RPA (Coverley 1992), XPA (Tanaka *et al.* 1990) and XPC (Mu *et al.* 1997), all of which show preferential binding for damaged DNA. After the three factors have bound to the DNA site, TFIIH is recruited and a pre-incision complex is formed. If the site has a lesion the DNA is unwound and XPG replaces XPC to form a more stable complex. XPF-ERCC1 is recruited to the damage site and the damage strand is incised at the 3'-end by XPG and at the 5' end by XPF-ERCC1 (Wakasugi and Sancar 1999). Transcription-coupled repair requires additional proteins in the form of CSA and CSB to detect DNA damage (Mu *et al.* 1997). After the oligomer is excised, the lesion is filled in and repaired in the same manner as described for base excision repair.

1.3.3.5 Recombinational repair

Double-stranded breaks are usually the result of reactive oxygen species, or ionizing radiation and are repaired by either homologous recombination (HR) or non-homologous end-joining (NHEJ) repair (Petrini 1999; Ischenko and Saparbaev 2002).

Homologous recombination repair is initiated by the resection of the break to provide 3' single-stranded DNA overhangs. These 3' ssDNA overhangs then invade into a homologous sequence after which DNA synthesis follows at the invading end. After strand invasion, two pathways can occur: the second double-stranded break end can be captured to form an intermediate with two Holliday junctions, and after DNA synthesis and DNA ligation the Holliday junctions can be resolved via non-crossover or crossover methods. Alternatively, synthesis-dependent strand

annealing can occur, through which the ssDNA strand anneals to the other break end followed by gap repair and ligation (Sung and Klein 2006). This process is illustrated in Figure 1.5.

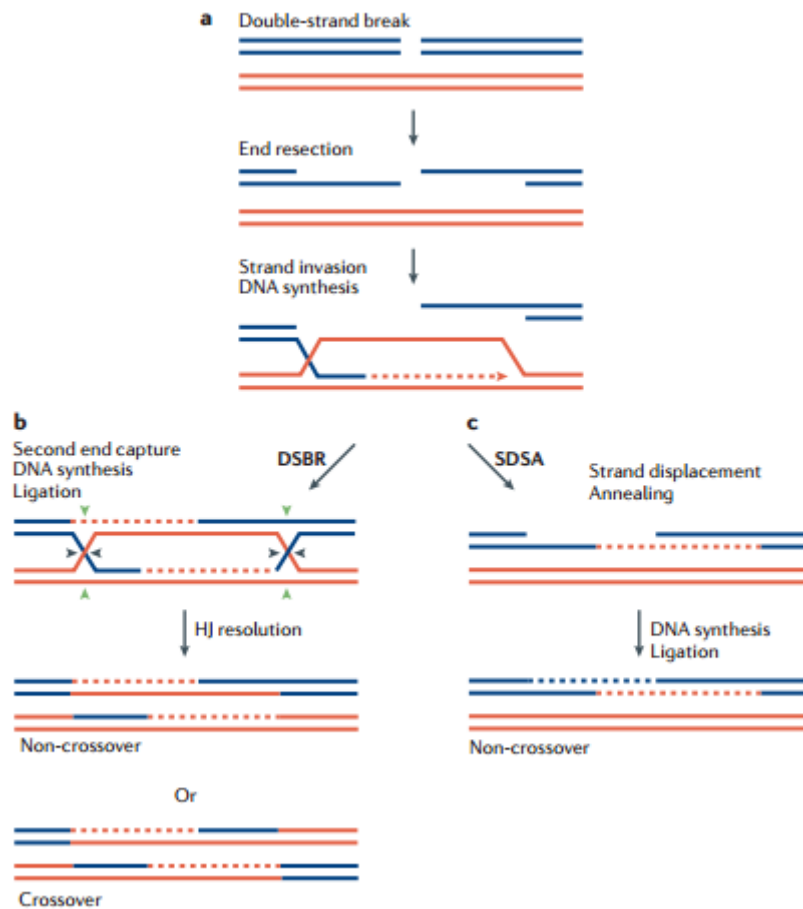


Figure 1.5: Schematic representation of the various homologous repair mechanisms to repair double-stranded breaks, taken from Sung, 2006.

Strand invasion and branch migration are initiated by Rad51 (Sung *et al.* 2003) which possess recombinase activity. The efficiency of HR is enhanced by mediator proteins that promote the loading of Rad51 onto single stranded DNA. The Rad51-ssDNA complex is disassociated by the Srs2 helicase (Aboussekhra *et al.* 1992), and other helicases control the level of crossover formation, with some such as Mer3 ensuring enough crossovers are made (Nakawaga and Ogawa 1999), while BLM helicases prevent spurious crossovers (Wu and Hickson 2003). BRC2, a well-known oncogene (Moynahan 2002) has been shown to be vital in HR (Jasin 2002), most likely via physical interaction with Rad51 (Sharan *et al.* 1997; P.-L. Chen *et al.* 1998).

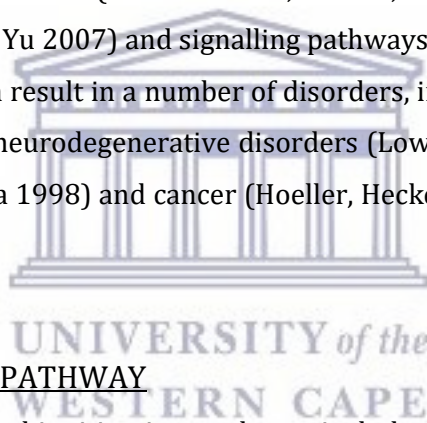
In non-homologous end-joining, the Ku heterodimer binds to the two ends of the double-stranded break and recruits DNA-PKcs (Gottlieb and Jackson 1993) and the ligase XRCC4 complex 4 to these ends (Ramsden and Geliert 1998). The two ends are then ligated, regardless

of whether the two ends come from the same chromosome (Nick McElhinny *et al.* 2000). This method of DNA damage repair is likely to be the major pathway for the repair of double-stranded breaks caused by ionizing radiation and chemical agents (Sancar *et al.* 2004).

1.4 UBIQUITINATION

1.4.1 INTRODUCTION

Ubiquitination is a cellular process whereby ubiquitin molecules are covalently attached to cellular proteins (Kerscher, Felberbaum, and Hochstrasser 2006). The most well characterized function of ubiquitination is the targeting of proteins for degradation via the proteasome, whereby ubiquitin is attached to the substrate to form a polyubiquitin chain that is recognised by receptors within the proteasome (Young *et al.* 1998). The ubiquitination pathway also serves other functions within the cell, including transcriptional regulation (Conaway, Brower, and Conaway 2002), cell cycle progression (Bai *et al.* 1996; Seufert, Futcher, and Jentsch 1995), DNA damage repair (Kim, Chen, and Yu 2007) and signalling pathways (Chen 2005). Dysregulation of the ubiquitination pathway can result in a number of disorders, including autoimmune diseases (Wang and Maldonado 2006), neurodegenerative disorders (Lowe *et al.* 1990; Alves-Rodrigues, Gregori, and Figueiredo-Pereira 1998) and cancer (Hoeller, Hecker, and Dikic 2006; Zhang *et al.* 2004).



1.4.2 THE UBIQUITINATION PATHWAY

The main components of the ubiquitination pathway include ubiquitin, ubiquitin activating enzymes (E1), ubiquitin conjugating enzymes (E2) and ubiquitin ligases (E3), as well as the 26S proteasome (Hershko *et al.* 1983). Figure 1.3 illustrates the components of the pathway and the various forms of ubiquitination that may occur. The initial activation of ubiquitin requires that the C-terminal of ubiquitin must be activated to be able to form bonds with other peptides (C M Pickart and Rose 1985). This activation is performed by E1, which adenylates ubiquitin, forming a ubiquitin-AMP intermediate. This intermediate is attacked by a sulfhydryl group on E1, forming a E1-ubiquitin thiolester (C M Pickart and Rose 1985). The ubiquitin is then transferred to an E2 through the formation of a thiolester bond between the C-terminus of ubiquitin and a catalytic cysteine on the E2 (Z. Chen *et al.* 1990). The ubiquitin is then finally transferred to a lysine on the target substrate via a substrate-specific E3 ligase (Hochstrasser 1996).

Further ubiquitin molecules can be added to form polyubiquitin chains and the specific lysine modification used in the formation of the polyubiquitin chain determines the cellular fate of the

protein. The formation of K48-linked polyubiquitin chains leads to proteasomal degradation (Hough, Pratt, and Rechsteiner 1986; Ganoth *et al.* 1988) while the formation of K63-linked chains allows the substrate to act as a scaffold and further participate in cellular activities such as DNA repair (Hofmann and Pickart 1999), protein kinase activation as well as assist in the localisation of proteins (Weissman 2001; Cecile M Pickart and Eddins 2004).

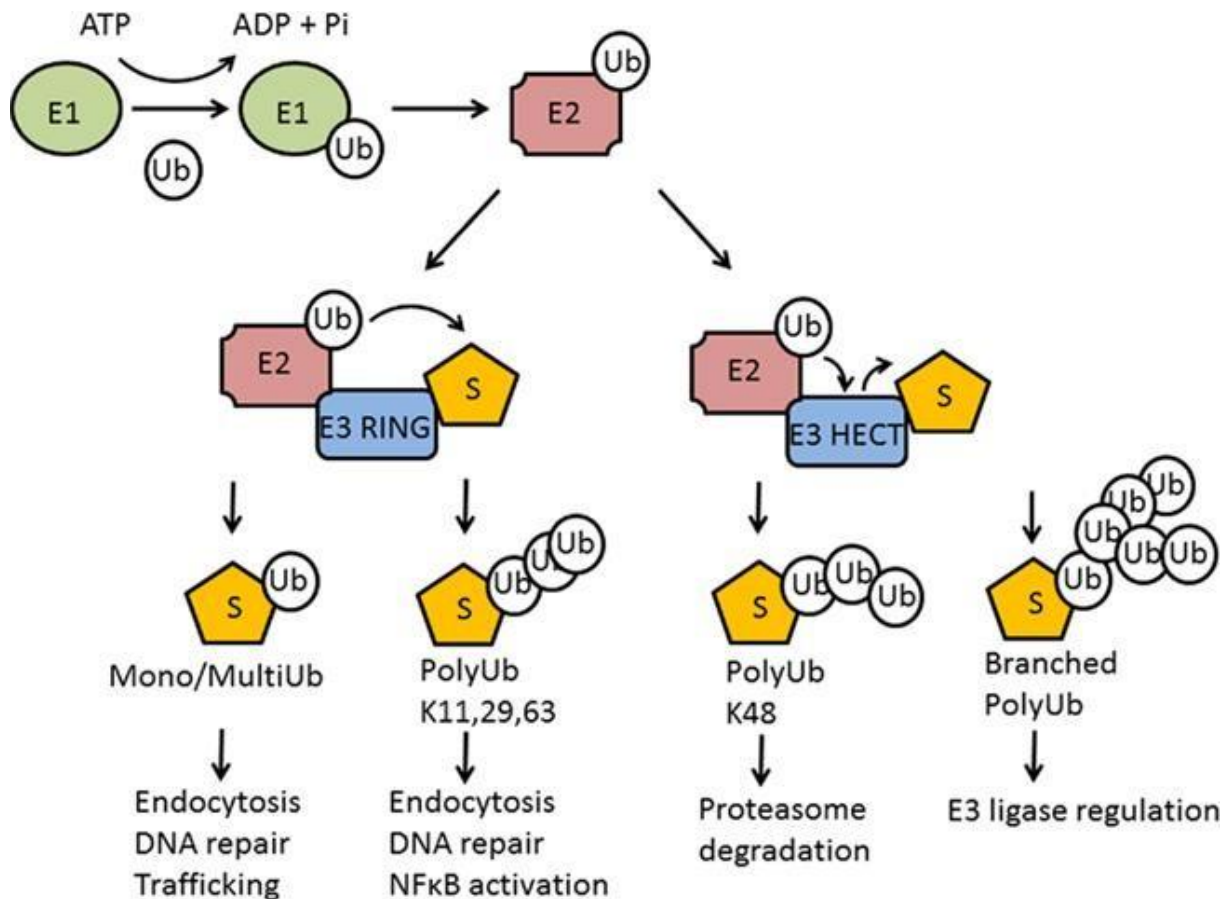


Figure 1.6: The ubiquitin-proteasome system illustrating the various forms of ubiquitination possible, taken from Perrett *et al.* 2011.

1.4.3. UBIQUITIN AND UBIQUITIN-LIKE MOLECULES

Ubiquitin was discovered in the early 1970s and was quickly found to be of vital importance in the labelling of intracellular proteins for degradation without involvement from the lysosome system (Hershko *et al.* 1983). Since then, a whole family of ubiquitin-like molecules (Ubl) has been identified. While these molecules may not all share high sequence homology, they all contain the ubiquitin-fold (Hochstrasser 2000). The most well studied ubiquitin-like molecules include SUMO and NEDD8, each of which display distinct, essential cellular functions and pathways (Schwartz and Hochstrasser 2003).

SUMO was first identified in 1996 by Matunis who found that RanGAP1, a protein required for the activation of nuclear Ras-like GTPase Ran was modified by a ubiquitin-like protein dubbed SUMO. SUMO conjugation, dubbed SUMOylation, is essential for cell viability in budding yeast (Müller *et al.* 2001) and has been shown to be necessary in chromosomal structure and dynamics (Bachant *et al.* 2002) and transcriptional regulation (Seeler and Dejean 2001; Sapetschnig *et al.* 2002).

NEDD8 was first identified as a gene that was downregulated in neural precursor cells in the development of the murine brain. This gene was found to code for a 9 kDa protein that bore a high sequence homology with ubiquitin, including the K48 residue (Kumar, Yoshida, and Noda 1993). Subsequent studies detected NEDD48 in a wide variety of cell-lines and tissues and named it “related to ubiquitin-1” (RUB1) in yeast (Liakopoulos *et al.* 1998). NEDD8 is remarkable because it can be processed by the ubiquitination system and can incorporate into polyubiquitin chains (Whitby *et al.* 1998). The main function of NEDD8 is as a regulator of ubiquitin protein ligases as it binds to cullins, preventing the recruitment of E2s (Liu *et al.* 2002), but it is also highly expressed in proliferating cells and is essential for the transition from the G₁ to S phase in the cell cycle (Tateishi *et al.* 2001).

1.4.4 UBIQUITIN-ACTIVATING ENZYME

It was long believed that there was only one E1 present in eukaryotic cells. However, a second E1-like protein, dubbed E1-L2, has recently been identified which has been shown to activate ubiquitin in eukaryotic cells (Jin *et al.* 2007).

1.4.5 UBIQUITIN-CONJUGATING ENZYMES

There are at least 35 active ubiquitin-conjugating enzymes in humans, with other species showing having between 16 and 35 active E2s (van Wijk and Timmers 2010). E2s share high sequence homology in the core ubiquitin-conjugation domain (UBC) which interacts with the E1 (Burroughs *et al.* 2008). This UBC provides the platform for the E1, activated ubiquitin and the E3 (Burroughs *et al.* 2008).

E2s are divided into classes based on the N- and C-terminal extensions present in the E2. These extensions can influence the specificity of E1 binding, subcellular localisation of the E2 as well as help modulate the interaction with the specific E3 (Winn *et al.* 2004). Class I E2s contain only the UBC and no other extensions, Class II E2s include N-terminal extensions, Class III include C-terminal extensions and Class IV E2s possess both N- and C-terminal extensions (Winn *et al.*

2004). E2s are also responsible for the type of polyubiquitination chain linkage through the selection of lysine residues on the ubiquitin (Rodrigo-Brenni, Foster, and Morgan 2010; David *et al.* 2010).

1.4.6 UBIQUITIN LIGASES

Ubiquitin ligases, also known as E3s, are the most numerous and diverse of the enzymes involved in the ubiquitin pathway, mainly because they play the pivotal role of determining substrate specificity (David *et al.* 2011). While the E2 enzyme is able to catalyse substrate polyubiquitination without the need for an E3, the lysine chosen for this reaction is non-specific. The E3 is required to select the correct ubiquitination site on the substrate and confer specificity to the ubiquitination reaction (David *et al.* 2011).

E3s fall into two broad groups depending on the types of domains they contain: namely the RING-containing E3s and the homologous to E6-AP carboxy-terminus (HECT)-containing E3s (de Bie and Ciechanover 2011). Smaller groups, such as U-box-containing E3s, zinc-finger-containing E3s and plant homologue domain-containing E3s have also been discovered, but they are found in relatively low numbers compared to the 600 RING-containing ligases and 30 HECT-ligases identified in humans (de Bie and Ciechanover 2011).

The RING finger was first described as a cysteine-rich motif with the consensus sequence CX2CX(9-39)CX(1-3)HX(2-3)C/HX2CX(4-48)CX2C (Katz and Marin 1991). Examination of the three dimensional structure of the domain showed that the conserved histidine and cysteine are found deep with the core of the domain where they keep the structure stable by binding two zinc ions (Barlow *et al.* 1994). Unlike traditional zinc fingers, the zinc coordination sites in the RING finger are interleaved, forming a rigid platform suitable for protein-protein interactions (Borden *et al.* 1995). RING-containing E3 ligases have been shown to play a role in many diverse cellular processes, with BRCA-1 and MDM2 being some of the more well-known examples, involved with DNA repair and proliferation respectively (Miki *et al.* 1994; Honda, Tanaka, and Yasuda 1997).

HECT-domain E3 ligases differ from RING-domain E3 ligases in that the ubiquitin is transferred from the E2 to an active site cysteine within the HECT domain before being transferred to the specific substrate (Scheffner, Nuber, and Huibregtse 1995). The HECT domain is a large lobe on the N-terminal of the protein which contains the E2 binding site and a smaller C-terminal domain containing the site-active cysteine (L. Huang *et al.* 1999). The two lobes are connected by a short linker and the conformational flexibility of this linker is vital to the transfer of the

ubiquitin to the active site cysteine and the formation of the thioester bond (Verdecia *et al.* 2003). The region upstream of the HECT domain determines the specificity of the E3 ligase and its localisation in the cell (Kee and Huibregtse 2007). The original HECT-domain E3 ligase, E6 associate protein (E6-AP), was found to interact with the E6 protein of human papillomavirus and form a stable dimer which subsequently targeted human tumour suppressor p53 for proteasomal degradation (Narisawa-Saito and Kiyono 2007).

1.5 NUCLEAR SPECKLES

1.5.1 INTRODUCTION

The nucleus is one of the largest and most complex organelles in the cell, and is highly compartmentalised, yet has the ability to be dynamic at the same time. A number of punctate structures are apparent when visualised using immunofluorescence microscopy, including Cajal bodies, polycomb bodies, nucleoli, paraspeckles and nuclear speckles (reviewed in Lamond and Earnshaw 1998). Nuclear speckles, which are also known as SC35 domains (Wansink *et al.* 1993) or splicing factor compartments (Phair and Misteli 2000), contain the pre-mRNA splicing machinery required to produce mature mRNA. Proteins found in nuclear speckles include small nuclear ribonucleoproteins (snRNPs), spliceosome subunits such as the Sm proteins and non-snRNP factors such as YB-1 (Raffetseder *et al.* 2003). Immunofluorescence labelling of splicing factors shows that they appear punctate only when they are in nuclear speckles, and are otherwise evenly distributed throughout the nucleus. These bodies are visible using electron microscopy and don't require immunofluorescence to visualise (Thiry 1995). Nuclear speckles are distributed in the interchromatin space of the nucleus and are linked together by thin fibrils (Cmarko *et al.* 1999) and for this reason are also referred to as interchromatin granules (Spector, O'Keefe, and Jimenez-Garcia 1993).

A number of signals targeting proteins to nuclear speckles have been identified. The most well-known is the arginine/serine rich domain (RS domain) that is found in a number of splicing factors. RS domains have been shown to be sufficient for localisation to speckles without the need for any additional factors (Cáceres *et al.* 1997). Two other domains reported to act as speckle localisation signals are the threonine/proline repeats of splicing factor SF3b1, a subunit of SF3b (Eilbracht and Schmidt-Zachmann 2001), and the forkhead-associated domain of NIPP1 (Jagiello *et al.* 2000). More recently, polyHis repeats were identified in 15 speckle-associated proteins, suggesting that these repeats function as a platform for the resident nuclear speckle constituents, most likely relying on charge effects to localise the proteins to nuclear speckles

(Salichs *et al.* 2009). These may not be the only signals sufficient for localisation to nuclear speckles and others may yet be discovered.

1.5.2 THE STRUCTURE AND FUNCTION OF NUCLEAR SPECKLES

Nuclear speckles form throughout the nucleoplasm in regions of little or no DNA (Thiry 1995). Although they don't contain any genes, nuclear speckles are observed close to highly active transcription sites, suggesting that they have a functional relationship with gene expression. This hypothesis is supported by the fact that particular genes preferentially localise close to nuclear speckles (Brown *et al.* 2008; Johnson *et al.* 2000; Moen *et al.* 2004; Xing *et al.* 1995), for example muscle-specific genes (Human β -cardiacmyosin heavy chain and myogenin) and COL1A1, encoding alpha-1 type I collagen. It has also been found that chromosomal regions rich in genes tend to be found along the edges of nuclear speckles more frequently than regions poor in genes (Shopland *et al.* 2003), and that genes expressed simultaneously tend to associate with the same speckle, suggesting that nuclear speckles organise active genes on their edges to form functional centres of transcription (Shopland *et al.* 2003).

An alternative view of nuclear speckles is that they serve as storage, assembly and modification compartments that supply active transcription sites, rather than being active transcription sites themselves (Lamond and Spector 2003). High resolution electron microscopy showed that pre-mRNA is localised outside of nuclear speckles in structures called perichromatin fibrils (Cmarko *et al.* 1999), making it more likely that most of the co-transcriptional splicing was taking place on these fibrils rather than within the nuclear speckles (Cmarko *et al.* 1999; Fakan 1994). Since perichromatin fibrils associate so closely with nuclear speckles, it is difficult to distinguish the two bodies using fluorescence microscopy, which has resulted in some postulating that nuclear speckles are direct sites of splicing, and it requires high resolution microscopy to make the distinction between the two (Spector and Lamond 2011).

Recent studies using antibodies which recognise a phosphorylated U2 snRNP protein that is only found in activated spliceosomes showed that these spliceosomes localised to areas of de-compacted chromatin in or around nuclear speckles (Girard *et al.* 2012), suggesting that nuclear speckles themselves are sites of mRNA processing. These findings support earlier studies that showed that introns of specific transcripts were spliced in nuclear speckles (Lawrence, Carter, and Xing 1993). Paraspeckles are structures formed at the periphery of nuclear speckles that have been implicated in the regulation of gene expression through RNA editing, particularly through the hydrolytic deamination of adenosine to inosine (A-to-I editing) controlled by

adenosine deaminases (Nakagawa and Hirose 2012), and also contain over 40 RNA-binding proteins of varying functions. This would suggest that paraspeckles play an important, though still poorly understood, role in RNA processing (Naganuma *et al.* 2012). Taken together, these findings suggest that nuclear speckles may play a more active role in transcription and mRNA processing than previously expected.

1.5.3 THE COMPOSITION OF NUCLEAR SPECKLES

The fact that so many pre-mRNA splicing factors associate with nuclear speckles allows for the identification of proteins involved with mRNA processing (Spector and Lamond 2011). Most snRNPs and SR proteins have been localised to nuclear speckles (Fu 1995), as well as several kinases, including Clk/STY (Colwill *et al.* 1996), hPRP4, (Kojima *et al.* 2001) and PSKHI, (Brede, Solheim, and Prydz 2002). Nuclear speckles also contain phosphatases (Trinkle-Mulcahy, Sleeman, and Lamond 2001) that activate and deactivate the components of splicing machinery through phosphorylation, which provides evidence that nuclear speckles are involved in the regulation of the factors used in transcription and splicing machinery (T Misteli and Spector 1997).

Analysis of an enriched interchromatin granule cluster fraction taken from mouse liver nuclei revealed 146 known proteins associated with nuclear speckles, in addition to unknown proteins (Mintz *et al.* 1999; Saitoh *et al.* 2004). Of particular interest is that the study revealed a number of proteins that are neither splicing factors, nor associated with splicing factors. Included in this list are a variety of transcription factors (Larsson *et al.* 1995; Zeng *et al.* 1997), 3'-end mRNA processing factors (Schul, van Driel, and de Jong 1998), the translation initiation factor eIF4E (Dostie, Lejbkiewicz, and Sonenberg 2000), a translation inhibition factor eIF4AIII (Li *et al.* 1999) and a variety of structural proteins. However, no factors associated with ribosome biogenesis or tRNA production were identified, cementing the relationship between nuclear speckles and mRNA processing (Spector and Lamond 2011). These findings are in agreement with other studies showing that assembled spliceosomes contain transcription factors and 3'-end processing factors in a higher order complex (Rappsilber *et al.* 2002).

While transcription and splicing are not thought to take place in nuclear speckles (Cmarko *et al.* 1999), the large subunit (LS) of RNA polymerase II, which is the enzyme primarily responsible for transcription, has been seen to localise to nuclear speckles through immunofluorescence (Bregman *et al.* 1995). This was confirmed through analysis of the IGC-enriched nuclear fraction discussed above (Mintz *et al.* 1999; Saitoh *et al.* 2004), suggesting that a pool of RNA polymerase

II is present in nuclear speckles. A number of transcription factors including FBI-1 (Pendergrast *et al.* 2002) and nucleosome binding protein HMG-17, which alters the structure of chromatin to enhance transcription (Hock *et al.* 1998), have also been found to partially localise to nuclear speckles. Nevertheless the data is contradictory, with other studies failing to report RNA polymerase II in speckles, in support of the idea that speckles are mainly used for storage and assembly of these factors (Grande *et al.* 1997; Zeng *et al.* 1997; Kimura, Sugaya, and Cook 2002) rather than being sites of active transcription. So while the link between nuclear speckles and transcription remains unclear, it is likely that the presence of transcription factors results in a higher order assembly that affects the transcription and modification of RNA (Spector and Lamond 2011).

The underlying scaffold on which nuclear speckles assemble has not yet been identified (Sacco-Bubulya and Spector 2002), though several candidates have been investigated. Lamin A has been detected in nuclear speckles (Jagatheesan *et al.* 1999), though studies in cells lacking lamin A did not display any change in nuclear speckle arrangement (Večeřová *et al.* 2004). The most promising candidate is Son, a ~270kDa protein that contains multiple serine-rich repeats and an RS domain. Son has been associated with nuclear speckles, and RNAi depletion of the protein results in changes of nuclear speckle structure, implying a role for scaffolding for the mRNA processing factors found in nuclear speckles (Sharma *et al.* 2010).

1.5.4 THE DYNAMICS OF NUCLEAR SPECKLES

Nuclear speckles are not static structures; they change in size, shape and number and are different depending on cell type and even the level of gene expression (Spector and Lamond 2011). If transcription is halted, either due to cell stress or to the use of transcriptional inhibitors, nuclear speckles become much larger, and splicing factors accumulate in these enlarged speckles (Spector, Schrier, and Busch 1984; Spector, Fu, and Maniatis 1991). The fact that speckles enlarge following stress, where transcription of stress factors is increased, provides additional support for the idea that the primary role of the speckles is storage and assembly of splicing factors and that direct sites of splicing are found elsewhere.

The use of fluorescence recovery after photo-bleaching (FRAP) has shown that the speckle components have an exceedingly rapid rate of exchange between the exterior and interior of the speckles (Phair and Misteli 2000). For instance, the recovery of splicing factor SF2/ASF occurs within thirty seconds of photo-bleaching, with half of the recovery occurring within five seconds. Further kinetic modelling of the dynamics indicates that the mean residence time for

the factor in speckles is about 50 seconds (Phair and Misteli 2000). This is the best example available to demonstrate that while the overall structure of nuclear speckles remains relatively steady, there is large flux of individual components into and out of speckles, allowing the cell to react rapidly to stress.

1.6 THE PRINCIPLES OF COLOCALISATION

1.6.1 INTRODUCTION

Colocalisation can be defined as the overlap in two or more fluorescence signals within a digital image recorded by fluorescence microscopy (Smallcombe 2001). Colocalisation is used to understand the function of a molecule based on its proximity to another in the cell (Zinchuk, Zinchuk, and Okada 2007). However, it should be noted that colocalisation is not suitable for identifying interactions between proteins, as even with super-resolution microscopy the resolution is not high enough to identify with certainty the physical location of two separate protein molecules (Dunn, Kamocka, and McDonald 2011). Colocalisation should instead be viewed as a tool to identify the localisation of proteins to the same sub-cellular or sub-nuclear structures. Further experiments such as fluorescence resonance energy transfer (FRET) or proximity ligation assay (PLA) should be performed to determine interactions between two proteins that show strong colocalisation.

1.6.2 ACQUIRING IMAGES FOR COLOCALISATION

As colocalisation requires high optical resolution to produce meaningful results, the choice of microscope is vital to the success of a colocalisation experiment (Bolte and Cordelières 2006). Confocal microscopes provide higher image resolution than traditional fluorescence microscopes by eliminating out-of-focus light via a pinhole on the detector. Images obtained with wide-field fluorescence microscopes may be subjected to a computational technique known as deconvolution to remove any out-of-focus light by reassigning the light to its origin, sharpening the image and providing enough resolution to mimic images taken by confocal microscopes (Wallace, Schaefer, and Swedlow 2001).

Accurate colocalisation analysis requires that the image meets a certain number of criteria. The background and auto-fluorescence of the cells should be accounted for and corrected by removing pixels with intensity values less than those generated by the features of interest.

Bleed-through, or cross-talk, is when signal from the red fluorophore leaks into the green channel or vice versa and is a large problem in colocalisation, as it can give false positive results.

Bleed-through is more common in fluorescence microscopes where band filters are poorly set up (Zinchuk, Zinchuk, and Okada 2007; Smallcombe 2001). To prevent the occurrence of bleed-through the microscope should be set up in a manner that avoids bleed-through by using optimised emission filters, acquiring images through sequential scanning and ensuring that the chosen fluorophores have excitation and emission spectra that are well-separated. The presence of bleed-through can be controlled for by using controls that contain only either the green fluorophore or red fluorophore and acquiring images for both channels. Unstained controls should be used to control for auto-fluorescence (Smallcombe 2001).

1.6.3 VISUALIZING COLOCALISATION

Initial colocalisation of two molecules can be identified visually. When the red and green signal merge due to superimposition, the signal turns yellow due to the combined contributions of the two fluorophores. One of the standard ways of showing colocalisation is to show the green image, the red image and a merge of the two showing yellow points of colocalisation (Dunn, Kamocka, and McDonald 2011). However, results shown in this manner can be ambiguous, because the presence of yellow signal will only occur if the intensities of the two individual signals are similar (Dunn, Kamocka, and McDonald 2011) which is not often the case when two fluorophores are used that differ in signal strength, or if the concentrations of the molecules in the cell vary (Bolte and Cordelières 2006).

Colocalisation can also be visualised graphically through the use of a scatterplot where the intensity of the one colour in each pixel is plotted against the intensity of the second colour in the same pixel. Under conditions where colocalisation is likely, the points in the plot will align to a straight line where the slope represents the ratio of fluorescence intensity between the two molecules. If colocalisation is not present the points will distribute into two separate groups (Dunn, Kamocka, and McDonald 2011). Scatterplots are useful as they provide an indication of the degree of colocalisation between the two molecules, as well as detecting the presence of different populations within cellular compartments (Dunn, Kamocka, and McDonald 2011).

While these visualizations of colocalisation produce intuitive results that are easily understood, they have limitations, namely they are unable to determine whether the amount of colocalisation detected is due to random chance, and they cannot compare the degree of colocalisation under differing experimental conditions. To overcome these limitations, further analysis using global statistical approaches is necessary. There are a number of approaches that can be used, each with their own specific uses and limitations (Bolte and Cordelières 2006; Dunn, Kamocka, and McDonald 2011).

1.6.4 QUANTIFYING COLOCALISATION

There are a number of specifically designed algorithms that can calculate a variety of coefficients applicable to colocalisation analysis. Correlation coefficients measure the strength of the linear variables such as the greyscale values assigned to fluorescence intensities of green and red image pairs (Bolte and Cordelières 2006). Each of these coefficients use varying approaches to evaluate colocalisation and the choice of which one to use depends heavily on the application and situation (Bolte and Cordelières 2006).

1.6.4.1 Pearson's Correlation Coefficient

Pearson's correlation coefficient was formulated in 1896 as a standard measure in pattern recognition (Pearson 1896), and it has since been adapted for use in colocalisation analysis (Manders, Verbeek, and Aten 1993). Pearson's coefficient is calculated using the following formula:

$$PCC = \frac{\sum_i (R_i - \bar{R}) \times (G_i - \bar{G})}{\sqrt{\sum_i (R_i - \bar{R})^2 \times \sum_i (G_i - \bar{G})^2}}$$

where R_i and G_i are the intensities of the red and green channel respectively in pixel i and \bar{R} and \bar{G} are the mean intensities of the red and green channels respectively, across the entire image. The sum is taken over all pixels. Pearson's correlation coefficient values range between -1 and +1, with +1 indicating perfect correlation, 0 indicating no significant correlation and -1 indicating complete negative correlation. The main limitation of Pearson's correlation coefficient is that it assumes that each pixel is an independent data point, which is not the case in images of cells where pixels are auto-correlated, meaning that pixels close to each other will have similar intensity values (McDonald and Dunn 2013). This autocorrelation is caused by the point-spread function of the imaging system where the signal of a point is sourced to several adjacent pixels, as well as due to the subcellular structures of the cell which typically occupy a number of pixels (McDonald and Dunn 2013). It has been well established that the expected distribution of Pearson's correlation coefficient under the null hypothesis is much broader when the points are auto-correlated as opposed to if the data points were independent (Student, 1914). This means that any pair of proteins in the cell can be shown to have significant colocalisation (McDonald and Dunn 2013).

Pearson's correlation coefficient may also be inadequate in a number of biological situations. As the coefficient measures the variability of green and red pixel intensities and expresses them in a simple linear relationship it is sensitive to the degree to which both individual red and green pixel intensity values are above or below background intensity, as well as the proportionality of the signal levels in the red and green channels (Bolte and Cordelières 2006; Dunn, Kamocka, and McDonald 2011). This means that values of the coefficient will be depressed in cells with varying proportions of proteins of interest in different compartments in the cell, for instance where a protein of interest is found diffused in the nucleus, but in high punctate concentrations in sub-nuclear compartments. In these cases, alternate coefficients should be used (Dunn, Kamocka, and McDonald 2011; McDonald and Dunn 2013).

1.6.4.2 Manders Overlap Coefficient

An adapted form of Pearson's coefficient was developed by Manders in 1993. The Manders overlap coefficient is described by the equation:

$$MOC = \frac{\sum_i (R_i \times G_i)}{\sqrt{\sum_i R_i^2 \times \sum_i G_i^2}}$$

where where R_i and G_i refer to the intensities of the red and green channel respectively in pixel i . The sum is taken over all pixels i . The values for the coefficient range between 0 and 1, with a value of 0 indicating no colocalisation and a value of 1 indicating 100 % colocalisation. A value of 0.5 would signify that half of the pixels in the image colocalise with each other.

One of the principal advantages of Manders' formulation is that it allows direct evaluation of the fraction of red pixels overlapping with green pixels and vice versa (Manders, Verbeek, and Aten 1993): these fractional coefficients are calculated using the formula:

$$M_1 = \frac{\sum_i R_{i,colocal}}{\sum_i R_i}$$

where $R_{i,colocal} = R_i$ if $G_i > 0$ and $R_{i,colocal} = 0$ if $G_i = 0$, and

$$M_2 = \frac{\sum_i G_{i,colocal}}{\sum_i G_i}$$

where $G_{i,colocal} = G_i$ if $R_i > 0$ and $G_{i,colocal} = 0$ if $R_i = 0$.

This provides a direct metric for measuring the population of the green channel colocalizing with the red channel and vice versa, which is of significance in many biological studies (Bolte and Cordelières 2006; Dunn, Kamocka, and McDonald 2011).

The main drawback of Manders over Pearson's is that, because it uses the absolute value R_i of the signal rather than first subtracting the background, $R_i - R$, it is extremely sensitive to background caused by auto-fluorescence, non-specific antibody labelling, and light leakage into the system. This background signal needs to be reliably identified and removed before the analysis can begin, either through setting threshold levels by locally determining background levels (Dunn, Kamocka, and McDonald 2011) by using an automated approach. An automatic approach to automatically identifying the threshold value used to identify background has been developed by Costes and co-workers, which determines the range of pixel values for which a positive Pearson's correlation coefficient is obtained (Costes *et al.* 2004) The coefficient is measured for each pixel in the image and then for lower red and green intensity values on a regression line, until the pixel values give a negative Pearson's correlation coefficient. These values are used as a threshold for identifying background levels and only pixels with higher intensity values are considered for the subsequent analysis. The automated Costes method provides an easily automated method for distinguishing background from labelled structures that eliminates user bias, allowing for accurate analysis using the Manders overlap coefficient (Bolte and Cordelières 2006; Dunn, Kamocka, and McDonald 2011).

1.7 RATIONALE FOR THE STUDY

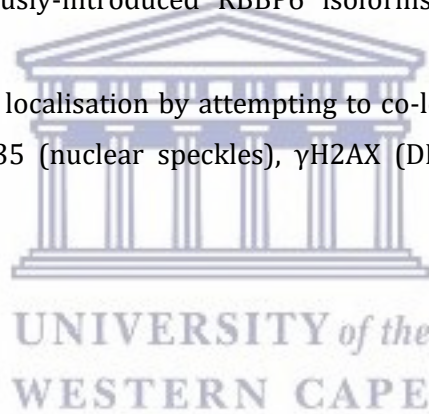
Through immunoprecipitation studies RBBP6 has been shown to interact directly with a number of proteins *in vivo*, including splicing factors and transcription factors. Some of these proteins, such as YB-1, are predominantly localised in the cytoplasm while others, like the Sm proteins, are localised exclusively in the nucleus. This raises the question as to whether RBBP6 localises to both the cytoplasm and the nucleus, or whether it shuttles between the two, either during the normal course of the cell cycle or in response to exceptional events such as heat shock or whether different isoforms of RBBP6 localise to different parts of the cell.

Determining the answer to this question may therefore provide invaluable information to the greater function of RBBP6 in the cell and help elucidate mechanisms that can lead to the disruption of normal cell function and result in cancer.

1.8 AIMS AND OBJECTIVES OF THE STUDY

The main objectives of the study were:

- 1) To investigate the localisation of different isoforms of endogenous RBBP6 before and after two different types of cell stress, namely heat shock and DNA damage, using immunofluorescence microscopy.
- 2) To investigate the time scale of observed changes in localisation using time course analysis.
- 3) To confirm that the detected protein was indeed endogenous RBBP6 by mimicking the results using exogenously-introduced RBBP6 isoforms tagged with highly specific immuno-tags.
- 4) To identify the sites of localisation by attempting to co-localise the signal with various markers, including SC35 (nuclear speckles), γ H2AX (DNA damage) and HSF-1 (heat shock).



CHAPTER 2 MATERIALS AND METHODS

2.1 CELL CULTURE

Details of the mammalian cell lines used in this study are shown in Table 2.1.

Table 2.1: Cell lines used in the study

CELL LINE	SPECIES	DERIVED FROM	CULTURED IN
A549	Human	Epithelial lung adenocarcinoma	DMEM
HeLa	Human	Cervical adenocarcinoma	DMEM
H157	Human	Non-small cell lung carcinoma	DMEM
HepG2	Human	Hepatocellular liver carcinoma	DMEM
KMST	Human	Human fibroblast, non-cancerous	DMEM

All cell lines were cultured at 37 °C in 25 cm² flasks in Dulbecco's modified eagle medium (DMEM, Gibco Life Sciences), supplemented with 10 % fetal bovine serum (Gibco Life Sciences, South Africa), 100 µg/ml penicillin and streptomycin (Gibco Life Sciences, South Africa), in a 5 % CO₂ humidified cell culture incubator (Farma International, USA). Cells were maintained in 25 cm² flasks and were trypsinised into 12-well plates for immunofluorescence studies. Trypsinisation was carried out by first removing the culture medium and rinsing the monolayer with 10 ml sterile 1X phosphate-buffered saline (PBS) (Life Technologies, South Africa). 2.5 ml of 0.25 % trypsin-ETDA (Gibco Life Sciences, South Africa) was added to the monolayer and incubated for 1 minute at 37 °C and the trypsin-ETDA solution removed. Cells were dislodged by the addition of 12 ml DMEM and gentle pipetting ensured complete re-suspension of cells. Cells were then distributed into the 12-well plate and grown for 12 – 24 hours before being subjected to cell stress.

When not in use cell lines were stored in a working bank at -80 °C. Cells were prepared for storage by trypsinising as described above and then re-suspended in a cryovial with 1 ml DMEM and 10 % v/v dimethyl sulfoxide (DMSO).

2.2 ADMINISTRATION OF CELL STRESS

Cell stress was administered using three different methods:

- Heat shock via incubation at 42 °C for 5 minutes. 12-well plates containing cells growing on coverslips were placed into an incubator set to 42 °C and incubated for 5 minutes, after which they were subjected to immunofluorescence techniques.
- DNA damage induced via UV irradiation using a Stratalinker UV Crosslinker 1800, (Stratagene, USA) at 40 J/m², as described by Koike and co-workers (Koike *et al.* 1997).
- DNA damage induced by 1 µg/ml cisplatin (Sigma) administered 1 hour prior to cell fixation, as described by Ogha and co-workers (Ogha *et al.* 1998).

2.3 IMMUNOFLUORESCENCE MICROSCOPY

Cells were grown on sterile coverslips (Lasec, South Africa) in 12-well plates for 24 hours at 37 °C in a 5 % CO₂ humidified cell culture incubator and subjected to cell stress as described in Section 2.2

Cells were then fixed to the coverslips in ice-cold 100 % methanol (Sigma, USA) for 5 minutes followed by incubation in 4 % paraformaldehyde (Sigma, USA), diluted in PBS for 5 minutes at room temperature. Methanol is an organic solvent that dissolves lipids from cell membranes, making them permeable to antibodies (Melan 1994). The coverslips were washed 3 times with sterile 1X PBS (5 minutes per wash), and then blocked with 1 % bovine serum albumin (BSA) in PBS for 1 hour before being incubated overnight with antibodies, as described in the respective sections as well as Section 2.5.

Antibodies were diluted in 1 % BSA immediately prior to use. After primary antibody incubation, the coverslips were washed again in 1X PBS 3 times for 5 minutes each and then incubated for 1 hour in the respective secondary. After secondary antibody incubation the cells were incubated for 5 minutes in 1 µg/ml of Hoechst 33342 (Cell Signalling, USA) diluted in deionised water. Coverslips were then washed again with 1X PBS and mounted onto slides using approximately 10 µl Mowiol (Sigma, USA). These were allowed to dry in a dark place for 24 hours before being viewed under a Zeiss Axiovert 200M LSM 510 Meta confocal microscope, using Zen 2009 software provided by Zeiss. Images were analysed using ImageJ (<http://rsbweb.nih.gov/ij/>) and colocalisation analysis was performed using the JaCoP plugin (<http://rsbweb.nih.gov/ij/plugins/track/jacop.html>).

Bleed through, also known as crosstalk, is when the emission of one fluorophore is detected in a channel reserved for another fluorophore. This can provide false positive colocalisation results, which may severely impact the validity of any colocalisation experiment. Band-pass filters

positioned between the sample and the detector ensure that only light of the correct wavelength enters the detector. To confirm that bleed through was not present in our colocalisation experiments, cells were stained with one of the two primary antibodies and the corresponding secondary antibody, conjugated to a fluorophore matched to channel 1, and the absence of any signal in channel 2 was confirmed. The control was then repeated using the other primary antibody.

2.4 ANTIBODIES USED

2.4.1 PRIMARY ANTIBODIES

2.4.1.1 Monoclonal antibodies

A mouse monoclonal antibody was raised against residues 1-81 of human RBBP6 (isoform 1), expressed recombinantly in *E. coli*, at the Monoclonal Antibody Core Facility, European Molecular Biology Laboratory, Monterotondo-Scalo, Italy.

2.4.1.2 Polyclonal antibody raised in Bellstedt laboratory

A rabbit polyclonal antibody was raised against residues 1 – 81 of human RBBP6, expressed recombinantly in *E. coli*, in the laboratory of Prof D. Bellstedt in the Biochemistry Department, University of Stellenbosch, Stellenbosch, South Africa, using the naked bacteria method (Bellstedt et al. 1987). The method uses acid treatment to strip *Salmonella minnesota* R595 bacteria of their natural antigens and replaces these with the antigen against which the antibody is to be raised. These bacteria are then used to immunize rabbits and antibodies are collected within 6 weeks of the first immunization. This antibody targets the DWNN domain of RBBP6, and pre-immune serum is provided as a control.

2.4.1.3 Commercially obtained antibodies

In addition to the antibodies generated specifically for the study of RBBP6 a number of commercial antibodies were obtained and used.

- A monoclonal mouse antibody against residues 1582-1692 of RBBP6 was purchased from LifeSpan Biosciences (LS-C133084). In order to distinguish this antibody from the non-commercial anti-DWNN antibodies, we refer to it throughout this thesis as “C133084”.
- A monoclonal mouse antibody against the phospho-epitope of SC35 was purchased from Abcam and is referred to as “mouse monoclonal anti-SC35” throughout the thesis.

- A rabbit polyclonal antibody generated against a synthetic peptide of phosphorylated (Ser139) human γ H2A.X was purchased from Abcam and is referred to as “rabbit anti- γ H2AX” or “rabbit polyclonal anti- γ H2AX” throughout the thesis.

The details of the commercially obtained antibodies are provided in Table 2.2 below.

Table 2:2: List of commercially obtained primary antibodies used in the study.

Antibody	Supplier	Catalogue number	Epitope	Dilution factor
Mouse monoclonal anti-SC35	Abcam	ab11826	Phospho-epitope of SC35	1:500
Mouse monoclonal anti-RBBP6	LifeSpan Biosciences	LS-C133084	Residues 1582 - 1692	1:200
Rabbit polyclonal anti- γ H2AX	Abcam	ab26350	synthetic peptide of phosphorylated (Ser139) human γ H2A.X	1:200

2.4.1.4 Specificity of antibodies targeting various RBBP6 epitopes and isoforms

Due to the fact that the antibodies raised against the DWNN domain of RBBP6 would recognise all isoforms of the protein, it was vital to keep in mind which isoforms of RBBP6 could be detected by which antibodies. Figure 2.1 illustrates where the various antibodies are expected to bind. Table 2.3 shows which isoforms of the protein are expected to be detected by which antibodies. It should be noted that only the commercial anti-RBBP6 antibody could distinguish between isoforms 1, 2, 4 and isoform 3.

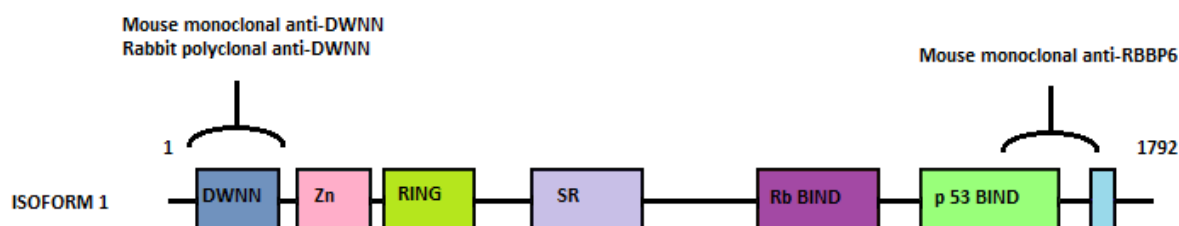


Figure 2.Schematic showing where the anti-DWNN and anti-RBBP6 antibodies are expected to bind; the anti-DWNN antibodies bind in the DWNN domain while anti-RBBP6 (C133084) binds at the C-terminal end.

Table 2:3 List of anti-RBBP6 antibodies used in the study and which isoforms of RBBP6 they are expected to detect.

Antibody	Epitope	Isoforms detected
Mouse monoclonal anti-DWNN	Residues 1-81	Isoforms 1, 2, 3 and 4
Mouse monoclonal anti-RBBP6 (C133084)	Residues 1582 - 1692	Isoforms 1, 2 and 4
Rabbit polyclonal anti-DWNN	Residues 1-81	Isoform 1, 2, 3 and 4

The specificity of the non-commercial antibodies for their target proteins were evaluated by Western blotting and peptide blocking as described in Section 2.5.

2.4.2 SECONDARY ANTIBODIES

To visualise the primary antibodies, several secondary antibodies conjugated to fluorophores were used in the study. These were diluted in PBS containing 1 % BSA at the dilutions given in Table 2.3 below.

Table 2:4: Secondary antibodies used during the study.

Antibody	Supplier	Catalogue number	Dilution factors
Anti-rabbit Cy3	Jackson ImmunoResearch Laboratories	711-165-152	1:500
Anti-rabbit Alexa488	Jackson ImmunoResearch Laboratories	711-545-152	1:1000
Anti-mouse Cy3	Jackson ImmunoResearch Laboratories	715-165-150	1:500
Anti-mouse Alexa488	Jackson ImmunoResearch Laboratories	715-545-150	1:1000
Anti-mouse conjugated HRP	Abcam	ab6728	1:1000
Anti-rabbit conjugated HRP	Abcam	ab6721	1:1000

2.5 WESTERN BLOTTING

2.5.1 PREPARATION OF CRUDE LYSATE

RIPA buffer was prepared as follows:

50 mM Tris, pH 7.4

1 % NP-40

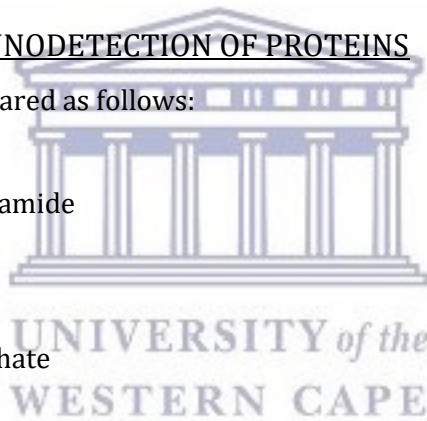
0.5 % Na-deoxycholate
0.1 % SDS
150 mM NaCl
2 mM EDTA
50 mM NaF

Culture medium from confluent A549 cells was removed and rinsed twice with PBS. The cells were detached using a cell scraper and the cell suspension transferred to a 1.5 ml Eppendorf tube. Cells were pelleted via centrifugation at 3000 rpm for 5 minutes and the supernatant was removed. The pellet was resuspended with 1 ml ice-cold RIPA buffer supplemented with PMSF (GeneTex, USA) and was allowed to stand on ice for 30 minutes with periodic vortexing every 10 minutes. The mixture was centrifuged at 14000 g for 15 minutes at 4 °C before being used for further analysis.

2.5.2 SDS-PAGE AND IMMUNODETECTION OF PROTEINS

16 % SDS-PAGE gels were prepared as follows:

2.1 ml H₂O
2 ml 40 % acrylamide:bis-acrylamide
1.31 ml 1.5M Tris, pH 8.8
42 µl 10 % SDS
20 µl 10 % ammonium persulphate
10 µl TEMED.



Stacking gels were prepared as follows:

1.27 ml H₂O
0.2 ml 40 % acrylamide:bis-acrylamide
0.5 ml 0.5 M Tris, pH 6.8
20 µl 10 % ammonium persulphate
10 µl TEMED.

Protein samples were prepared by adding an equal volume of prepared lysate and 2X SDS sample buffer which was then vortexed briefly and boiled at 95 °C for 5 minutes before being loaded on the prepared SDS-PAGE gel. Electrophoresis was carried out at a constant voltage of 150 V.

Proteins were then transferred to a PVDF membrane using a transfer buffer comprising of 25 mM Tris, 0.2 M glycine and 20 % methanol. Following the transfer, membranes were blocked with 0.5 % BSA and then incubated overnight with the relevant primary antibodies. After primary antibody incubation, the membranes were washed three times for 5 minutes each with PBS supplemented with 0.1 % Tween-20. Secondary antibody incubation was carried out for an hour and after a further three wash steps the membranes were incubated with SuperSignal® WestPico chemiluminescent substrate solution (Pierce Biotechnology, USA) and visualised using the GelDoc Imager (UVP, LLC, Canada).

2.6 TRANSFECTIONS

2.6.1 THE PRINCIPLE OF LIPID-BASED TRANSFECTION

Specifically designed cationic lipids can be used to transfer DNA and siRNA into cells (Chesnoy and Huang 2000). Cationic lipids contain a positively charged head group, which binds to the negatively-charged DNA forming a liposome/nucleic acid complex, and a hydrocarbon chain which mediates interaction with the lipid bilayer of the cell membrane. The positively charged liposome interacts with the cell membrane and mediates the fusion of the liposome/nucleic acid complex to the negatively charged cell membrane, and afterwards the complex enters the cell through endocytosis. The DNA then escapes the endosomal pathway, diffuses through the cytoplasm and is carried into the nucleus where it is expressed.

2.6.2 METHODS USED IN TRANSFECTION

Transfections were carried out in A549 and HeLa cells using TransIT-LT1 transfection reagent (Mirus, USA). A plasmid containing isoform 1 of RBBP6 cloned into the pCMV-HA mammalian expression vector was kindly provided by coworker Ms Andronica Ramaila. Isoform 3 of RBBP6, cloned into the same vector, was kindly provided by Ms Lauren Jooste.

Cells were plated on sterile coverslips in 6-well plates at an approximate density of 3×10^5 per well in 2 ml complete DMEM 24 hours prior to transfection. The DNA/transfection reagent complex was prepared by adding 3 µg of DNA to 155 µl serum-free DMEM and adding 10 µl of TransIT-LT1. The complex was mixed thoroughly through gentle pipetting and then incubated for 30 minutes at room temperature. 150 µl of the complex was then added to the well containing the cells, and the cells were incubated for 24 hours at 37 °C in a 5 % CO₂ humidified cell culture incubator.

Cells were then subjected to cell stress via heat shock or DNA damage, as previously described, after which coverslips were fixed with methanol and paraformaldehyde. Cells were then stained with Hoechst and mounted in Mowiol and viewed under the Zeiss Axiovert 200M LSM 510 Meta confocal microscope, using Zen 2009 software provided by Zeiss. Images were analysed using ImageJ <http://rsbweb.nih.gov/ij/>

2.7 QUANTITATIVE ANALYSIS OF IMAGES

The ImageJ software package was used for quantitative analysis of the images. The analysis determines the mean intensity values of pixels specified in a particular region of interest (ROI). Signal intensities correspond to a user-defined Region of Interest (ROI) and are defined as the mean intensity across all pixels in the ROI. Intensity values range from from 0 (black) to 225 (white).

The ROIs were defined manually, as shown in Figure 2.1, to record either nuclear (left) or cytoplasmic (right) values. Intensity measurements were made using the “Measure” function found in the ROI Manager of ImageJ.

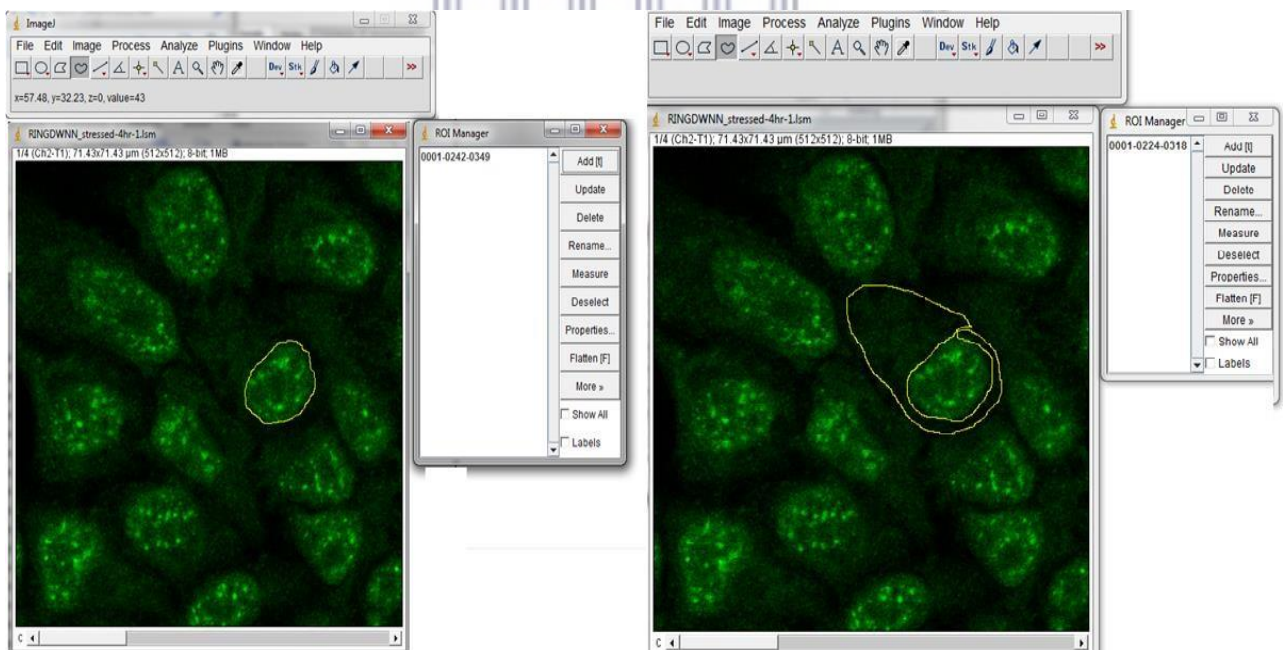


Figure 2.1: Manual definition of a Region of Interest (ROI). The region inside the yellow border was measured and a mean value of the intensity recorded. On the left is the selection of a nuclear ROI, while the cytoplasmic ROI can be seen on the right.

2.8 COLOCALISATION ANALYSIS

Colocalisation images were analysed using the JaCoP plugin in ImageJ. Care needs to be taken when setting up a co-staining immunofluorescence assay that the signal observed in one channel emanates exclusively from one of the two proteins of interest, and the signal in the other channel exclusively from the other protein. For example, when one of the two signals is much more intense than the other it is possible that the stronger signal may “bleed-through” into the other channel, leading to it masquerading as the other protein. In that case the same protein would appear in both channels, which would present as colocalisation. However in reality it would be one protein colocalising with itself.

While bleed-through is an artifact that arises from within the microscope itself, other artifacts may arise from within the sample, through inappropriate binding of the antibodies. Binding of the primary antibody to a molecule other than its expected target is a problem which is investigated in Section 3.2. Binding of the secondary antibody to a molecule other than the appropriate primary antibody commonly leads to background which can be mitigated by setting thresholds high enough, and by using secondaries matched to the primary antibody, so they do not bind to the “other” primary antibody.

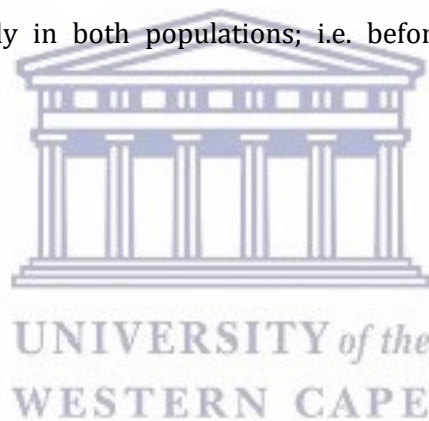
Both bleed-through and the secondary-related problems described above can be controlled by repeating each co-localisation with both secondaries but only one of the two primary antibodies. So, for example, if the primary corresponding to the green-labelled secondary is omitted, no signal should be apparent in the green channel. Any signal that is apparent in the green channel cannot emanate from the protein recognised by that primary antibody and can legitimately be removed by adjusting thresholds using the automated Costes method to remove any user bias. The same procedure is followed for the red channel.

Mander’s coefficient is a measure of the true overlap of two signals. Compared with the widely-used Pearson’s Correlation Coefficient it has the additional benefit of taking the varying intensities of the fluorescent signal into account by providing measures of the fraction of total probe fluorescence that colocalises with the fluorescence of a second probe, making it a more reliable indicator of true colocalisation. The coefficient takes values in the range 0-1, with a coefficient of 0.4, as an example, indicating that 40% of the analysed pixels of one channel colocalise with pixels from the other channel, after thresholds have been taken into account. Different Mander’s coefficients can be calculated to distinguish between the overlap of channel 1 with channel 2 and vice versa.

2.9 STATISTICAL ANALYSIS

Statistical analysis was performed using functions built into Excel. The centre and spread of repeated observations were calculated using the MEAN and STDEV functions respectively. The significance of changes in intensity values before and after stress was assessed using the p -value, which represents the likelihood that the second set of measurements could have been obtained without stress. The smaller the p -value, the more significant the change following stress. A p -value less than 0.05 is generally accepted to represent a significant change.

p -values were calculated using the students t-test, which is implemented in Excel as `TTEST(array1, array2, tails, type)`. *Array1* and *array2* are the sets of data before and after stress respectively. The parameter *tails* was generally set to 1, corresponding to a 1-tailed or 1-sided t-test, because the direction of the change was not at issue; i.e. the intensity was generally found to increase and not decrease. The parameter *type* was set to 3, corresponding to an unpaired t-test. This is appropriate because the cells used to measure intensity values before and after stress were selected randomly in both populations; i.e. before and after values were not measured on the same cells.



CHAPTER 3 ISOFORM 3 OF RBBP6 TRANSLOCATES TO NUCLEAR SPECKLES FOLLOWING CELL STRESS

3.1 INTRODUCTION

RBBP6 is implicated in a number of different cellular functions, which take place in a number of different cellular locations. It has also been reported to interact with a number of different proteins, including YB-1, p53, MDM2, zBTB38 and Sm splicing proteins (Chibi *et al.* 2008, Li *et al.* 2017, Miotto *et al.* 2014), which are known to localise variously in the cytoplasm and the nucleus. For example, Scott and co-workers reported that RBBP6 localises to the periphery of chromosomes in mitotic cells (Gao *et al.* 2002). Simons and co-workers showed that RBBP6 can be identified within punctate structures in the nucleus which they identified as nuclear speckles (Simons *et al.* 1997). Manley and co-workers showed using mass spectrometry that RBBP6 forms part of the 3'-end processing complex, which is located in the nucleus (Shi *et al.* 2009).

Since the first report of RBBP6 localising in nuclear speckles, no further investigation has been carried out to confirm that the bodies to which it localises are indeed nuclear speckles, rather than one of the many other types of punctate nuclear bodies. Nuclear speckles, also known as splicing speckles or SC35 domains, are bodies within the nucleus primarily associated with transcription and splicing (Mintz and Spector 2000; reviewed in Spector and Lamond 2011) and as centres of localisation of a number of splicing factors, including SC35.

Recently Manley and co-workers have shown that isoforms 1 and 3 both interact directly with the polyadenylation-associated protein CstF-64, and proposed a model in which isoform 3 suppresses the activity of RBBP6 by binding competitively to CstF-64 (Di Giammartino *et al.* 2014). If this model is true, then the overall effect of this competition will be determined by the localisation of both isoforms relative to CstF-64. Hence the localisations of isoforms 1 and 3, whether in nuclear speckles or not, becomes of even greater interest. We therefore decided to use immunofluorescence microscopy to investigate the intra-cellular localisation of different isoforms of RBBP6 in greater detail. And due to the reported association of RBBP6 with stress response proteins (Simons *et al.* 1997, Kappo *et al.* 2012) we decided furthermore to investigate whether stress played any role in the localisation of RBBP6 by subjecting cells to a variety of different cytotoxic stresses.

Immunofluorescence studies were carried out using antibodies targeting various regions of endogenous RBBP6. To provide supporting evidence that the proteins detected were indeed RBBP6, HA-tagged isoforms of RBBP6 were exogenously introduced into cells and detected using highly-specific antibodies targeting the HA immunotag. Once the localisation of RBBP6 had been determined, we used colocalisation analysis to identify the exact bodies to which RBBP6 localises.

Since nuclear localisation of isoform 3 follows DNA damage, it is possible that isoform 3 localises directly to sites of DNA damage. Chromatin structure is modulated in response to certain forms to DNA damage, such as the phosphorylation of histone variant H2AX to γ H2AX which flanks the sites of double-stranded DNA breaks as part of the DNA damage signalling pathway (Matsuoka *et al.* 2007). It should be noted that while cisplatin does not directly induce double-stranded DNA breaks, these breaks occur during the NER and JER repair processes, and as such γ H2AX can be viewed as an indicator to the extent of the repair process (X. Huang *et al.* 2004). Immunofluorescence microscopy using antibodies specifically targeting γ H2AX provides a reliable method of visualising sites of DNA damage and repair, and as such is an excellent colocalisation target for isoform 3 in order to determine whether isoform 3 localises directly to site of double-stranded DNA breaks or sites of DNA repair in the case of cisplatin.

3.2 SPECIFICITY OF THE ANTIBODIES GENERATED AGAINST THE DWNN DOMAIN OF RBBP6

The DWNN domain of human RBBP6 (residues 1-81) was produced recombinantly in *E. coli* and used to produce two antibodies targeting the DWNN domain. A monoclonal antibody was raised at the Monoclonal Antibody Core Facility, Monterotondo-Scalo, Italy. A polyclonal antibody was raised in rabbits in the laboratory of Prof Dirk Bellstedt, University of Stellenbosch, South Africa, using the naked bacteria method described in Section 2.4.1. Before using either of these antibodies in immunofluorescence microscopy we needed to confirm that they recognised only proteins containing the DWNN domain. All four known isoforms of RBBP6 – isoform 1 (200 kDa), isoform 2 (197 kDa), isoform 3 (13 kDa) and isoform 4 (106 kDa) – contain the DWNN domain and therefore may be expected to be detected by the antibodies.

A lysate was prepared from HeLa cells and probed with both antibodies, as shown in Figures 3.1 and 3.2. Using the monoclonal antibody a single band was observed with a molecular weight of less than 20 kDa (Figure 3.1, lane 2), which is consistent with the expected size of isoform 3.

Bands corresponding to the other isoforms were not visible; this may be due to the other isoforms being expressed at low levels in HeLa cells. Alternatively it may be due to the highly basic nature of the C-terminus of RBBP6, which is present in all isoforms except isoform 3, and may prevent the protein from entering the SDS-PAGE gel, as suggested by Simons and co-workers (Simons *et al.* 1997). More importantly, no other proteins in the cell lysate reacted with the antibody.

In order to confirm that the low molecular weight band is caused by antibodies reactive with the DWNN domain, and not with some other protein, the antibody was incubated with recombinant DWNN domain for an hour prior to using it in the western blot. The low molecular weight band was not observed in lane 4, from which we conclude that the recombinant DWNN out-competed the epitope giving rise to the low MW band on the western blot. This makes it highly likely that the band corresponds to the 13 kDa isoform 3.

The same result was obtained when the rabbit polyclonal antibody was used, as shown in Figure 3.2. A band consistent with isoform 3 was observed (lane 2) which disappeared when the antibody was pre-incubated with recombinant DWNN domain (lane 4). As before, none of the higher molecular weight isoforms of RBBP6 were observed and no other proteins in the cell lysate reacted with the antibody.

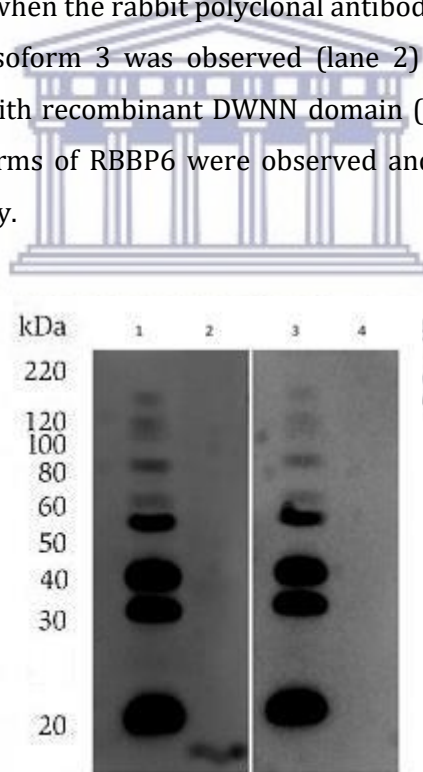


Figure 3.1: Western blot analysis of the specificity of the mouse monoclonal anti-DWNN antibody. Lanes 1 and 3 contain a molecular weight marker. Lane 2 represents cell lysate probed with the monoclonal anti-DWNN antibody. Lane 4 represents the probing with the same antibody that has been pre-treated with a DWNN peptide before blocking. A band of low molecular weight can be seen in lane 2, but no bands are visible in lane 4, indicating that the mouse monoclonal anti-DWNN antibody is specific for the DWNN peptide.

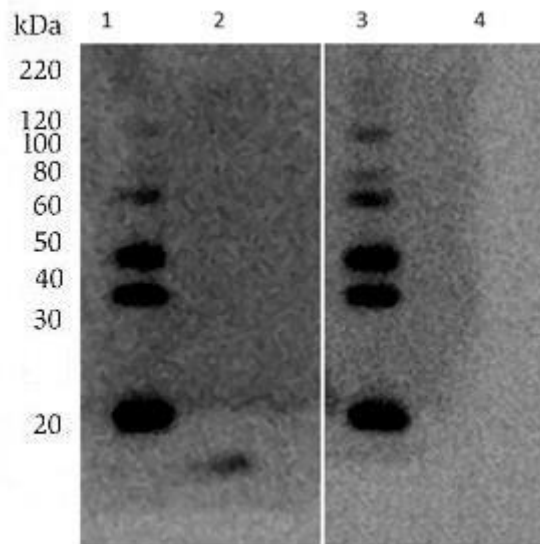


Figure 3.2: Western blot analysis of the specificity of the rabbit polyclonal anti-DWNN antibody. Lanes 1 and 3 are a marker indicating the size of the bands. Lane 2 represents cell lysate probed with the rabbit polyclonal anti-DWNN antibody. Lane 4 represents the probing with the same antibody that has been pre-treated with a DWNN peptide before blocking. A band of low molecular weight can be seen in lane 2, but no similar band is visible in lane 4, indicating that the antibody is specific for the DWNN peptide.

The successful peptide blocking of these two antibodies confirms that they are specific for the DWNN domain, and that immunofluorescent signal generated using these two antibodies is likely to result only from isoforms of endogenous RBBP6.

3.3 LOCALISATION OF RBBP6 AND ITS ISOFORMS IN UNSTRESSED CELLS

Three antibodies were used to examine the localisation of RBBP6 in the cell: mouse monoclonal anti-DWNN, rabbit polyclonal anti-DWNN and a commercial antibody targeting residues 1582 – 1692 of RBBP6 purchased from LifeSpan Biotechnologies. Since the DWNN domain is found in all four isoforms of RBBP6, the antibodies raised against the DWNN domain were not able to distinguish between them in the context of immunofluorescence microscopy, where the sizes of detected proteins are not apparent. The antibody purchased from LifeSpan (referred to in this thesis as “C133084”) targeted a region of the protein found in isoforms 1, 2 and 4, but not in 3, thus allowing us to distinguish the localisation of isoform 3 from those of the other three isoforms.

Immunofluorescence microscopy was first used to investigate the localisation of RBBP6 and its isoforms in unstressed cells. HeLa cells were grown on coverslips for 24-48 hours at 37 °C with 5 % CO₂. The coverslips were then fixed, blocked and treated with one of three antibodies: a

1:10 dilution of mouse monoclonal anti-DWNN, a 1:500 dilution of rabbit polyclonal anti-DWNN or a 1:1000 dilution of the C133084 antibody. After overnight incubation, the coverslips were washed and stained with the appropriate secondary antibody and then mounted on slides. Images were viewed on a Zeiss Axiovert 200M LSM 510 Meta confocal microscope using Carl Zeiss Zen 2009 software and were acquired at 40x magnification at a resolution of 512x512 pixels per image. The results are shown in Figures 3.3, 3.4 and 3.5 below.

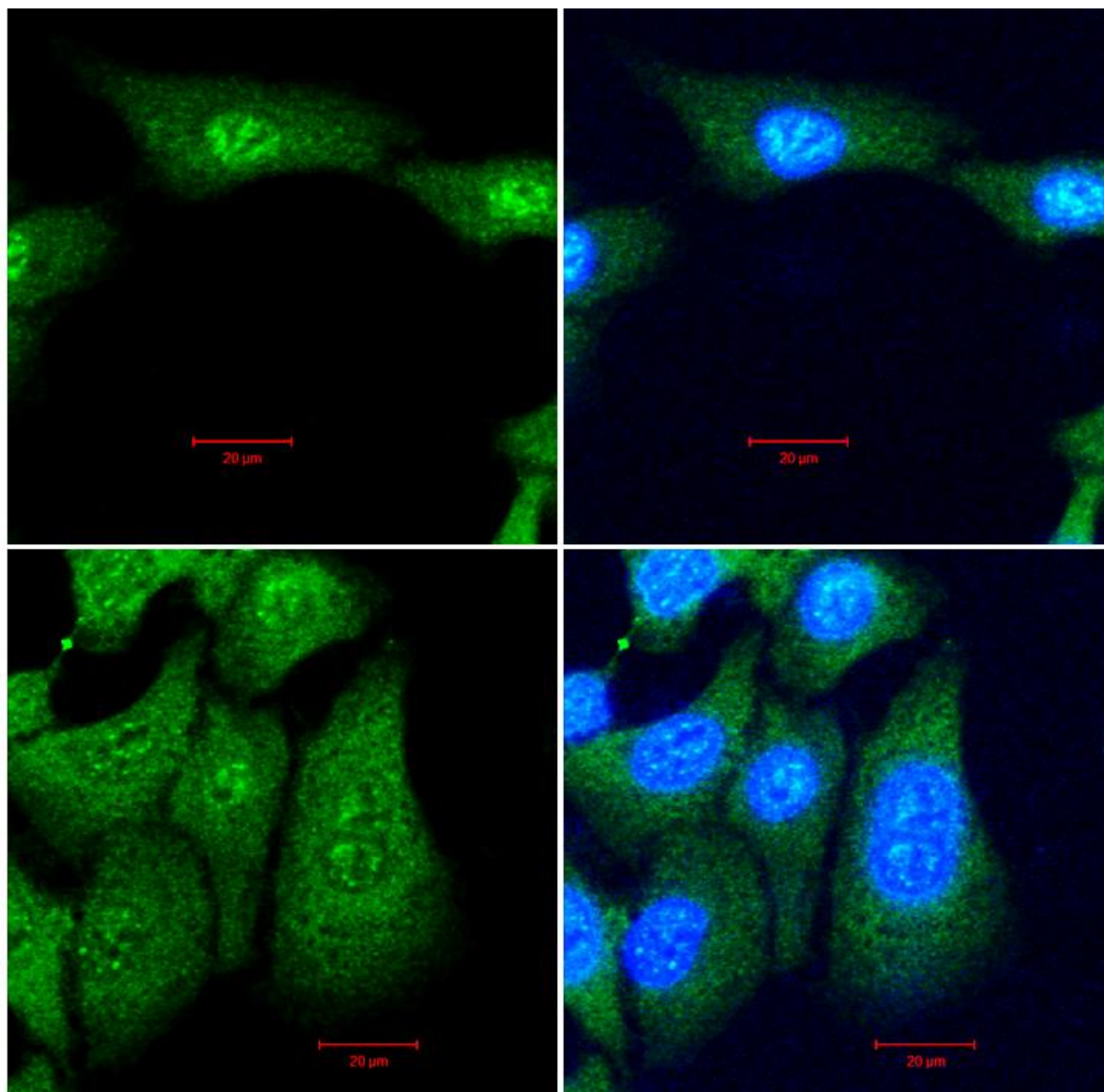


Figure 3.3 HeLa cells stained with mouse monoclonal anti-DWNN. Green indicates staining with mouse monoclonal anti-DWNN while the blue indicates the DNA dye Hoechst staining the nucleus. There is clear signal in both the cytoplasm and the nucleus, with punctate structures clearly visible in the nucleus.

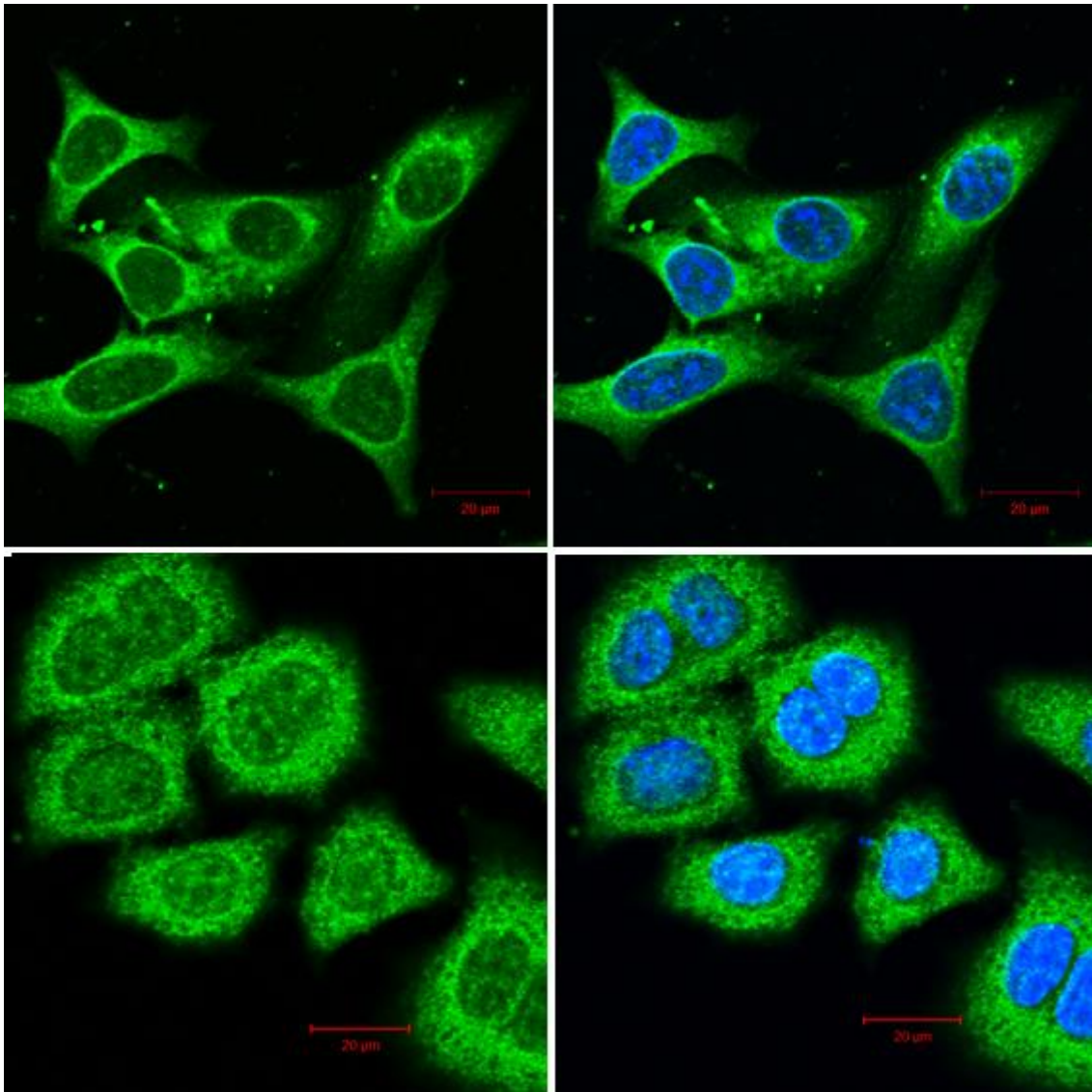


Figure 3.4: HeLa cells stained with rabbit polyclonal anti-DWNN. Green indicates staining with rabbit polyclonal anti-DWNN while the blue indicates the DNA dye Hoechst staining the nucleus. There is clear signal in both the cytoplasm and the nucleus, and punctate structures within the nucleus are clearly visible.

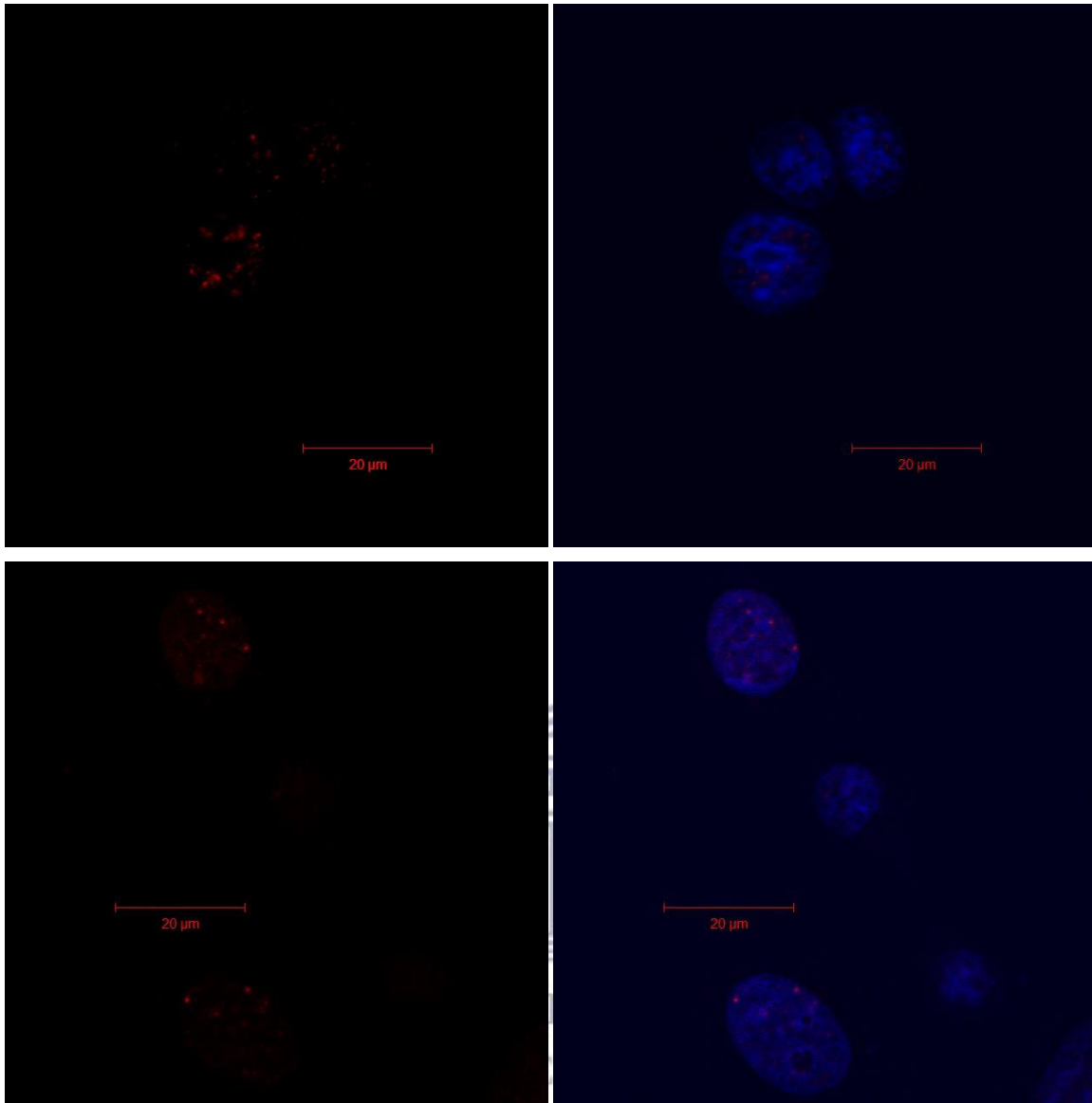


Figure 3.5 HeLa cells stained with C133084. Red indicates staining with the C133084 antibody while the blue indicates the DNA dye Hoechst staining the nucleus. There is no detectable signal in the cytoplasm, but both diffuse and punctate signal is visible in the nucleus.

Staining with the mouse monoclonal anti-DWNN (Figure 3.3) and rabbit polyclonal anti-DWNN antibodies (Figure 3.4) shows significant cytoplasmic staining, in addition to weaker nuclear staining with clear evidence of speckle-like bodies. Since evidence has been presented above showing that both of these antibodies are specific for the DWNN domain, this cytoplasmic staining is likely to correspond to one of the isoforms of RBBP6. Furthermore, since isoforms 1, 2 and 4 show no evidence of cytoplasmic staining, we conclude that isoform 3 is at least partly localised in the cytoplasm. On the strength of this evidence we cannot decide whether isoform 3 is also found in the nucleus or in speckle-like bodies or whether isoforms 1, 2 and 4 are exclusively responsible for the nuclear signal.

Since C133084 recognises an epitope found in all isoforms except 3, we conclude from Fig 3.5 that isoforms 1, 2 and 4 are found exclusively in the nucleus, in particular in speckle-like bodies.

3.4 ISOFORMS OF RBBP6 FORM SPECKLES IN THE NUCLEUS THAT BECOME MORE PRONOUNCED AFTER CELL STRESS

3.4.1 Visualisation of RBBP6 isoforms after cell stress

Three main sources of cell stress were examined: (i) heat shock, (ii) DNA damage induced via UV and (iii) DNA damage induced by cisplatin. UV damages DNA through the formation of pyrimidine dimers which distort the structure of DNA by introducing kinks and bends, interfering with DNA replication and transcription. Attempts by the cell to repair these dimers can lead to double- and single-strand breaks within the DNA molecule as a consequence of excision repair breaks on opposite sides of the DNA strand (Greinert *et al.* 2012). Cisplatin interacts directly with DNA forming cisplatin-DNA adducts which interfere with DNA replication and translation. (Basu and Krishnamurthy 2010).

Heat shock was elicited by growing HeLa cells on coverslips for 24-48 hours at 37 °C with 5 % CO₂ and then placing them in a 42 °C incubator for 5 minutes. DNA damage was produced either by subjecting the cells to 40 J/m² UV using a Stratalinker 1800 or else with 0.6 µg/ml of cisplatin. Previous experiments with YB-1 showed that these two DNA damage inducers elicit the same effect and utilise the same DNA repair pathways (Ohga *et al.* 1998). Our time of 5 minutes was significantly shorter than the several hours used by Ohga and co-workers.

Following stress, cells were fixed and blocked and then stained overnight with a 1:10 dilution of anti-DWNN monoclonal mouse primary antibody followed by a 1:1000 dilution of either Alexa488-conjugated anti-mouse or Cy3-conjugated anti-mouse secondary antibody. Images were viewed on a Zeiss Axiovert 200M LSM 510 Meta confocal microscope using Carl Zeiss Zen 2009 software (http://microscopy.zeiss.com/microscopy/en_de/products/microscope-software/zen-2012.html). Images were acquired at 40x magnification at a resolution of 512x512 pixels per image.

As above, the DWNN domain was found to be uniformly distributed across both the cytoplasm and the nucleus in resting cells, but with additional localisation in punctate structures within the nucleus (Figure 3.6, left panel). The intensity of this punctate signal increased markedly following heat shock (right panel). The same effect was observed following UV stress (Figure 3.7, right panel) and following treatment of the cells with cisplatin (Figure 3.8)

Since both stressed and unstressed cells were grown under identical conditions, and identical microscope settings were used in both cases, the increase in nuclear intensity is concluded to be due to the stressing of the cells.

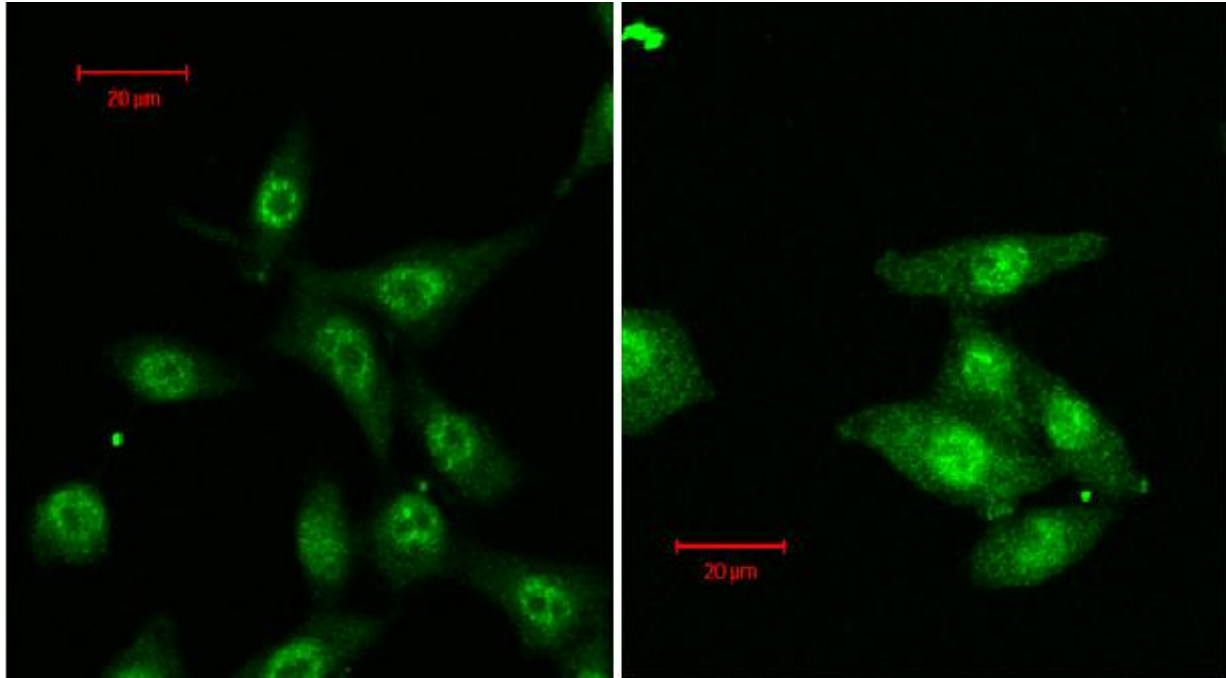


Figure 3.6: Localisation of the DWNN domain following heat shock. HeLa cells stained with mouse monoclonal anti-DWNN antibody before (left) and after (right) heat shock treatment. Clear evidence of punctate structures can be seen in the nucleus, whose intensity increases sharply following heat shock.

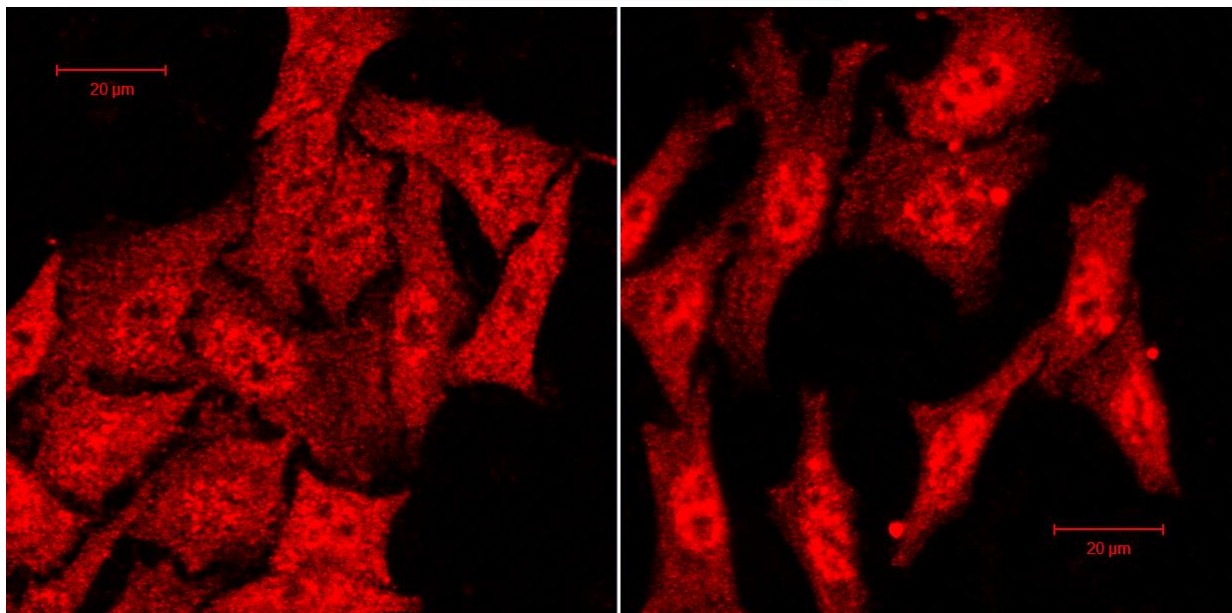


Figure 3.7: Localisation of the DWNN domain following UV shock. HeLa cells stained with mouse monoclonal anti-DWNN antibody before (left) and after (right) UV treatment. Speckling can be clearly seen in the nucleus, and this increases in intensity after UV treatment, whereas the cytoplasmic signal appears to be unchanged or possibly reduced.

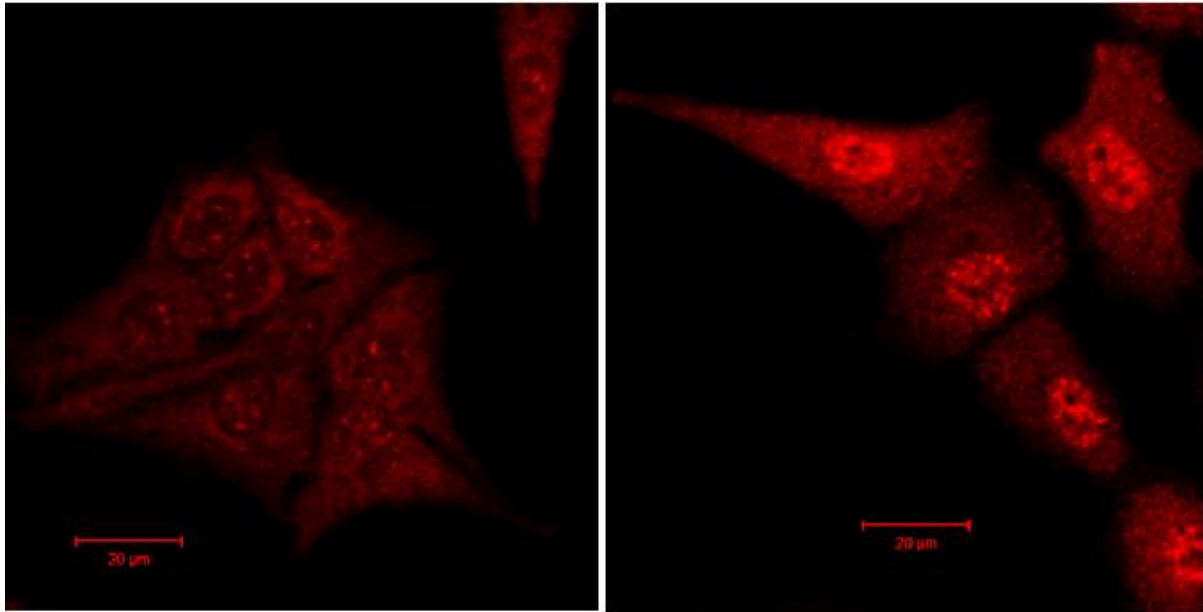


Figure 3.8 Localisation of the DWNN domain following exposure to cisplatin. HeLa cells stained with mouse monoclonal anti-DWNN antibody before (left) and after (right) cisplatin treatment. Speckling can be clearly seen in the nucleus, and this increases in intensity after cisplatin treatment, whereas the cytoplasmic signal appears to be unchanged or possibly reduced.

3.4.2 Quantitative analysis of nuclear and cytoplasmic intensity values after heat shock and DNA damage

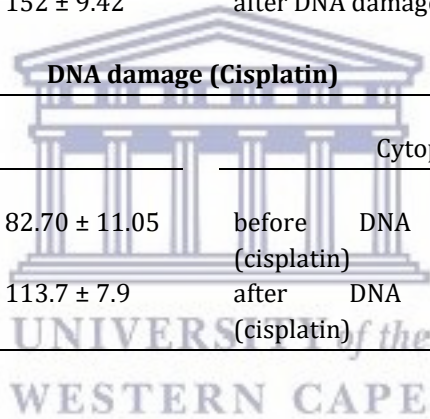
The intensities of the DWNN signal in heat shocked and UV-treated cells were quantified using the ImageJ software package (<http://rsbweb.nih.gov/ij/index.html>). Two slides were used per experimental condition and a total of ten cells were selected from these two slides. Intensity values ranged from 0 (black) to 225 (white). The procedure was repeated for three independent experiments performed on different days, resulting in a pool of 30 nuclear intensity measurements and 30 cytoplasmic intensity measurements ($n = 30$). The values can be found in Appendix A.

Secondary antibodies can generate non-specific signal that can be mistaken for the protein of interest. In addition some cells, including HeLa cells, generate strong auto-fluorescent signal which may also be mistaken for the true signal generated by the proteins under examination. To ensure that all signals reflect recognition of the DWNN domain by the primary antibody, slides incubated only with Alexa488- or Cy3-conjugated secondary antibodies were used as negative controls. Exposure times and digital gain were set to ensure that no signal was detected from the secondary antibodies or from the cell, and thereafter were kept constant throughout the course of the experiment.

Mean cytoplasmic and nuclear intensities recorded before and after stress are presented in Table 3.1 and Figure 3.9.

Table 3:1: The effect of heat shock and DNA damage (UV and cisplatin) on nuclear and cytoplasmic signal from stressed and unstressed cells. 30 different cells were used for each measurement (n = 30).

Heat shock			
Nuclear intensity		Cytoplasmic intensity	
before heat shock	34.37 ± 6.8	before heat shock	14.9 ± 2.6
after heat shock	53.6 ± 2.5	after heat shock	17.03 ± 2.2
DNA damage (UV)			
Nuclear intensity		Cytoplasmic intensity	
before DNA damage (UV)	114.2 ± 6.48	before DNA damage (UV)	84.96 ± 9.4
after DNA damage (UV)	152 ± 9.42	after DNA damage (UV)	66.69 ± 6.51
DNA damage (Cisplatin)			
Nuclear intensity		Cytoplasmic intensity	
before DNA damage (cisplatin)	82.70 ± 11.05	before DNA damage (cisplatin)	72.9 ± 6.66
after DNA damage (cisplatin)	113.7 ± 7.9	after DNA damage (cisplatin)	83.86 ± 8.88



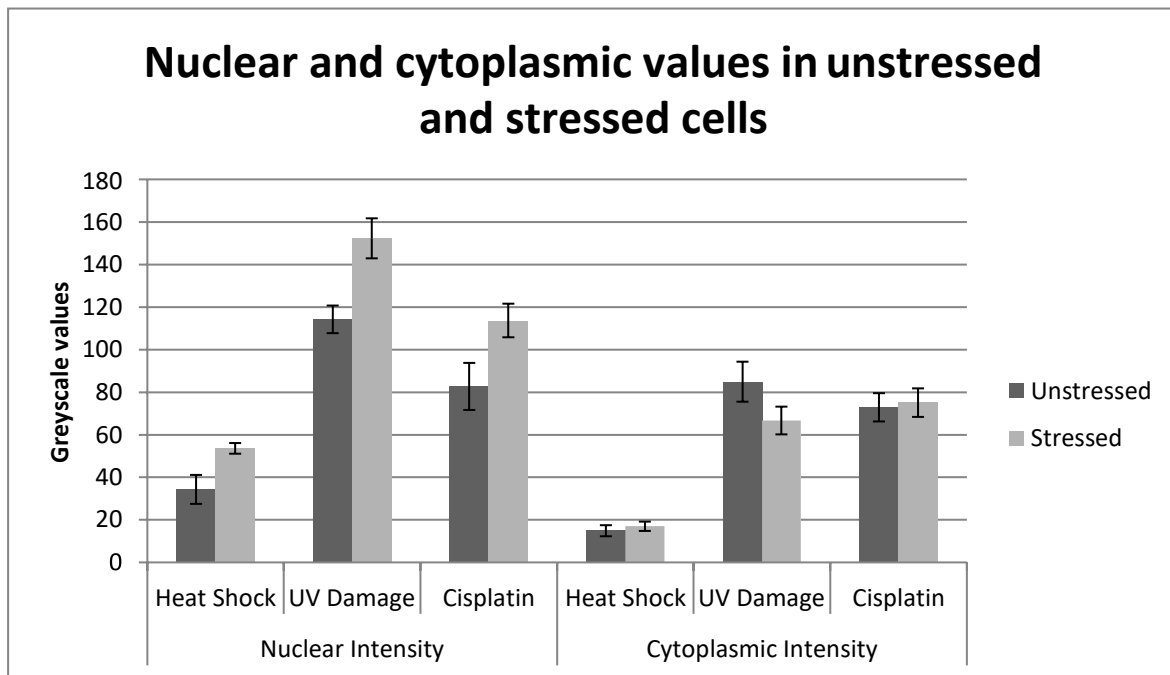


Figure 3.9: Nuclear and cytoplasmic intensity values of cells stressed by three different stressors, namely heat shock, DNA damage via UV and DNA damage via cisplatin. In all cases it is clear that there is an increase in nuclear intensity following cell stress, while cytoplasmic intensity increases slightly in the case of heat shock, decreases slightly in the case of UV damage and remains unchanged following cisplatin treatment. The increase in intensity in the nucleus due to heat shock was statistically significant ($p = 2.03E-08$) whereas the cytoplasmic intensity did not change significantly ($p = 0.07$). As a result of UV treatment the increase in intensity in the nucleus was significant ($p = 2.99E-07$), whereas a significant decrease in cytoplasmic intensity was observed ($p = 4.43E-08$). Cisplatin treatment gave a significant increase in nuclear intensity ($p = 6.6E-15$) and a non-significant increase in cytoplasmic intensity ($p = 0.1$).

The increase in intensity in the nucleus due to heat shock was statistically significant ($p = 2.03E-08$) whereas the cytoplasmic intensity did not change significantly ($p = 0.07$). As a result of UV treatment the increase in intensity in the nucleus was significant ($p = 2.99E-07$), whereas a significant decrease in cytoplasmic intensity was observed ($p = 4.43E-08$). Cisplatin treatment gave a significant increase in nuclear intensity ($p = 6.6E-15$) and a non-significant increase in cytoplasmic intensity ($p = 0.1$). This is consistent with a model in which the DWNN domain has translocated from the cytoplasm to the nucleus.

In order to further confirm that only the nuclear intensity was increasing, relative to the cytoplasmic intensity, we calculated the ratio of nuclear intensity versus cytoplasmic. The values confirm our findings that nuclear intensity increases (Table 3.2 and Figure 3.10). The ratio increased from 2.11 to 3.67 in the case of heat shock, 1.42 to 2.32 in the case of UV exposure and from 1.13 to 1.52 in the case of cisplatin exposure. All these findings were statistically significant, with $p < 0.0001$ in all cases.

Table 3:2 Quantitative analysis of nuclear/cytoplasmic intensity ratios of cells after being subjected to various forms of cell stress

Heat shock			
before heat shock	2.11 ± 0.25	after heat shock	3.67 ± 1.82
DNA damage (UV)			
before DNA damage (UV)	1.42 ± 0.32	after DNA damage (UV)	2.23 ± 0.32
DNA damage (Cisplatin)			
before DNA damage (cisplatin)	1.13 ± 0.13	after DNA damage (cisplatin)	1.52 ± 0.19

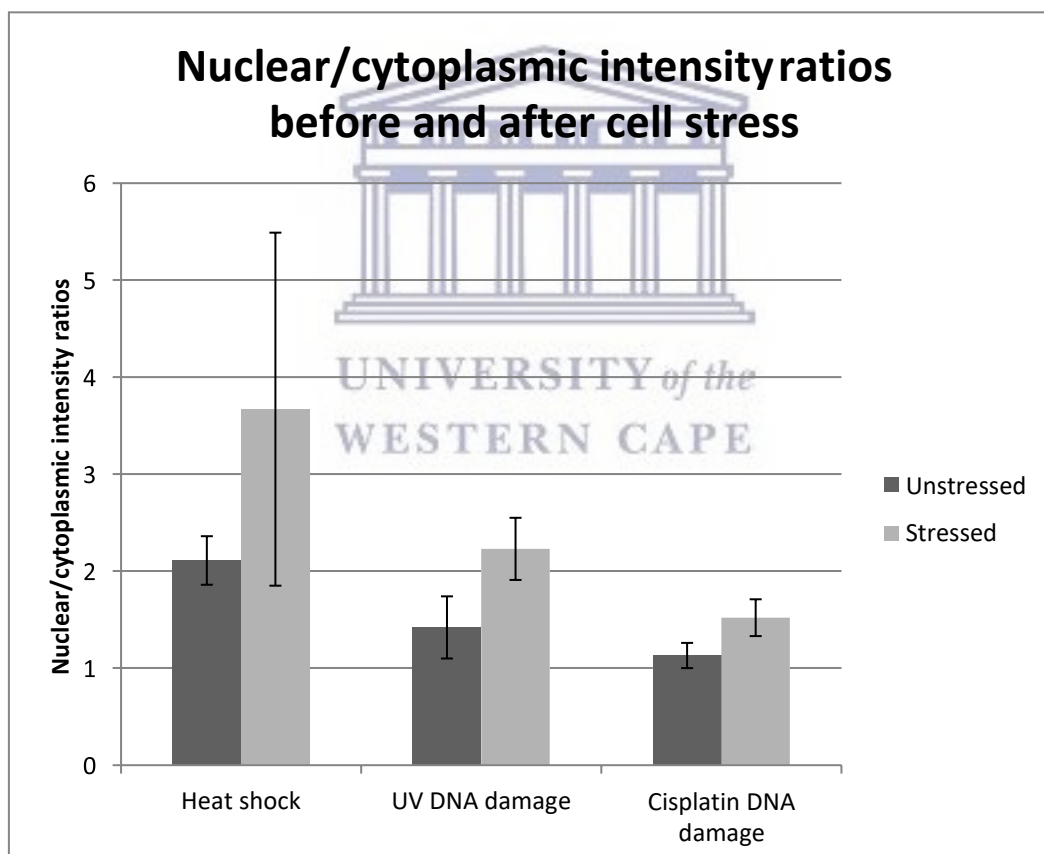


Figure 3.10 Nuclear/cytoplasmic ratios in cells subjected to various forms of cell stress. In all cases, the ratio increased after cell stress, indicating an increase of nuclear signal relative to cytoplasmic signal.

3.4.3 Analysis of nuclear signal intensity over time

In order to assess the speed of accumulation of the signal in the nucleus, a time course was performed. HeLa cells were grown on coverslips and stressed using heat shock or UV as

described previously. Coverslips were collected immediately after stress and thereafter in one-hour intervals up to 8 hours. Nuclear and cytoplasmic intensities recorded as described in 3.2.1.2. The experiment was repeated in triplicate and five cells were sampled from each replicate slide, giving a total of 15 measurements for each time point, which can be found in Appendix A. The average values are shown in Figures 3.11 and 3.12.

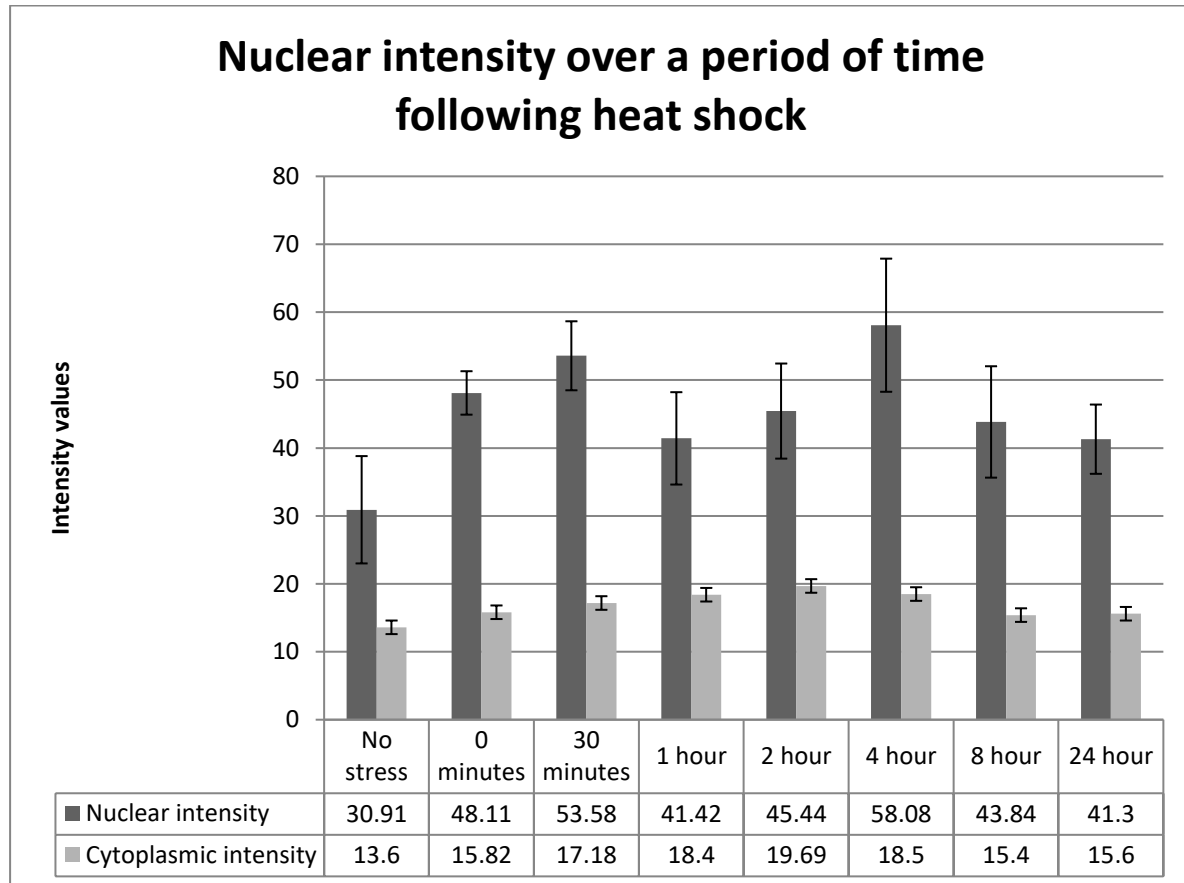


Figure 3.11: Nuclear and cytoplasmic intensity values following heat shock. Nuclear intensity increases dramatically after cell stress and reaches peak intensity at 4 hours, after which it decreases to almost baseline levels.

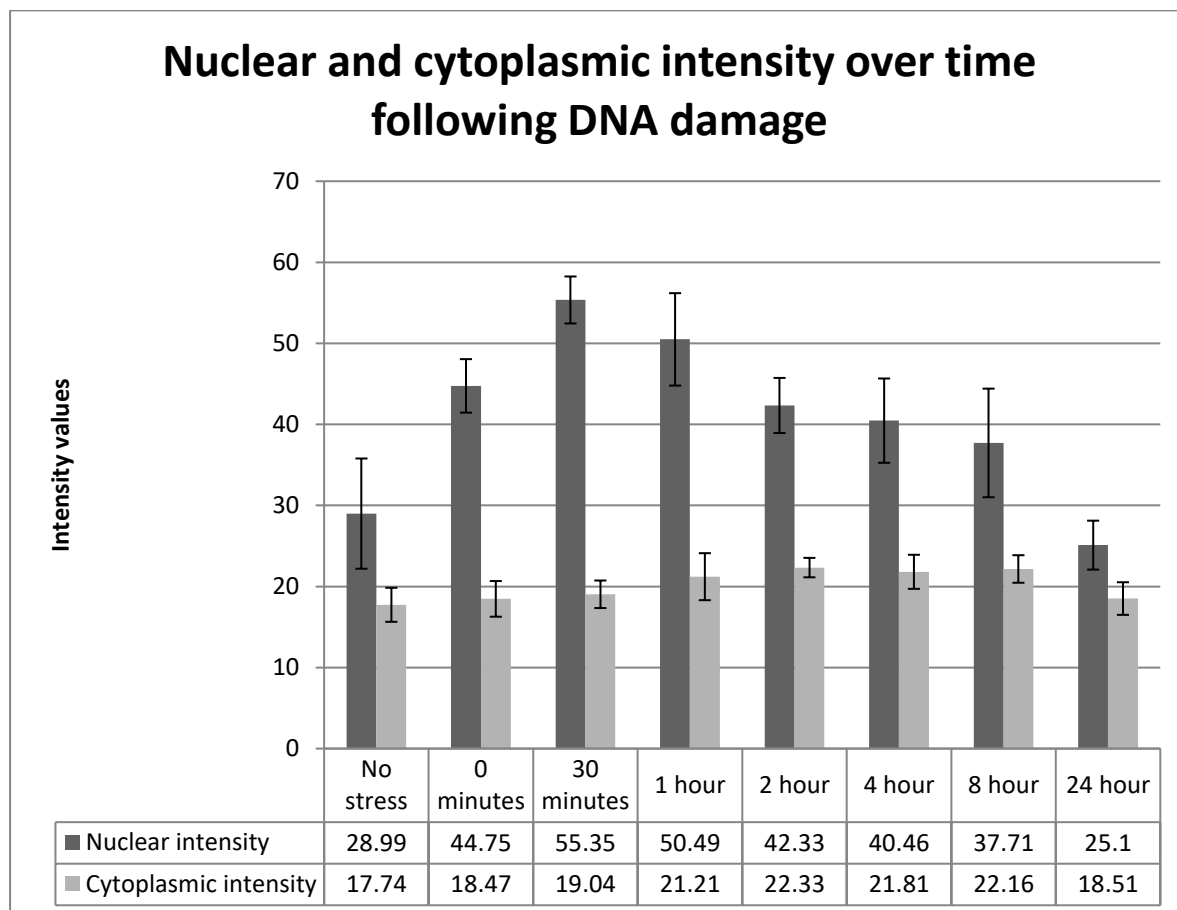


Figure 3.12: Nuclear and cytoplasmic intensity values following DNA damage induced by UV. Nuclear intensity increases after DNA damage and then slowly comes back to baseline levels within 24 hours of the UV exposure.



The 0-minute time point represents a period of time between the cessation of cell stress (removal from the incubator, cessation of UV irradiation, washing off of cisplatin-containing media) and fixing of the cells. It includes travel time between equipment and the bench and can represent anything from 30 seconds to 2 minutes of time in which signal can accumulate. As it is also likely that some signal accumulation happens during the time of cell stress exposure, the 0 minute point can represent dead time ranging from 1 to 5 minutes from the start of cell stress, or even longer in the case of cisplatin exposure.

Nuclear intensity increased rapidly following heat shock and then stayed elevated for up to 24 hours, with a downward trend after approximately 4 hours (Figure 3.11). Cytoplasmic intensity also shows a slight increase in intensity, but not to the same magnitude as for the nucleus. This also showed a downward trend after 4 hours. A similar effect was observed following DNA damage inflicted by UV. Nuclear intensity increased rapidly after exposure to DNA damage and remained elevated for up to eight hours after stress. After twenty four hours, the levels had

returned to normal. Cytoplasmic intensity also increased slightly and remained elevated for up to twenty four hours after the experiment (Figure 3.12), although the increase is not significant.

In addition to shedding light on the time-scale of the effect, the above results increase the significance of the effect by providing a number of independent measurements which are consistent with one another. The smooth variation of the signal with time shows that the effect is robust and does not depend very strongly on the precise time at which the measurement is made. The smooth variation of the signal with the amount of stress shows that the effect is robust and does not depend very strongly on the amount of stress applied.

3.4.4 Analysis of the length of heat shock exposure time on the increase in nuclear intensity

Studies that examine the effect of heat shock on the cell use a wide variety of exposure times to elevated temperatures. For example Royer and co-workers, investigating the effect of heat shock on the nuclear localisation of YB-1, used 40 °C and 43 °C for 15, 30, 60 and 120 minutes, respectively (Stein *et al.* 2001). As the conditions used above were relatively mild, a range of exposure times from 30 seconds to 30 minutes was examined to ensure that the stress was sufficient to elicit a robust heat shock response. Cells were grown on coverslips, subjected to 42 °C for a range from 30 seconds to 30 minutes, and immediately fixed and stained using the mouse monoclonal anti-DWNN antibody as described previously. Each condition was replicated in duplicate and ten cells were sampled from each replicate slide, giving a total of 20 signal intensity readings per exposure time.

Figure 3.13 shows a dose-dependent increase in the amount of nuclear signal, up to 5 minutes, with no further increase thereafter even up to 30 minutes. The results are consistent with previous results obtained following heat shock (Figures 3.7 and 3.10), and have a significance value of 2.68×10^{-16} .

As above, the results increase the significance of the overall effect by providing a number of independent measurements which are consistent with one another. The smooth variation of the signal with the amount of stress shows that the effect is robust and does not depend very strongly on the amount of stress applied. Since no further increase in the response was found after 5 minutes, we decided to adopt 5 mins at 42 °C as our heat shock conditions in all subsequent experiments, even though they are significantly milder than those commonly used in experiments of this type. It should be noted that, whereas the increase in the nuclear signal could be due to the increase in the length of time for which the heat shock was applied, it could

also reflect the time required for the DWNN-containing proteins to translocate to the nucleus, or a combination of the two. On the basis of the current results it is not possible to distinguish between these two causes.

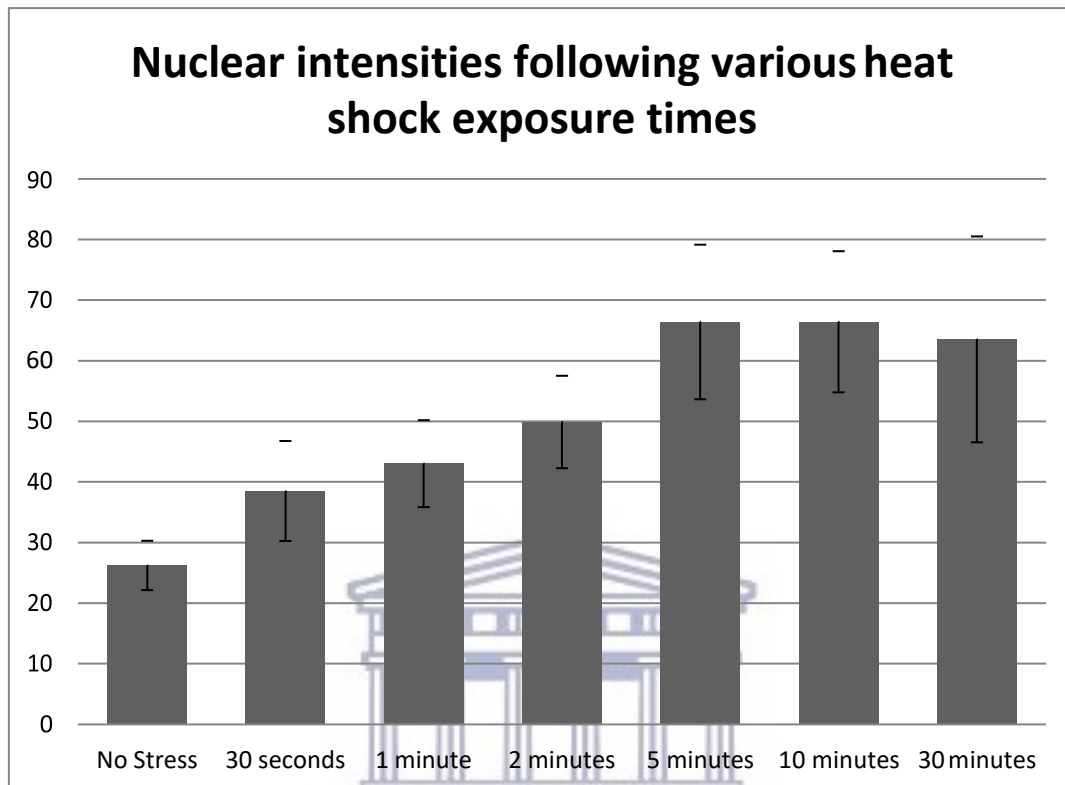


Figure 3.13: Measured nuclear intensity as a function of heat shock exposure time, which is a measure of the amount of shock applied. Nuclear intensity increases the longer cells are exposed to heat shock, until 5 minutes, at which point it levels off.

3.5 INCREASE IN NUCLEAR INTENSITY IS CAUSED BY ISOFORM 3 ALONE

Since the above results were obtained using an antibody raised against the DWNN domain (residues 1-81), which is present in all four isoforms of RBBP6, it is not possible to distinguish which of the isoforms are responsible for the increase in nuclear signal following stress. In order to distinguish between the isoforms a commercial antibody raised against residues 1582 – 1692 of human RBBP6, was procured from LifeSpan Biosciences (C133084). As this was a commercial antibody and stocks were low, we did not verify the antibody, instead relying on the verification performed by the manufacturer. Since then, the antibody has been discontinued and replaced with B12177. From Figure 1.2 and Table 2.3 it is clear that this antibody should detect isoforms 1, 2 and 4, but not isoform 3.

Figure 3.14 shows HeLa cells stained with C133084 before and after heat shock. The signal is entirely nuclear and concentrated in punctate bodies, consistent with previous reports that it localises to nuclear speckles. This is different from what is observed using the antibody targeting the DWNN domain, which is more evenly distributed in the cytoplasm in addition to punctate nuclear signal. Importantly, there is no clear evidence of an increase in the intensity of the signal following cell stress. Numerical validation can be found in Table 3.2. Figure 3.14 shows the results of heat shock stress and Figure 3.15 shows similar results using DNA damage applied using UV.

A number of conclusions can be drawn from Figures 3.14 and 3.15. Firstly, since C133084 is expected to recognise only isoforms 1, 2 and 4, whichever of those is expressed in HeLa cells is entirely nuclear and primarily localised in speckle-like bodies. This is in agreement with previous reports (Li *et al.* 2007). Secondly, if isoform 1, 2 and 4 are not affected by stress, then by a process of elimination our previous results obtained with anti-DWNN antibody suggest that the increase in nuclear intensity following stress is due to isoform 3 alone. Thirdly, since isoforms 1, 2, and 4 are entirely nuclear, the cytoplasmic signal seen above using the anti-DWNN antibodies can only originate from isoform 3. Taken together, we conclude that isoform 3 is located in both the cytoplasm and the nucleus, but that the nuclear speckle-like signal increases rapidly following cell stress. Whether isoform 3 is found in speckle-like bodies in the absence of stress cannot be decided on the basis of the evidence presented so far.

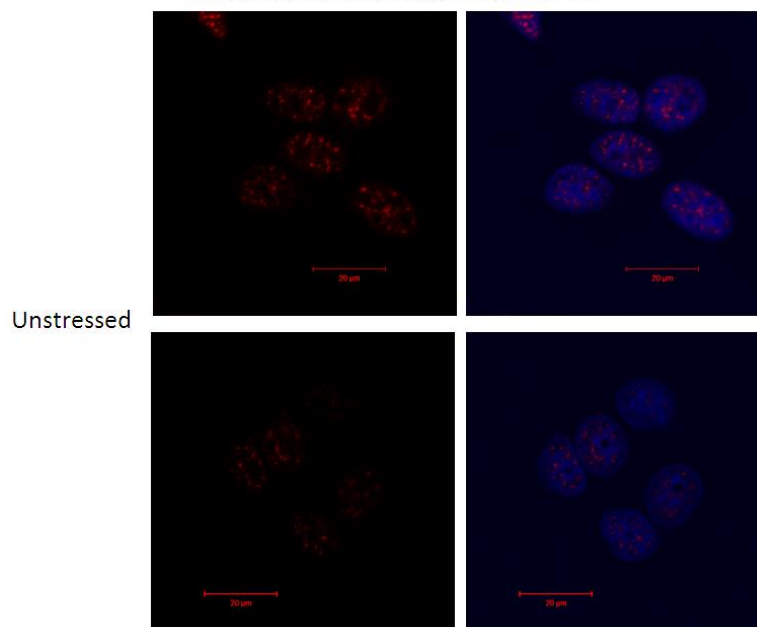


Figure 3.14 Antibody C133084, which is expected to target isoforms 1, 2 and 4 but not 3, is found exclusively in the nucleus in speckle-like bodies in the absence of stress. Unstressed HeLa cells stained with C133084 antibody in red (left) and merged with DNA stain Hoechst in blue (right).

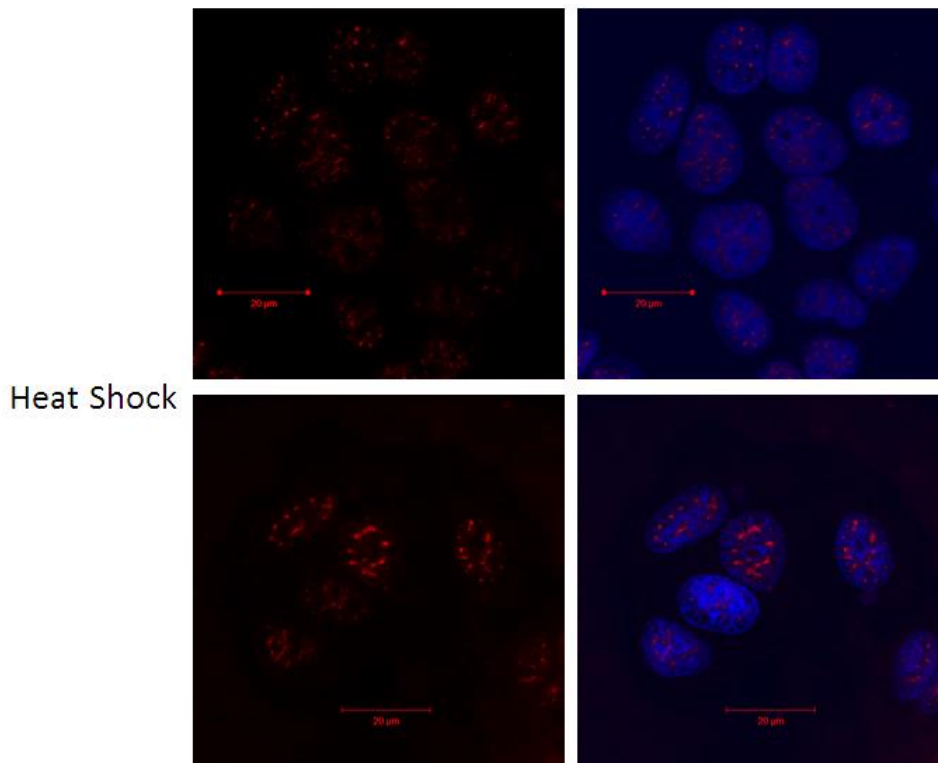


Figure 3.15 Antibody C133084, which is expected to target isoforms 1, 2 and 4 but not 3, is found exclusively in the nucleus in speckle-like bodies following heat shock. Heat shocked HeLa cells stained with C133084 antibody in red (left) and merged with DNA stain Hoechst in blue (right). There is no clear evidence of increased nuclear speckling following exposure to increased temperatures.

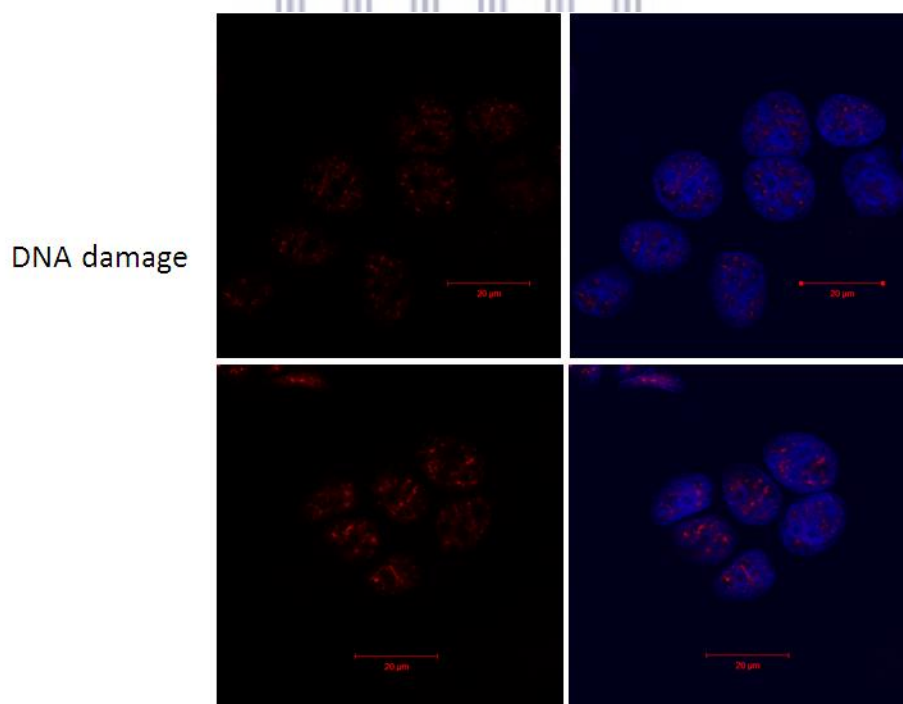


Figure 3.16: Antibody C133084, which is expected to target isoforms 1, 2 and 4 but not 3, is found exclusively in the nucleus in speckle-like bodies following UV-treatment. UV-treated HeLa cells stained with C133084 antibody in red (left) and merged with DNA stain Hoechst in blue (right). There is no clear evidence of increased nuclear speckling following DNA damage.

Table 3:3: Nuclear intensity values corresponding to isoforms 1, 2 and 4, before and after heat shock treatment. Measurements were carried out in HeLa cells using heat shock of 42 °C for 5 minutes. There is no significant increase in intensity following heat shock or DNA damage caused by UV.

Nuclear Intensity			
Heat Shock		DNA Damage (UV)	
before heat shock	10.79 ± 1.7	before DNA damage	11.49 ± 2.23
after heat shock	10.47 ± 1.8	after DNA damage	11.01 ± 1.39

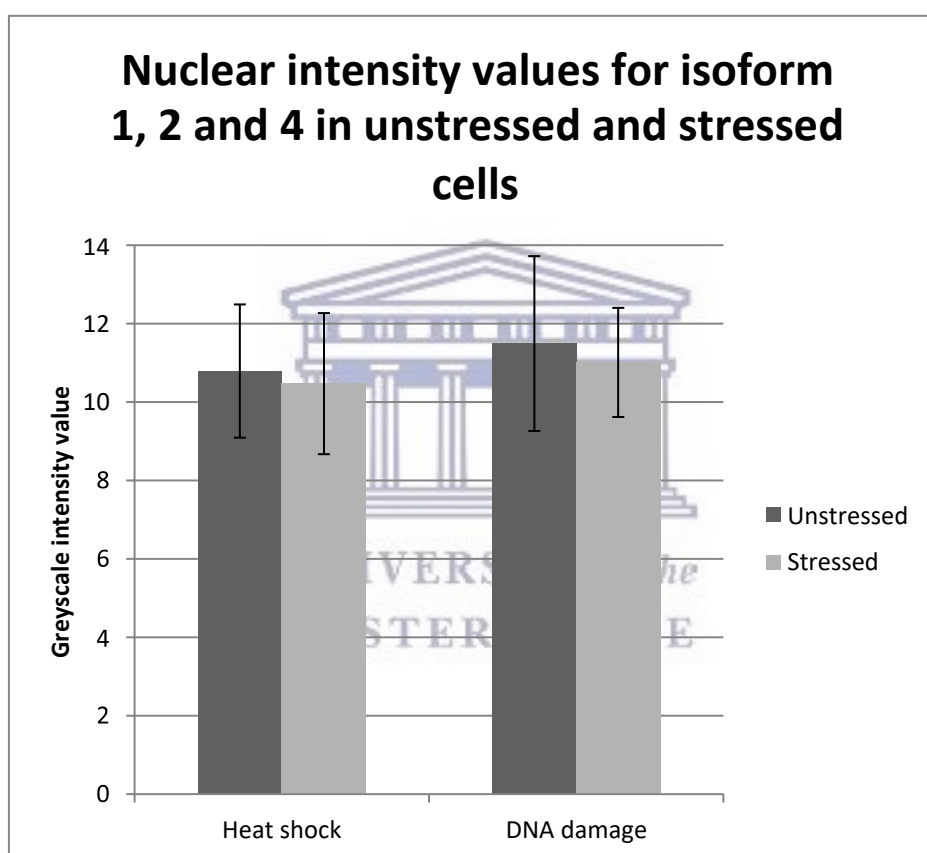


Figure 3.17 Nuclear intensity values corresponding to isoforms 1, 2 and 4, following heat shock and DNA damage caused by UV. There is no evidence for increase in nuclear intensity following either type of stress.

3.6 STRESS-INDUCED INCREASE IN NUCLEAR INTENSITY IS NOT DUE TO *DE NOVO* PROTEIN SYNTHESIS

The rapid increase in the intensity of the nuclear signal detected using the monoclonal anti-DWNN antibody suggests that it cannot be caused by *de novo* protein synthesis from the RBBP6 gene. In order to interrogate this conclusion, A549 cells were pre-treated with 50 µg/ml

cycloheximide (Sigma) for 30 minutes prior to induction of stress induced by cisplatin. Cycloheximide is known to block translation by interfering with the translocation step. Cisplatin was used instead of UV as the DNA damaging agent due to the lack of suitable equipment (Stratalinker) at the time when the experiment was being conducted. While the DNA damage and subsequent cellular response elicited by UV and cisplatin differ (reviewed in Chapter 1.3.3.2), our previous experiments show that both UV and cisplatin elicit the stress response in equal measure and thus the two induction methods could be used interchangeably for our purposes.

Coverslips were collected 30 minutes after stress and the nuclear intensity measured in the presence and absence of cycloheximide respectively, using the monoclonal mouse anti-DWNN antibody. The experiment was repeated in duplicate and 10 cells were sampled from each replicate slide. The recorded values can be found in Table 3.3.

Table 3:4: Nuclear intensities measured using the mouse monoclonal anti-DWNN antibody in cells treated with cycloheximide and subjected to DNA damage.

Nuclear intensity			
Without cycloheximide		With cycloheximide	
before DNA damage	83.94 ± 7.70	before DNA damage	79.6 ± 2.78
after DNA damage	114.99 ± 6.9	after DNA damage	121.61 ± 4.05

Visual examination of Figure 3.18 suggested that cycloheximide had no significant impact on the stress effect, as both treated and non-treated cells show essentially the same response. This conclusion is supported by the measured intensity values set out in Table 3.3. The increase in intensity after cell stress without cycloheximide was significant ($p < 0.001$), in agreement with previous results, as was the increase in intensity in the presence of cycloheximide ($p < 0.001$). However the difference between the two stressed experiments was not significant ($p = 0.5$), indicating that the stress had the same effect in both the presence and absence of cycloheximide. This suggests that the increase in the intensity of the signal in the nuclei is not affected by cycloheximide, from which we conclude that the increase induced by cisplatin treatment cannot be due to *de novo* protein synthesis. The most likely alternative is that it is due to translocation of isoform 3 from the cytoplasm into the nucleus.

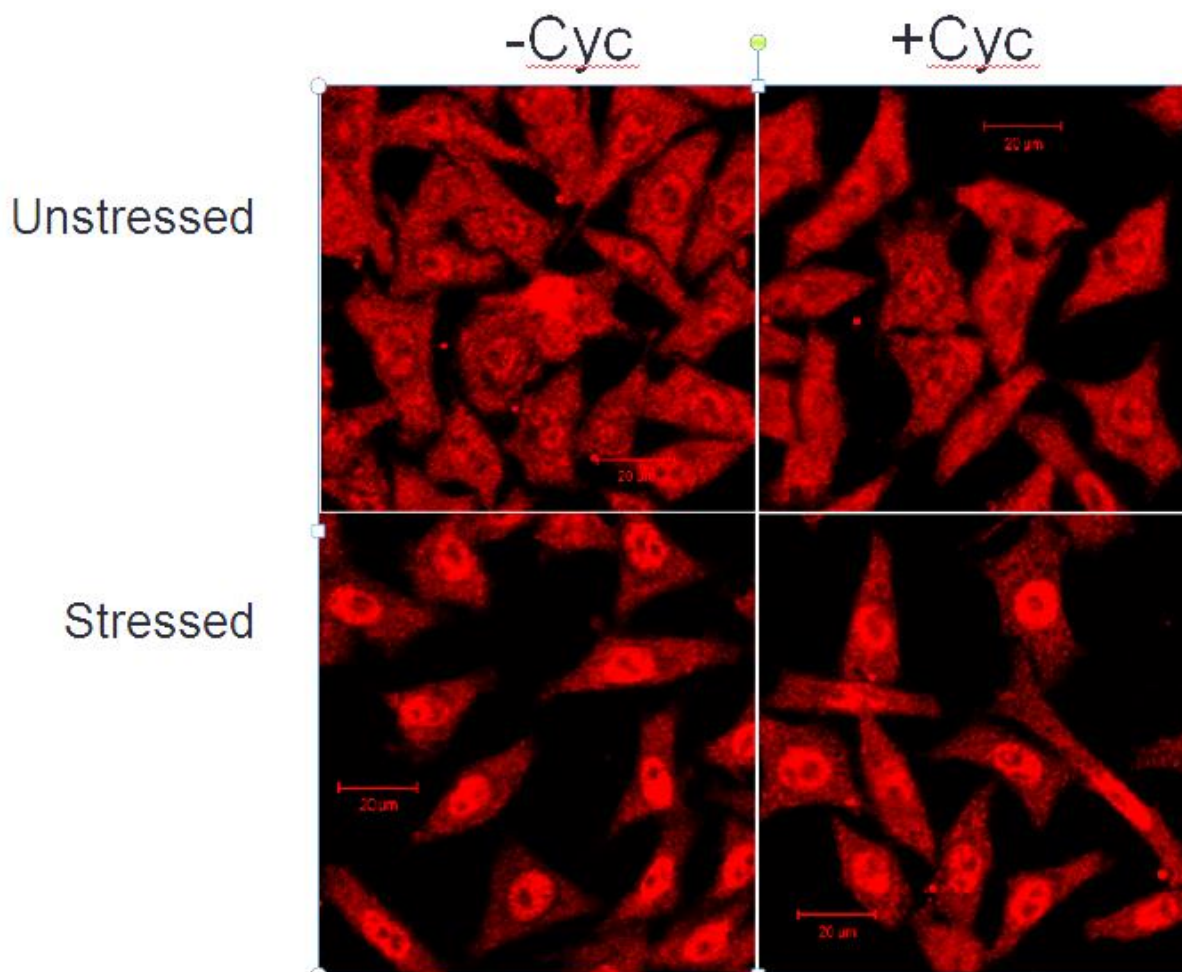


Figure 3.18: Cycloheximide has no effect on changes of nuclear intensity induced by cisplatin. HeLa cells pre-treated with cycloheximide and subjected to stress induced by cisplatin. Immunofluorescence microscopy was carried out using the mouse monoclonal anti-DWNN antibody. No difference was observed between cells that have been treated with cycloheximide and those that were not.

3.7 TRANSLOCATION OF ISOFORM 3 OCCURS IN A VARIETY OF CELL LINES

To test whether or not the translocation of isoform 3 was exclusive to a particular cell line, or only occurred in cell lines derived from cancer cells, or having mutant p53, a number of cell lines were tested in addition to the HeLa and A549 cell lines previously used (Table 3.4). The cells were subjected to DNA damage using UV, then were fixed and blocked and then stained overnight with a 1:10 dilution of the monoclonal mouse anti-DWNN antibody and then processed as previously described. The results are presented in Table 3.5.

Table 3:5: Cell lines used in DWNN translocation experiment. The p53 status of each cell line is taken from the IARC TP53 database, version R17, <http://p53.iarc.fr>. All of the cells, with the exception of KMST cells, are derived from carcinomas. All of the cells, with the exception of HeLa and H157, have normal levels of functional p53.

CELL LINE	SPECIES	CELL TYPE	p53 STATUS
A549	Human	Epithelial lung adenocarcinoma	Wild type, normal levels in the cell
HeLa	Human	Cervical adenocarcinoma	Wild type, low levels in the cell.
H157	Human	Non-small cell lung carcinoma	Missense mutation, non-functional
HepG2	Human	Hepatocellular liver carcinoma	Wild type, normal levels in the cell
KMST	Human	Human fibroblast, non-cancerous	Wild type, normal levels in the cell

Table 3:6: Nuclear intensity values for a number of cell lines, before and after UV-induced stress. Measurements were taken as previously described (section 3.2.1 and others) for either a total of 20 (for A549) or 30 (all other cell lines) measurements of unstressed and stressed cells respectively.

Cell line	Before stress	After stress	p value
A549 (n=20)	84 ± 8	114 ± 7	< 0.001
HeLa (n=30)	34 ± 7	53 ± 2	< 0.001
H157 (n=30)	46 ± 9	75 ± 13	< 0.001
HepG2 (n=30)	91 ± 23	96 ± 19.8	0.2
KMST (n=30)	61 ± 8	87.89 ± 29	< 0.001

In all cell lines there is evidence of the DWNN domain being present in both the cytoplasm and the nucleus of resting cells; on the basis of earlier evidence the cytoplasmic signal is likely to be due to isoform 3 alone. There is also evidence in resting cells of localisation to punctate nuclear bodies which is likely to be due to all four isoforms. However there is a significant increase following UV-induced stress which, if these cells follow the same pattern as HeLa cells, is due to isoform 3 alone. Although highly likely, this conclusion cannot be confirmed without investigation of these cells using antibody C133084, which does not detect isoform 3. However this was not performed due to the fact that we did not have the C133084 antibody at the time of the experiment.

All cell lines demonstrate some evidence of nuclear speckling and some increase in nuclear intensity following cell stress. Of these cell lines H157, KMST, A549 and HeLa cells displayed the greatest increases in intensity (Figures 3.19, 3.20, 3.22 and 3.23 respectively), while HepG2 displayed weaker increases (Figure 3.21) that are not statistically significant. This indicates that the stress effect is not exclusive to cancer cell lines and suggests that the p53 status of the cell line does not affect the translocation of isoform 3.

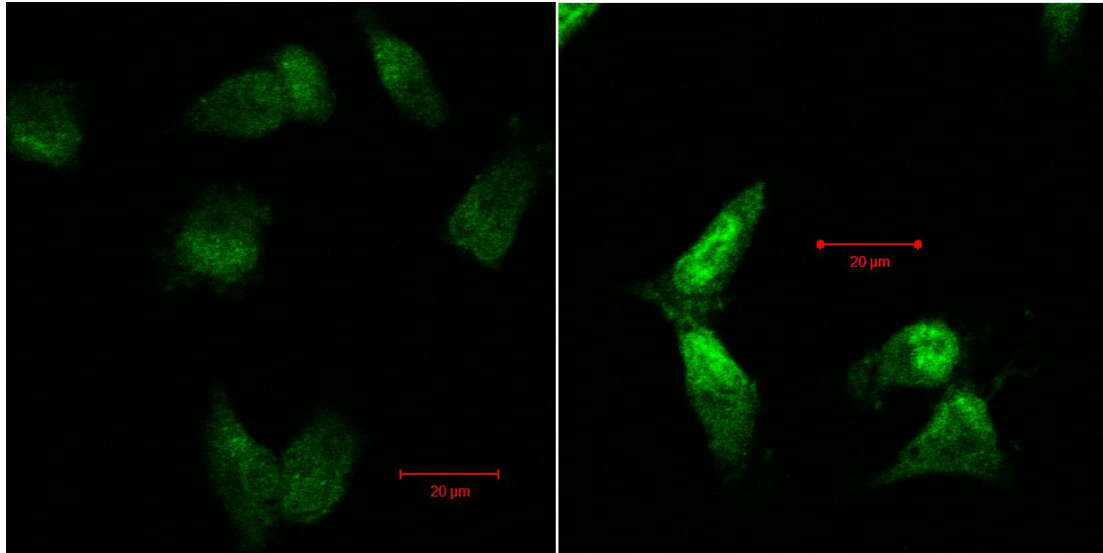


Figure 3.19: H157 cells stained with mouse monoclonal anti-DWNN antibody before (left) and after (right) DNA damage inflicted using UV.

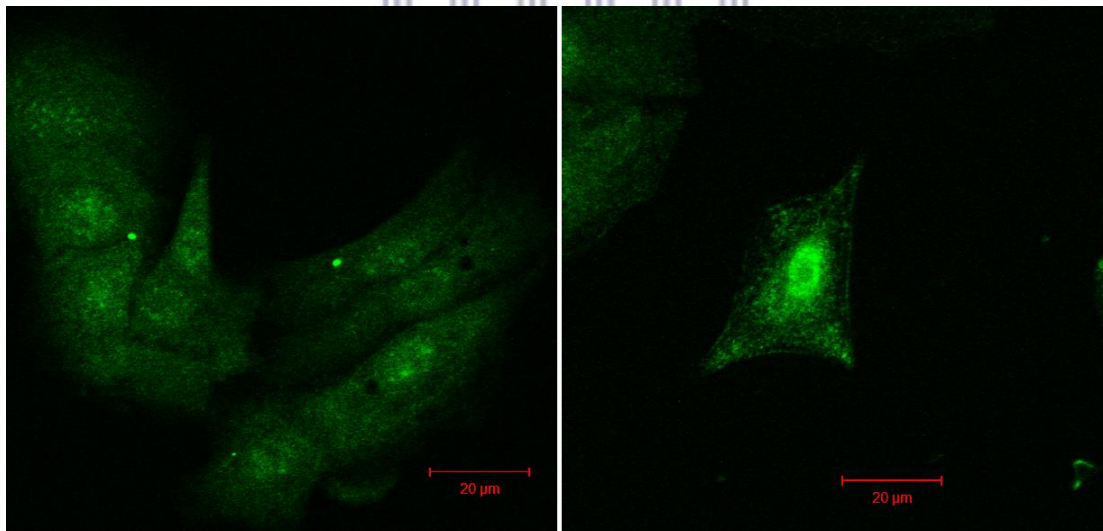


Figure 3.20: KMST cells stained with mouse monoclonal anti-DWNN antibody, before (left) and after (right) DNA damage inflicted using UV.

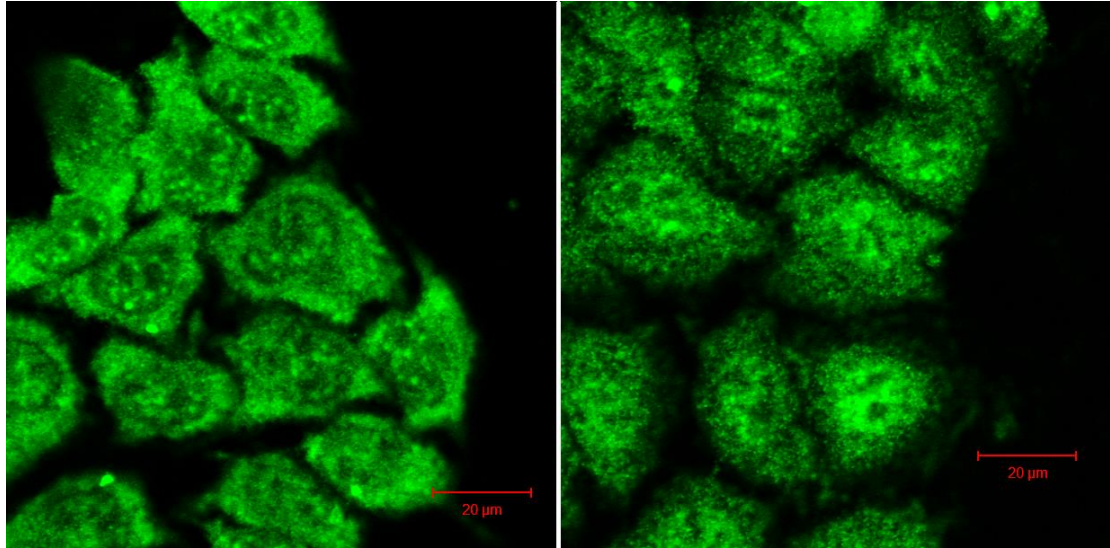


Figure 3.21: HepG2 cells stained with mouse monoclonal anti-DWNN antibody, before (left) and after (right) DNA damage inflicted using UV.

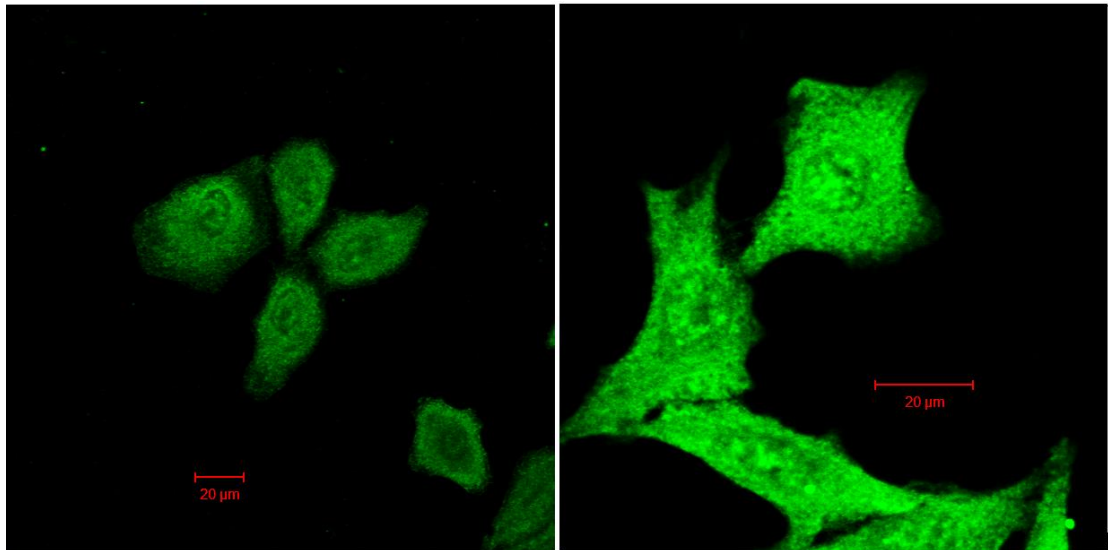


Figure 3.22: A549 cells stained with mouse monoclonal anti-DWNN antibody, before (left) and after (right) DNA damage inflicted using UV.

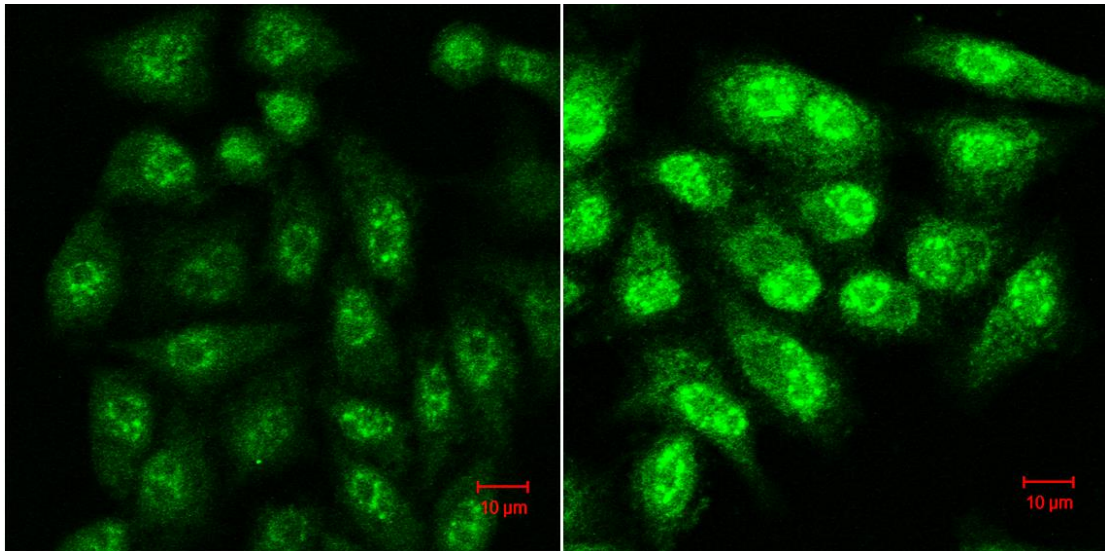


Figure 3.23: HeLa cells stained with mouse monoclonal anti-DWNN antibody before (left) and after (right) DNA damage inflicted using UV.

We conclude that the stress-dependent localisation of isoform 3 observed in HeLa or A549 cells is not exclusive to these cell lines. Isoform 3 is present in the cytoplasm of all cell lines tested and shows evidence of translocation to speckle-like bodies following UV-induced stress, with the possible exception of HepG2 cells. The effect does not appear to be restricted to cells with functional p53, nor to cells derived from carcinomas. As in the case of HeLa cells, the above conclusions rely on the conclusion that isoforms 1, 2 and 4 are entirely nuclear in all of these cells and do not increase following stress. This conclusion was not explicitly checked. Again, as with HeLa cells, is not possible to determine from these results whether isoform 3 is present in speckle-like bodies in resting cells.

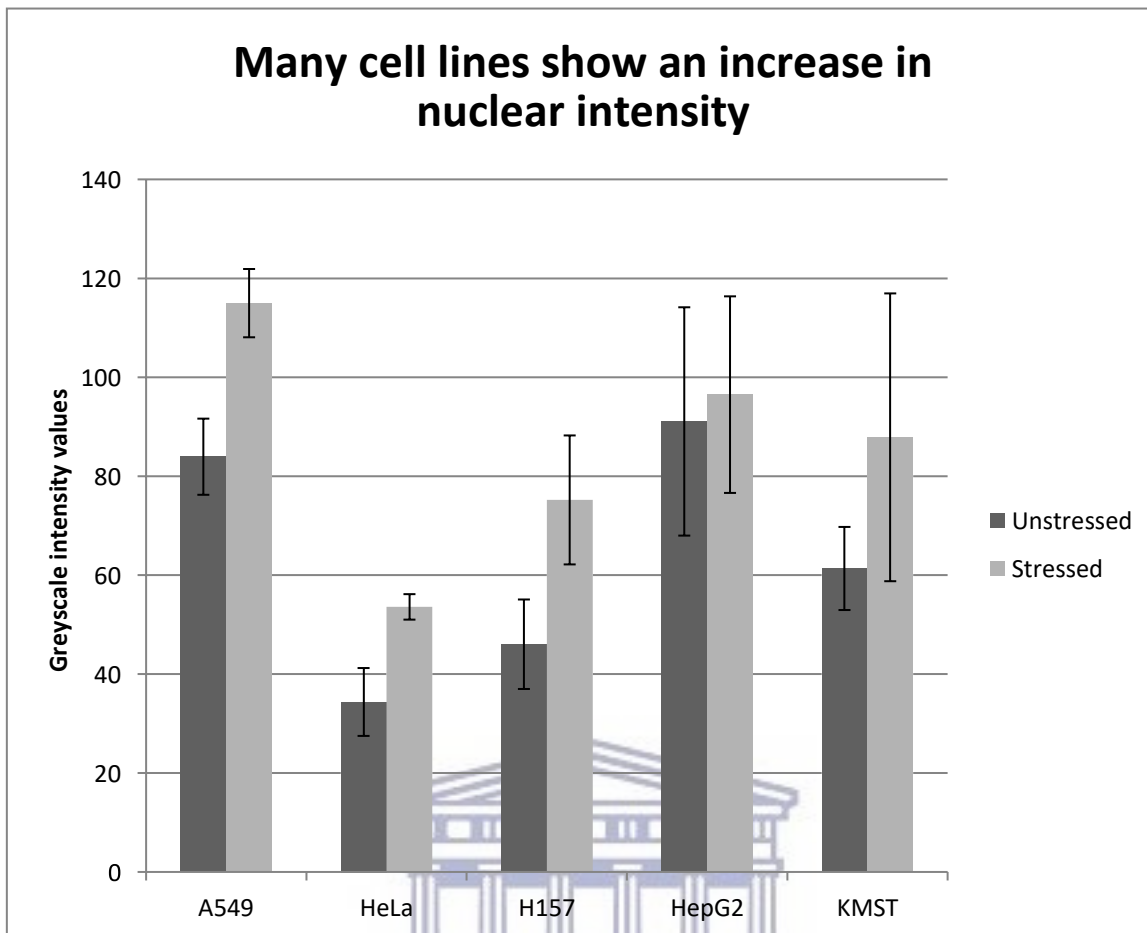


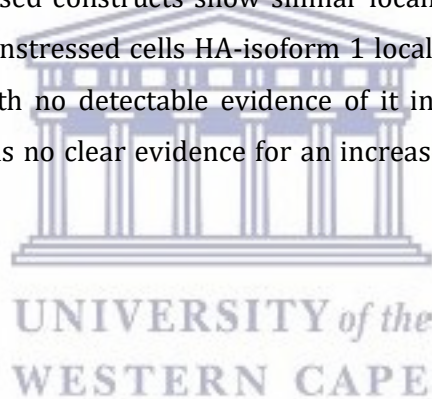
Figure 3.24: Translocation of isoforms 3 to nuclear speckle-like bodies in a number of cell lines. The difference between the nuclear intensities of anti-DWNN in stressed and unstressed cells is highly significant (p -value < 0.001) in all except HepG2 cells (p -value = 0.2).

3.8 CONFIRMATION OF ENDOGENOUS FINDINGS USING OVER-EXPRESSED CONSTRUCTS

The above conclusion was derived using antibodies targeting endogenous RBBP6 isoforms. To provide further evidence that the effect is due to RBBP6 and not another, off-target, protein, HeLa cells were transfected with pCMV constructs over-expressing exogenous isoforms 1 and 3 of RBBP6. These constructs included an N-terminal HA-immunotag, allowing detection by anti-HA antibodies. These antibodies have been shown in countless reports in the literature to be specific for the HA-tag, ruling out the possibility of off-target effects. Another important advantage of using exogenous constructs is that it provides a means of observing isoform 3 directly, which previously had only been observed indirectly by comparing results obtained using antibodies specific for the DWNN domain on the one hand and for isoforms 1, 2 and 4 on the other.

A third reason for using exogenous constructs is that they are expressed from a constitutive CMV promoter that is not expected to be induced by stress. This would totally rule out the possibility of stress-dependent changes being due to *de novo* protein expression from a stress-responsive promoter. The constructs are described in detail in Chapter 2. The cells were stressed using heat shock as described previously and stained using goat-anti-HA primary antibody and a donkey anti-goat secondary antibody conjugated to Cy3. Exposure times were set so that no signal was apparent in un-transfected cells, and the same settings were used for transfected cells. The results are presented in Figures 3.25-28.

Large cell-to-cell variability is apparent using both HA-isoform 1 and HA-isoform 3, as is expected for transient transfections (Smith and Mueller 2012). The signal is also highly granular, both in the nucleus and in the cytoplasm, which makes identification of nuclear speckles difficult and contributes further to high variability in measured densities. Despite these shortcomings, the over-expressed constructs show similar localisation and behaviour to their endogenous counterparts. In unstressed cells HA-isoform 1 localises exclusively in the nucleus within speckle-like bodies, with no detectable evidence of it in the cytoplasm (Figure 3.25). Following heat shock there was no clear evidence for an increase in the nuclear signal (Figure 3.26).



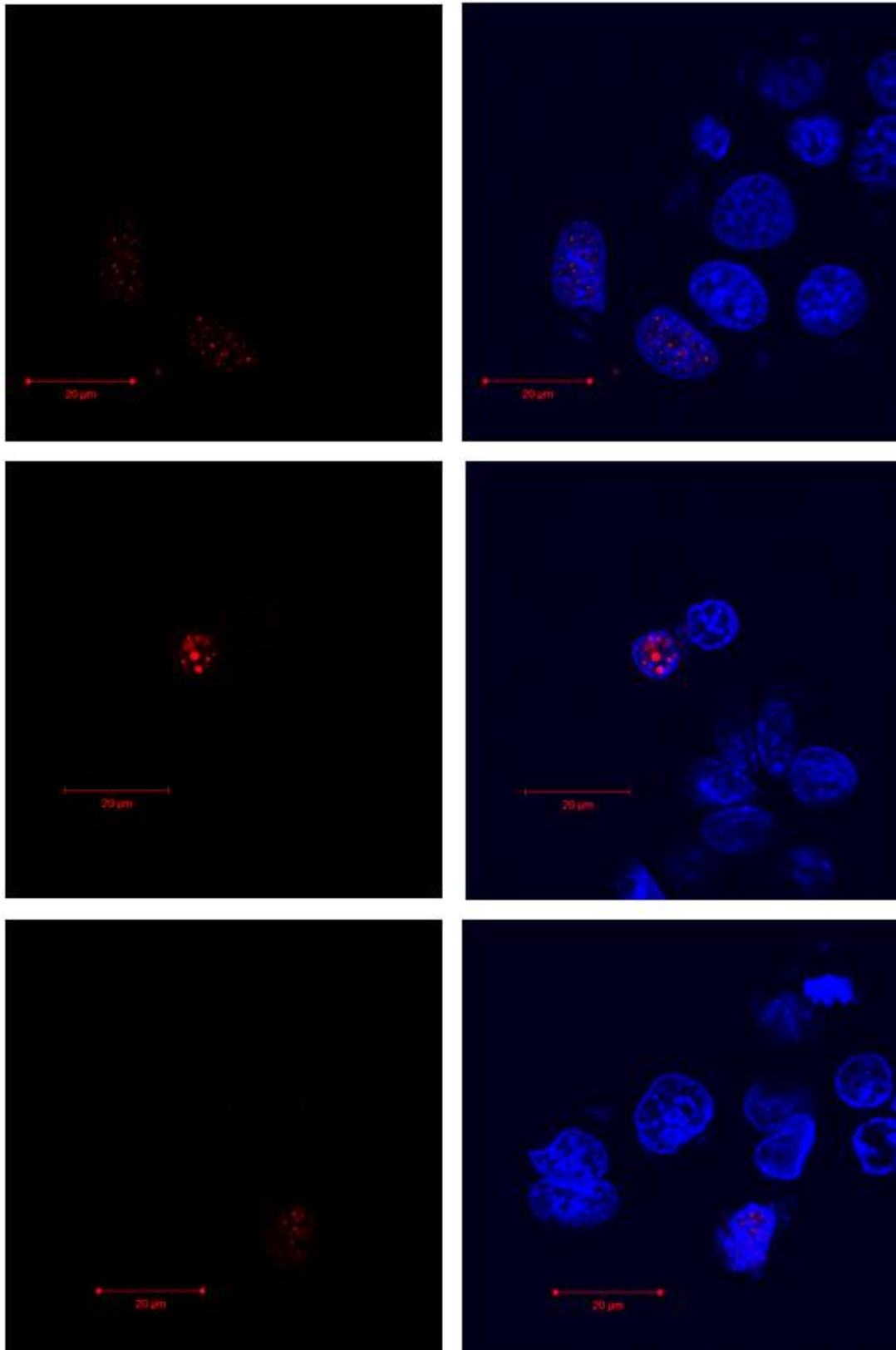


Figure 3.25: Unstressed HeLa cells transfected with HA-isoform 1 and detected using an anti-HA antibody. Red indicates the HA-isoform 1 signal (left) while blue represents the nuclear stain, Hoechst (right). As with endogenous isoform 1, the signal is punctate and exclusively nuclear with no detectable cytoplasmic signal. The nuclear intensity varies greatly between cells as is expected for transient transfection.

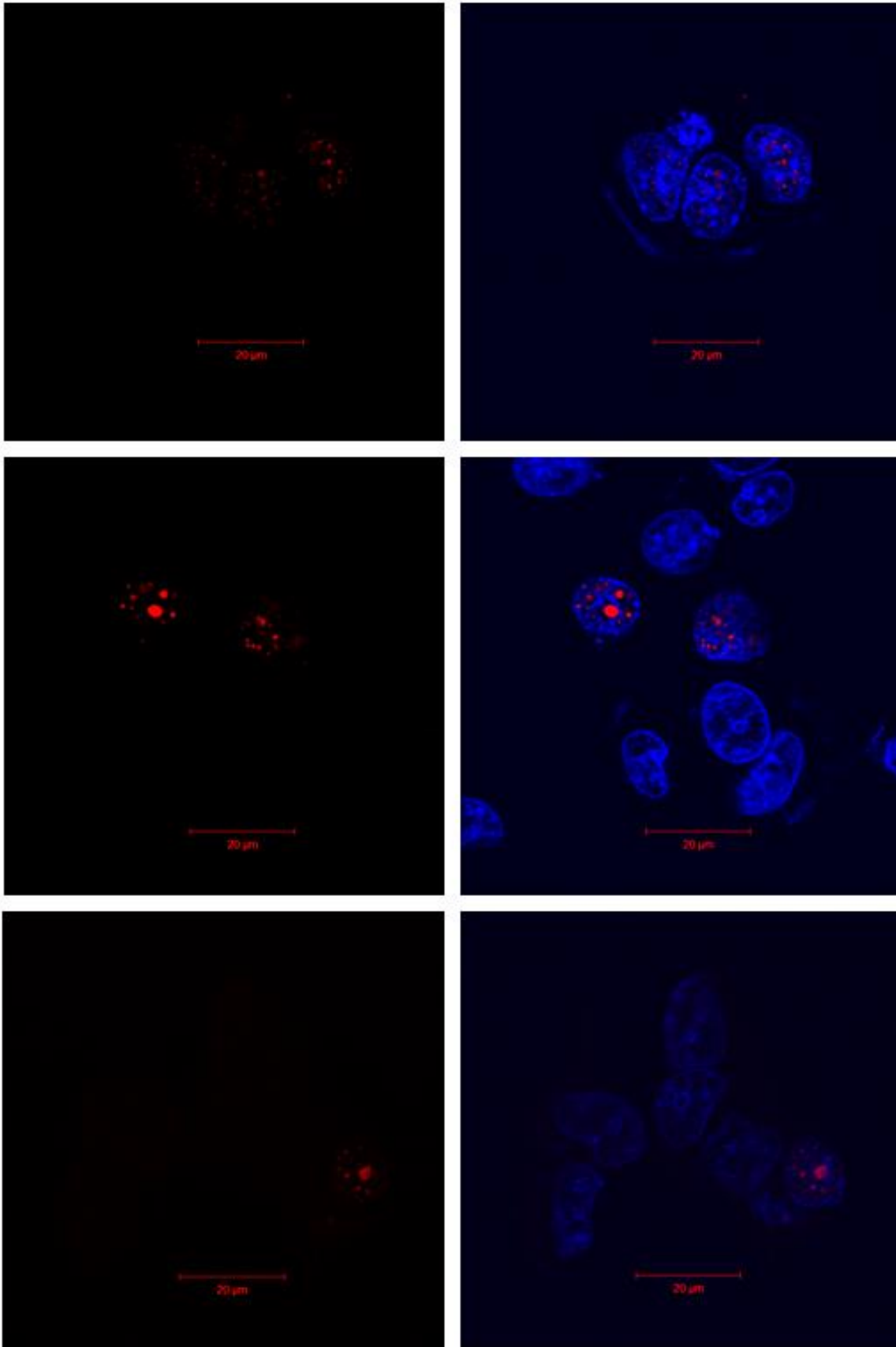


Figure 3.26 Heat-shocked HeLa cells transfected with HA-isoform 1 and detected using an anti-HA antibody. Red indicates the HA-isoform 1 signal (left) while blue represents the nuclear stain, Hoechst (right). As with endogenous isoform 1, the signal is punctate and exclusively nuclear with no detectable cytoplasmic signal. The nuclear intensity varies greatly between cells as is expected for transient transfection.

In resting cells, HA-isoform 3 is largely cytoplasmic in many cells, consistent with the endogenous form (Figure 3.27), although there is very high cell-to-cell variability. Following heat-shock the density of HA-isoform 3 increases in the nucleus, as is apparent from Figure 3.28, although again the cell-to-cell variability is high. Nevertheless these observations are borne out by numerical analysis of the data: there is no significant change in the cytoplasmic density following stress (p -value = 0.06), whereas there is a significant increase in the nuclear density (p -value = 0.002).

Scrutiny of the raw data (see Appendix) suggests that there may be some correlation between the nuclear and cytoplasmic intensities; i.e. when the nuclear intensity is high, so is the cytoplasmic intensity, and when the nuclear intensity is low, so is the cytoplasmic intensity. If that is the case then the ratio of the nuclear intensity and the cytoplasmic intensity is likely to be less variable than the individual intensities.

The ratio increases from 0.96 ± 0.24 before stress to 1.39 ± 0.21 after stress. The change is significant, with a p -value of 0.015. Also of interest is that the standard deviations before and after stress are both significantly smaller than those of the raw intensity values, which supports the hypothesis that the nuclear and cytoplasmic intensities are indeed correlated.

HA-isoform 3 was predominantly localised in the cytoplasm in resting cells (Figure 3.27), consistent with what is seen in the endogenous case. However there was some evidence for punctate structures in the nucleus, from which we conclude that isoform 3 is also present in nuclear speckles in resting cells, although at low levels. Following heat-shock HA-isoform 3 is found at significantly higher density in the nucleus than in the cytoplasm, (Figure 3.28). This is confirmed by quantitative analysis, where the ratio of nuclear to cytoplasmic intensity increases from 0.96 in resting cells to 1.39 in stressed cells, with a significance value of $p = 0.01$. The relatively high value of 0.96 implies that the nuclear intensity in resting cells is almost equal to that of cytoplasmic intensity. The images appear to indicate that there is much more cytoplasmic intensity, however, as the nuclear values take into account both the punctate (brighter) structures in addition to the diffuse signal in the rest of the nucleus, which may serve to explain this discrepancy between image and value. It should also be noted that the nuclear/cytoplasmic values are similar calculated during the study of endogenous proteins where a similar discrepancy occurs.

This implies that in resting cells, mean nuclear and cytoplasmic values are almost equal, while in stressed cells there is a higher proportion of nuclear signal relative to cytoplasmic signal.

Relative intensities were calculated in this case rather than comparing absolute intensities because the large cell-to-cell variability of the over-expressed proteins masked the significance of the relative changes within each cell (See Appendix A for cytoplasmic and nuclear intensity values).

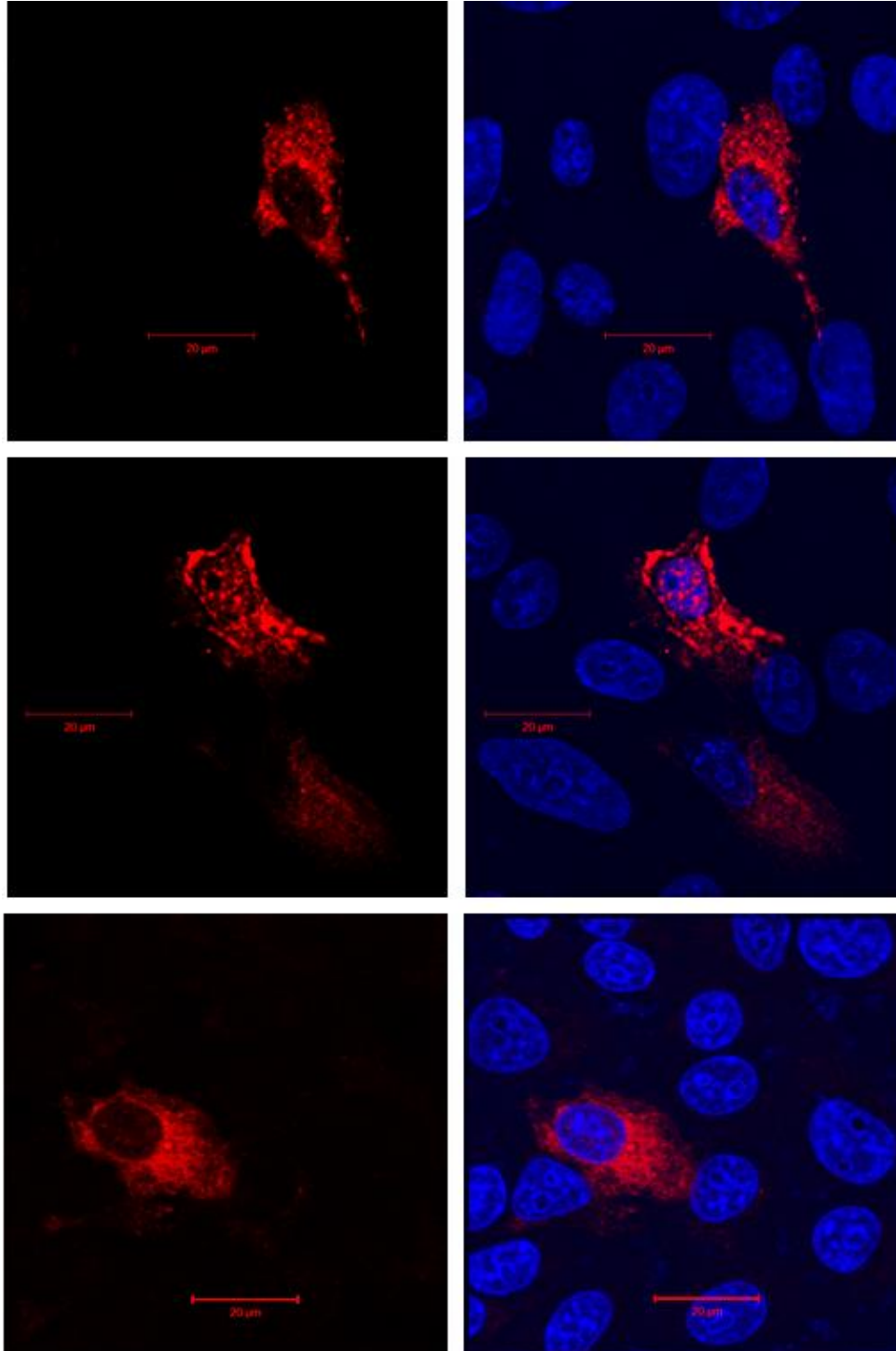


Figure 3.27: Unstressed HeLa cells transfected with HA-isoform 3. Red indicates the HA-isoform 3 signal (left) while blue represents the nuclear stain, Hoechst (right). As with endogenous isoform 3, the signal occurs both in the cytoplasm and the nucleus. There are detectable punctate structures in the many of unstressed nuclei, but most of the signal originates in the cytoplasm.

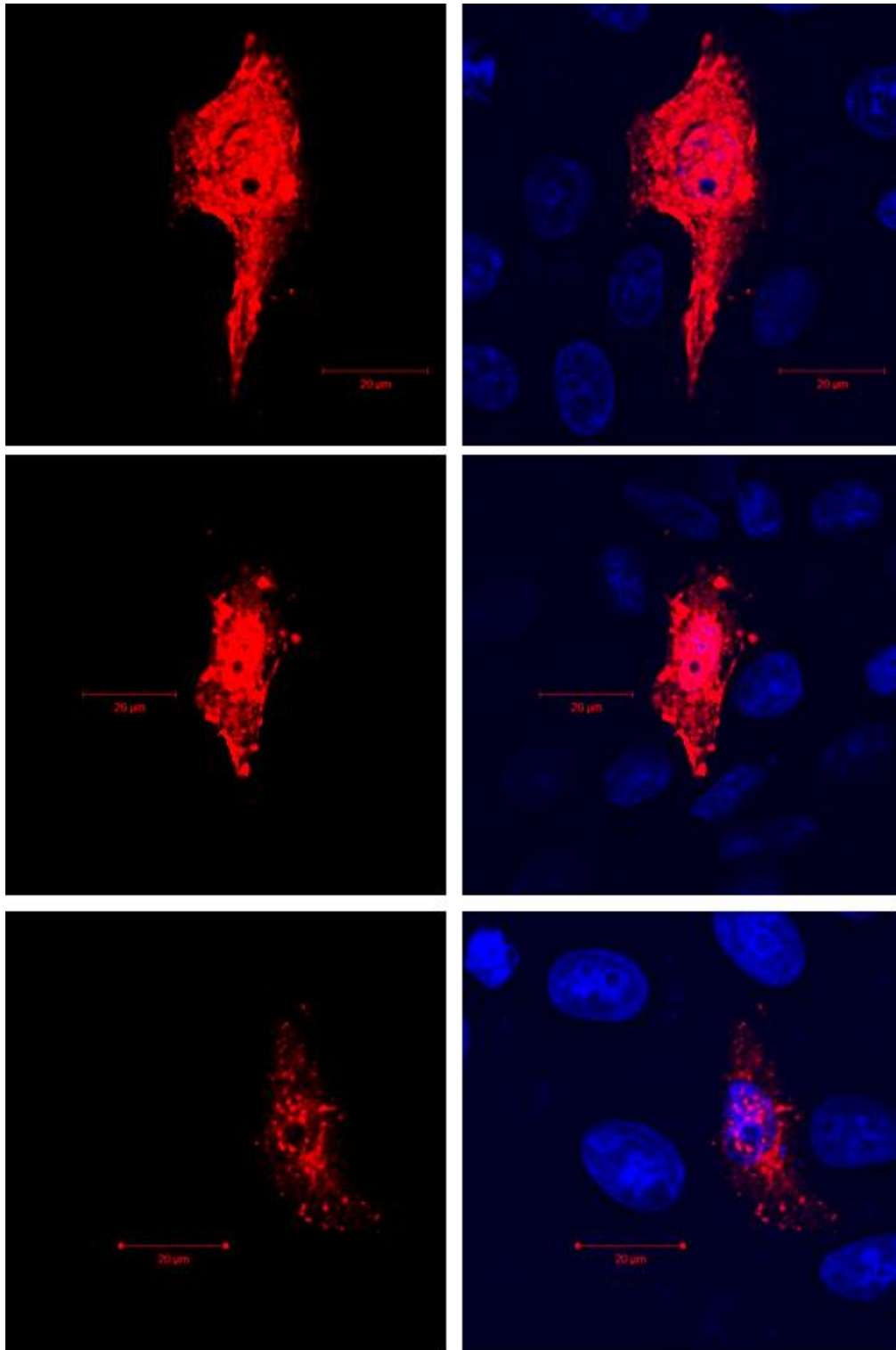


Figure 3.28 Stressed HeLa cells transfected with HA-isoform 3. Red indicates the HA-isoform 3 signal (left) while blue represents the nuclear stain, Hoechst (right). As with endogenous isoform 3, the signal occurs both in the cytoplasm and the nucleus. There are detectable punctate structures in the all of the stressed nuclei, but most of the signal originates in the cytoplasm.

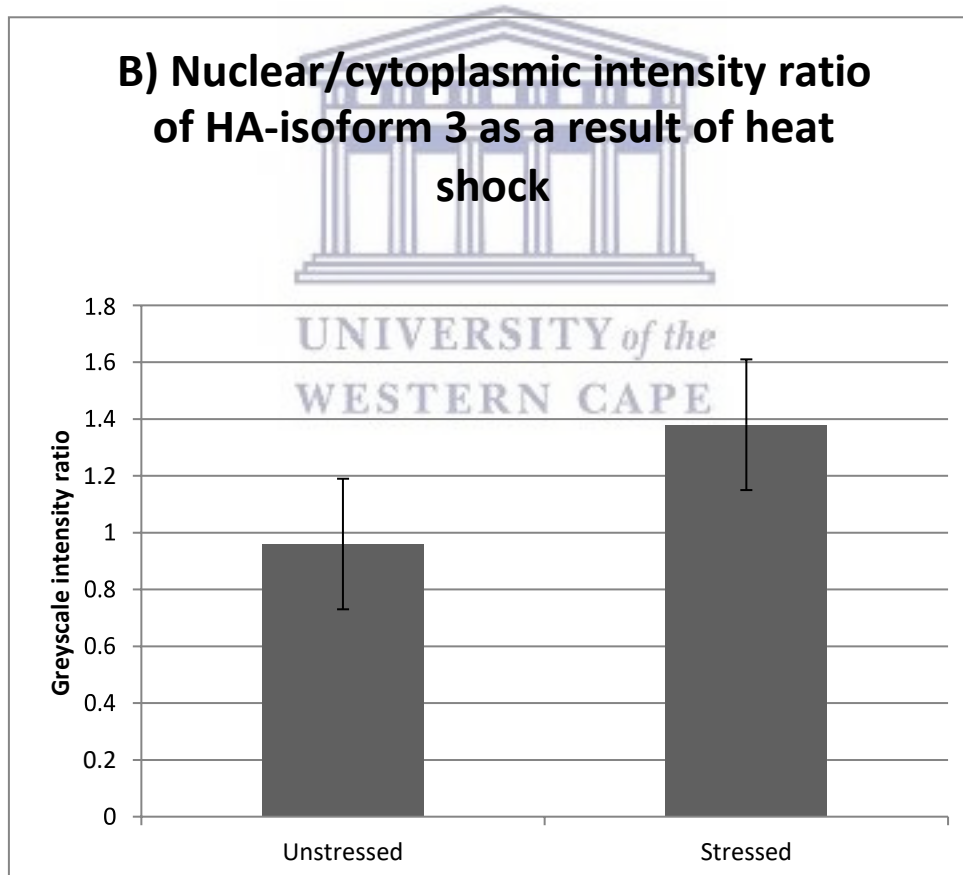
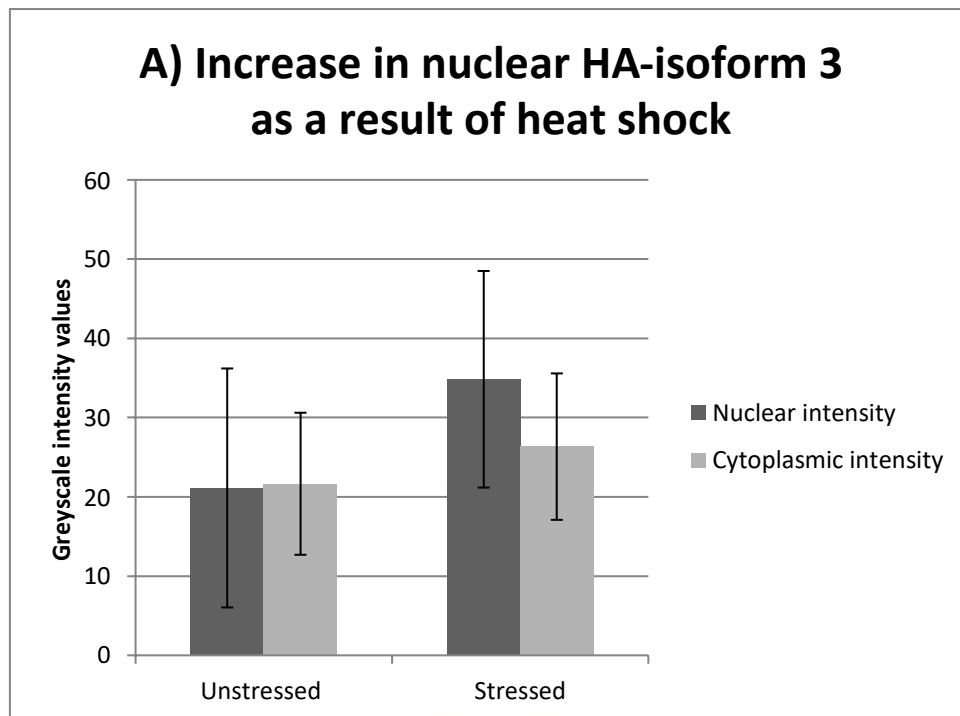


Figure 3.29: The ratio of nuclear to cytoplasmic intensity in stressed and unstressed cells. A) Nuclear and cytoplasmic intensities of unstressed and stressed cells with high SDs related to high variation in signals. B) Nuclear/cytoplasmic intensity ratio of unstressed and stressed cells. Unstressed cells show slightly higher levels of cytoplasmic intensity compared to nuclear intensity. However, after cell stress, this value rises, indicating a higher proportion of nuclear intensity to cytoplasmic intensity and indicating a rise in nuclear intensity. The change in ratio is significant with a *p*-value of 0.015.

Table 3:7: Table showing both the raw mean nuclear and cytoplasmic intensity values as well as the ratio of nuclear/cytoplasmic intensity in unstressed and stressed cells

Nuclear and cytoplasmic intensity values of cells expressing HA-isoform 3			
Nuclear intensity		Cytoplasmic intensity	
before stress	21.13 ± 15.08	before stress	21.65 ± 8.96
after stress	34.84 ± 13.66	after stress	26.34 ± 9.24
Nuclear intensity/cytoplasmic intensity values of cells expressing HA-isoform 3			
Unstressed Cells		Stressed Cells	
0.96 ± 0.23		1.38 ± 0.21	

3.9 RBBP6 LOCALISES TO NUCLEAR SPECKLES

SC35 is an mRNA splicing factor which localises exclusively in punctate nuclear bodies known as nuclear speckles, splicing speckles or SC35-speckles. The function of these bodies is not fully understood, but a number of possible functions have been outlined (see section 1.5), of which the most popular is that speckles are involved in mRNA processing, from splicing to 3'-end processing, as well as showing potential involvement in transcription. RBBP6 has previously been reported to localise to nuclear speckles (Simons *et al.* 1997), but to our knowledge the punctate bodies in which it localises have not previously been confirmed to be nuclear speckles.

In order to determine whether endogenous RBBP6 does indeed localise to nuclear speckles, A549 cells were co-stained with mouse antibodies against SC35 and rabbit polyclonal antibodies against the DWNN domain. As the available anti-SC35 primary was raised in mouse, to avoid cross-reactivity we were obliged to use the polyclonal rabbit anti-DWNN, rather than the mouse monoclonal antibody used in prior experiments. After incubation with the primary antibodies, anti-rabbit and anti-mouse secondary antibodies conjugated to Alexa488 and Cy3 respectively were used to fluorescently label the respective proteins, which were then visualised under the confocal microscope. Colocalisation analysis was performed using the Zeiss AxioVision 4.8 software with colocalisation plugin and verified with ImageJ with the assistance of the JaCoP plugin (Bolte and Cordelières 2006). Cell stress was induced through incubation at 42 °C for five minutes after which the same staining and visualization procedures were used.

In order to control for bleed-through and non-specific secondary antibody signal A549 cells were separately stained with only rabbit anti-DWNN or with only mouse anti-SC35 and then incubated with both secondary antibodies, conjugated to Alexa488 (green) and Cy3 (red) respectively, as described in Section 2.3. As is apparent from Figure 3.30, in the presence of the anti-DWNN primary the DWNN was detected in the green channel (top row, left panel); the distribution is consistent with what was observed previously (e.g. Figure 3.4). Nothing was observed in the red channel, confirming that there was no bleed-through of the green fluorophore into the red detector, and nor was there any non-specific binding of the Alexa488- conjugated secondary. In the presence of the anti-SC35 primary punctate nuclear bodies were observed in the red channel (second row, right panel), consistent with what is expected for SC35; nothing was observed in the green channel, confirming that there was no bleed-through of the red fluorophore into the green detector, and nor was there any non-specific binding of the Cy3-conjugated secondary.

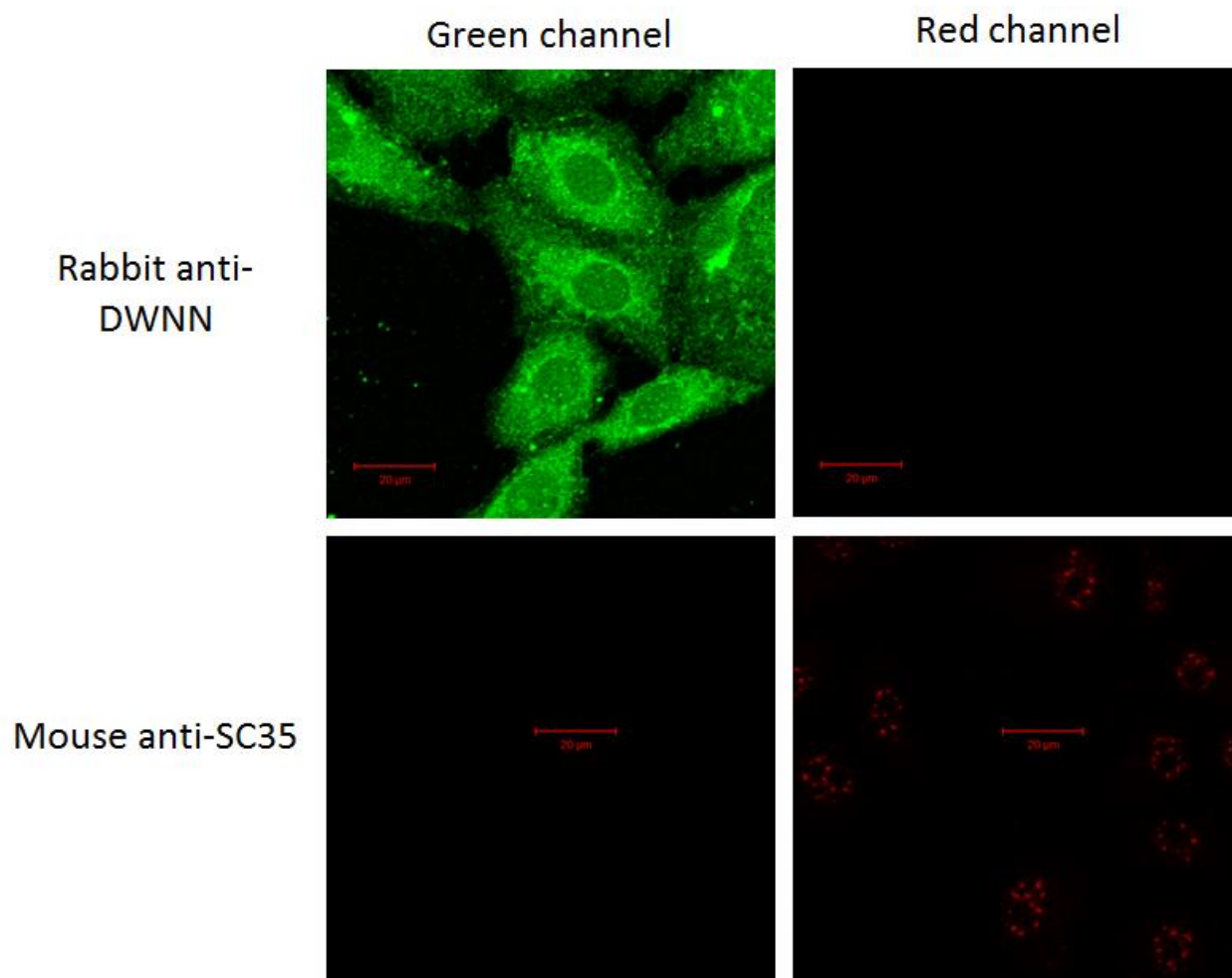
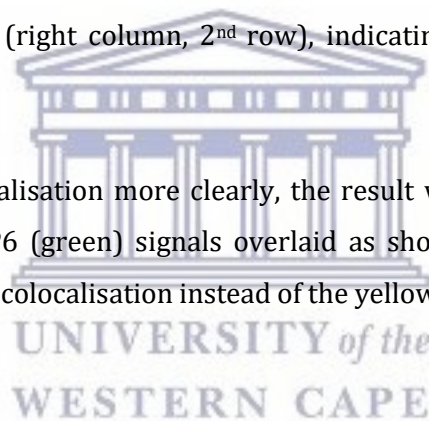


Figure 3.30: Bleed through and non-specific secondary antibody control. The rabbit anti-DWNN antibody produces strong signal in the green channel but none in the red channel, despite being incubated with both secondary antibodies (anti-mouse Cy3 and anti-rabbit Alexa488). This shows that there is no signal in the red channel resulting from either bleed through or non-specific secondary antibody binding. Similarly, mouse-anti SC35 shows strong signal in the red channel but none in the green channel.

Colocalisation assays, in the presence of both primary antibodies, are shown in Figure 3.31, both for unstressed cells (top row) and DNA-damage stressed cells (second row). As expected, the localisation of SC35 is not significantly affected by cell stress, as can be seen by comparing the 1st and 2nd rows of the middle column. In unstressed cells the DWNN signal shows both cytoplasmic and nuclear signal (left column, 1st row), with pronounced perinuclear staining, consistent with what was previously observed using the polyclonal rabbit antibody (Figure 3.4). Weak speckle-like bodies are visible in the nucleus. As was previously concluded the cytoplasmic staining is likely to emanate from isoform 3 alone, whereas it is impossible to distinguish which isoform of RBBP6 is responsible for the speckle-like bodies, since all contain the DWNN domain. Importantly isoform 3 localises colocalise with SC35, both in unstressed cells and, more significantly, in stressed cells. As can be seen in the overlay in the right-hand column, the yellow/orange colour of the speckles in the 1st row provides evidence that RBBP6 colocalises with SC35 already in resting cells. Following stress there is a clear increase in the yellow colour of the speckles (right column, 2nd row), indicating co-localisation of SC35 and RBBP6.

In order to visualise the colocalisation more clearly, the result was repeated using A549 cells and the SC35 (red) and RBBP6 (green) signals overlaid as shown in Figure 3.32, where the white pixels represent areas of colocalisation instead of the yellow colour shown in Figure 3.31.



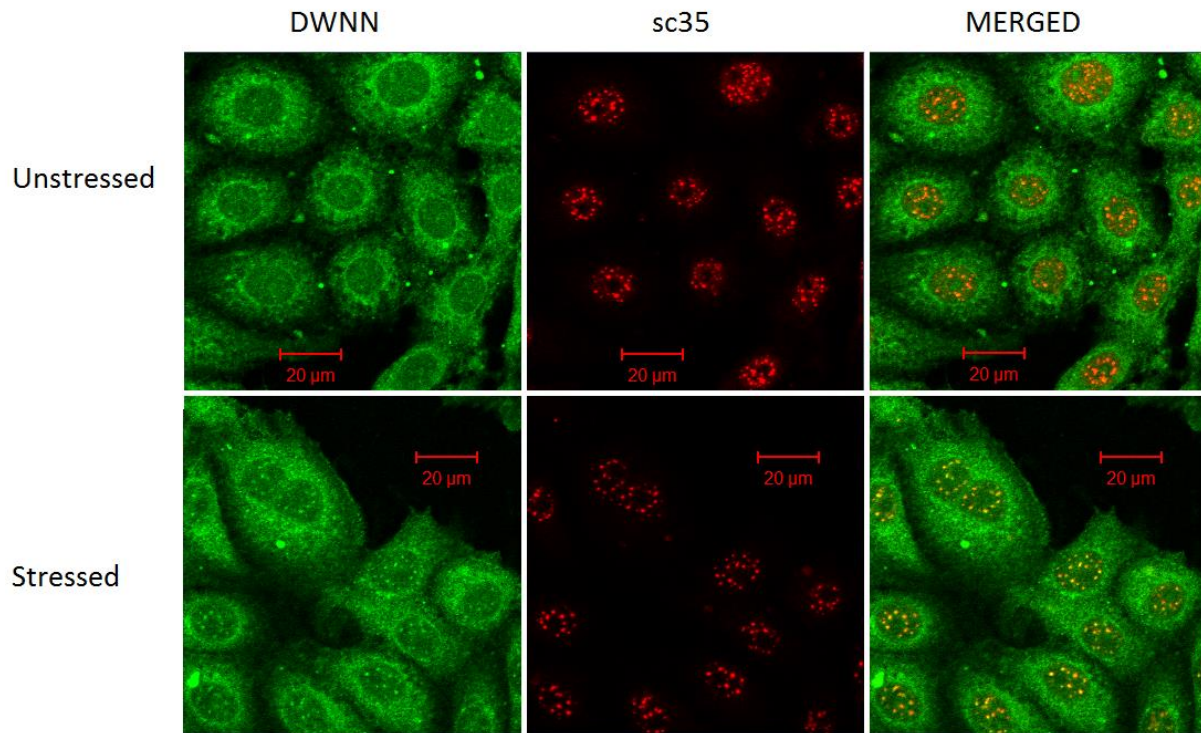


Figure 3.31: A549 cells co-stained with rabbit polyclonal anti-DWNN (green) and mouse monoclonal anti-SC35 (red) showing that the DWNN domain localises to the same nuclear speckles as SC35 following stress induced by heat shock. SC35 shows the expected punctate, exclusively nuclear, pattern, which is not affected by stress (middle column). Although there is evidence that DWNN is found in similar punctate bodies in the absence of stress (top left panel), they increase significantly following stress, as shown earlier (bottom left panel). The increase in the amount of yellow colour in the speckles following stress indicates increasing co-localisation (right column).

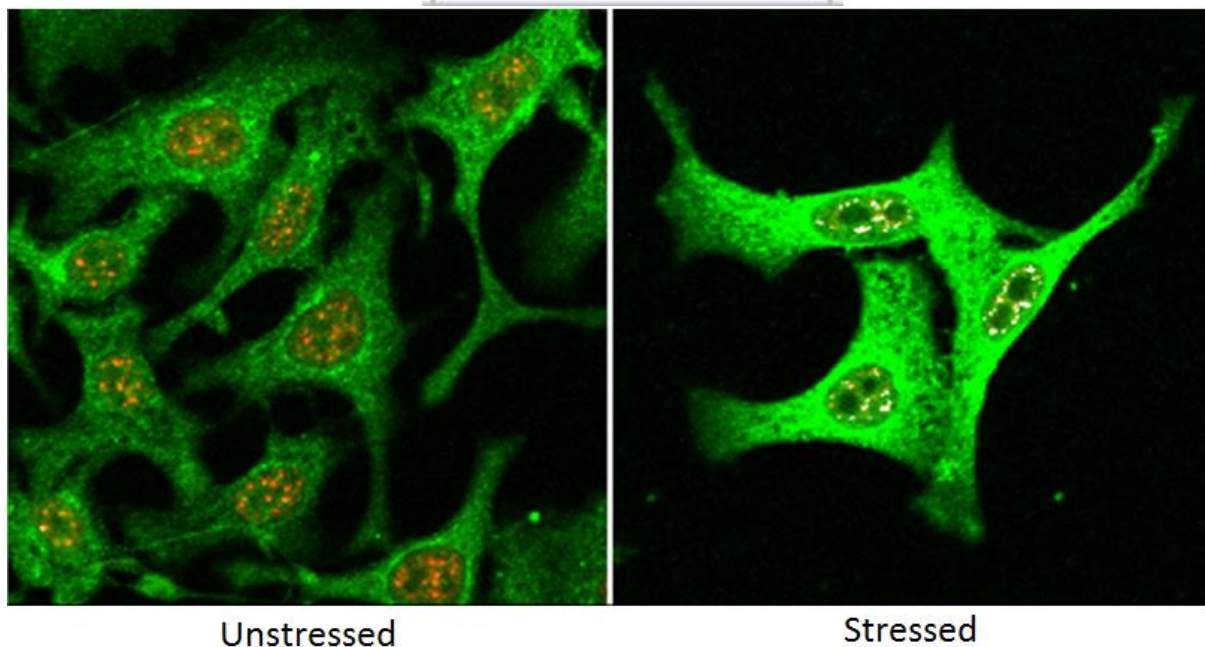


Figure 3.32: Colocalisation analysis of A549 cells stained with rabbit polyclonal anti-DWNN (green) and mouse monoclonal anti-SC35 (red). Stress was administered via heat shock as previously described. White spots within the nucleus show areas of colocalisation. The conclusion that can be drawn is that isoform 3 localises to nuclear speckles (SC35 speckles) following cell stress

Quantitative colocalisation analysis was carried out using the Zeiss AxioVision 4.8 colocalisation software. One of the largest challenges in immunofluorescence microscopy is determining whether a signal is genuine or part of non-specific background. In order to ensure that the colocalisation analysis takes into account only genuine signal, a threshold value of intensity is set, above which the signal can be considered genuine and not background signal. These thresholds can be set manually, particularly if there is a clear distinction between genuine signal and background, or can be set automatically using the Costes method (Costes *et al.* 2004) in both the Zeiss AxioVision 4.8 colocalisation plugin or the JaCoP plugin for ImageJ. As the threshold values impact heavily on the Mander's coefficient measurement, having an unbiased, automated way to do so is essential. Once the intensity thresholds have been set, pixels where the intensities for both channels (green and red) have been exceeded are considered to colocalise (indicated in white). Thresholds for all colocalisation experiments were set using the Costes method.

We took measure of the Manders coefficient to evaluate colocalisation. As we wished to examine the colocalisation of RBBP6 with SC35, we only took readings of the amount of RBBP6 colocalising with SC35, and not SC35 colocalising with RBBP6.

The amount of co-localisation increases significantly following stress (right) compared to the absence of stress (left). Quantitative analysis of the images confirms these findings. Thresholds were set to 150 in the green channel and 100 for the red channel, intensity levels at which we say the two dyes are colocalised. The experiment was repeated three times and 5 Mander's coefficient values were calculated per experiment (see Appendix). The mean Mander's coefficient in unstressed cells was found to be 0.178, indicating that only 18% of the RBBP6 in the nucleus colocalised with SC35. This increased to 0.749 following stress, indicating that 75% of RBBP6 in the nucleus was to be found in nuclear speckles following stress.

3.10 ISOFORM 3 DOES NOT LOCALISE TO SITES OF DNA DAMAGE REPAIR

We have previously shown that the nuclear translocation of isoform 3 of RBBP6 can be induced by DNA damage, either through double-stranded breaks induced by UV or by DNA crosslinks induced by cisplatin. The phosphorylation of H2AX serves as a marker of double-stranded DNA damage. Cisplatin does not cause double-stranded DNA breaks itself, but during the process of DNA repair through nuclear excision, double-stranded DNA breaks are generated. Thus, in the case of cisplatin, the presence of γ H2AX corresponds to the progress of DNA repair through NER.

This makes γ H2AX an ideal candidate to examine whether isoform 3 is directly involved in the DNA damage repair pathway. Cisplatin was chosen to induce DNA damage as at the time of the experiment we did not have access to the Stratalinker used to generate DNA damage via UV induction.

In order to determine whether γ H2AX colocalises with isoform 3 after cell stress, A549 cells were grown on coverslips for 24 hours, after which DNA damage was induced using 0.6 μ g/ml cisplatin (Sigma) for 1 hour before fixing the cells, as previously described. Cells were then stained using 1:10 mouse anti-DWNN and 1:200 rabbit anti- γ H2AX primary antibodies overnight. Cells were incubated with 1:1000 anti-rabbit Alexa488 and 1:500 anti-mouse Cy3 and visualised as previously described. Colocalisation analysis was performed using ImageJ with the assistance of the JaCoP plugin (Bolte and Cordelières 2006). As γ H2AX occurs exclusively in the nucleus and only after cell stress (Figure 3.33), only nuclear signal from stressed cells was considered for colocalisation. Colocalisation thresholds were set at 200 for the green channel and 575 for the red channel and maintained throughout the experiment. The experiment was repeated three times and 5 Mander's coefficient values were calculated per experiment. These values can be found in the Appendix.

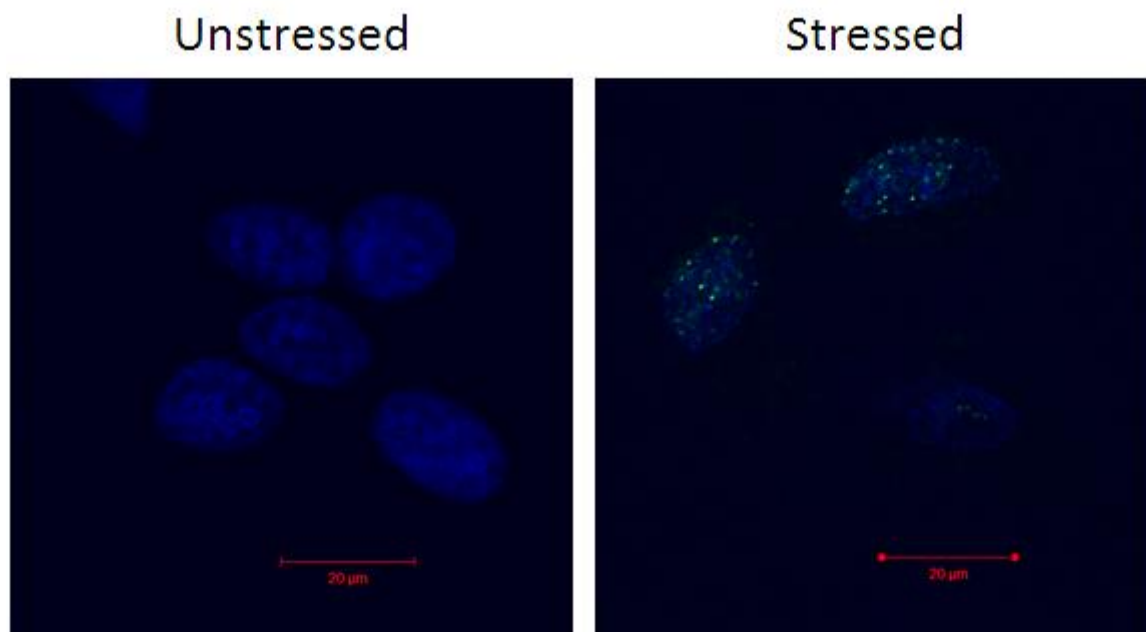


Figure 3.33: Stain showing that γ H2AX (green) localises to the nucleus (stained blue) and only appears after DNA damage induced using cisplatin (right). It should be noted that γ H2AX levels vary per cell,

To confirm that neither bleed through nor non-specific secondary antibody staining were affecting the results of the colocalisation experiment, we performed the same controls as discussed in the previous section and the results are shown in Figure 3.34.

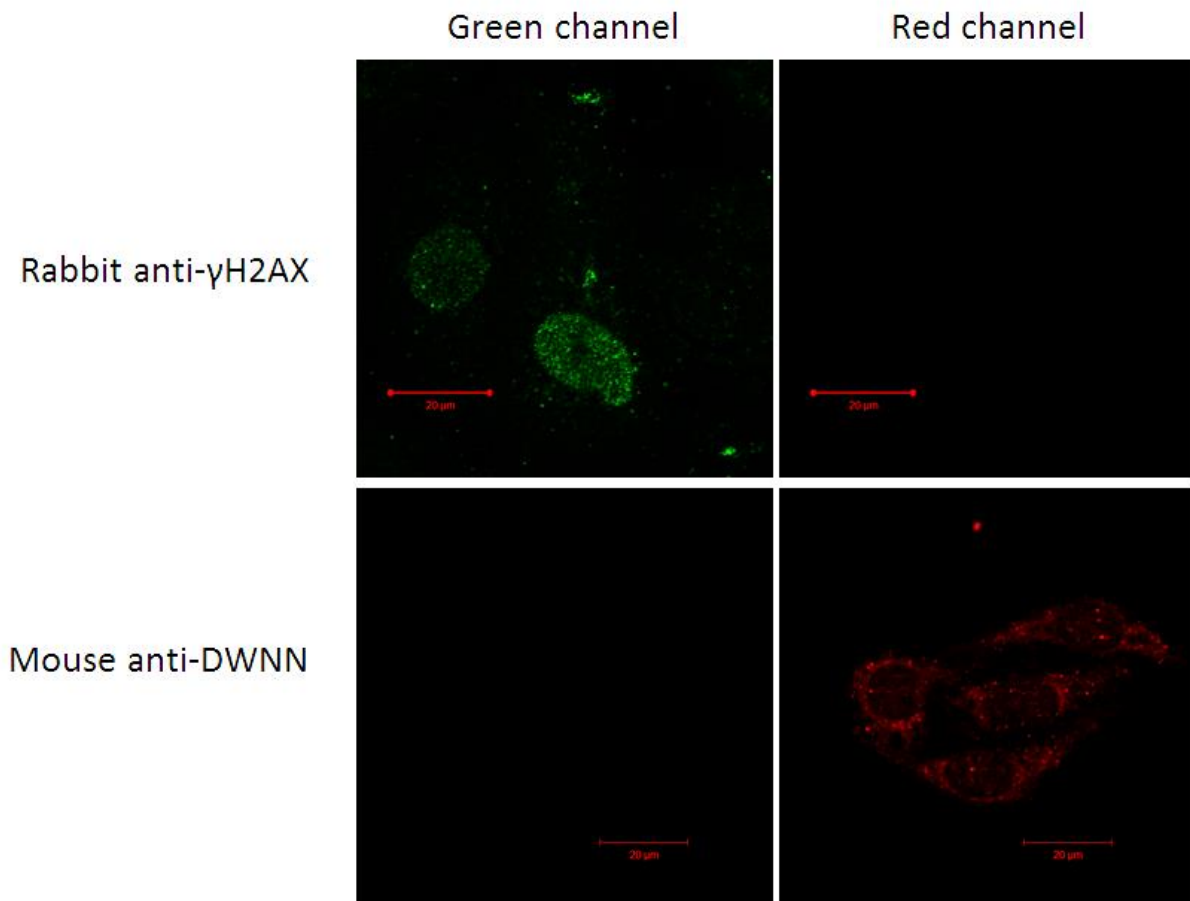


Figure 3.34 Bleed-through controls and non-specific secondary antibody controls. The rabbit anti- γ H2AX antibody produces strong signal in the green channel but none in the red channel, despite being incubated with both secondary antibodies (anti-mouse Cy3 and anti-rabbit Alexa488). This shows that there is no signal in the red channel resulting from either bleed-through or non-specific secondary antibody binding. γ H2AX is found only in the nucleus of these cisplatin-stressed cells, consistent with what is seen in Figure 3.33 above. Similarly, mouse-DWNN shows strong signal in the red channel but none in the green channel. The DWNN signal is nuclear and cytoplasmic, with nuclear speckles visible.

Despite both γ H2AX and isoform 3 being punctate nuclear signals after cell stress, visual analysis (Figure 3.35) shows that the two signals do not colocalise and in fact appear to be almost mutually exclusive. Quantitative analysis using JaCoP for ImageJ confirmed these visual results, with average values for M1 and M2 of 0.2 ± 0.06 and 0.12 ± 0.7 respectively, indicating very little colocalisation between the two channels.

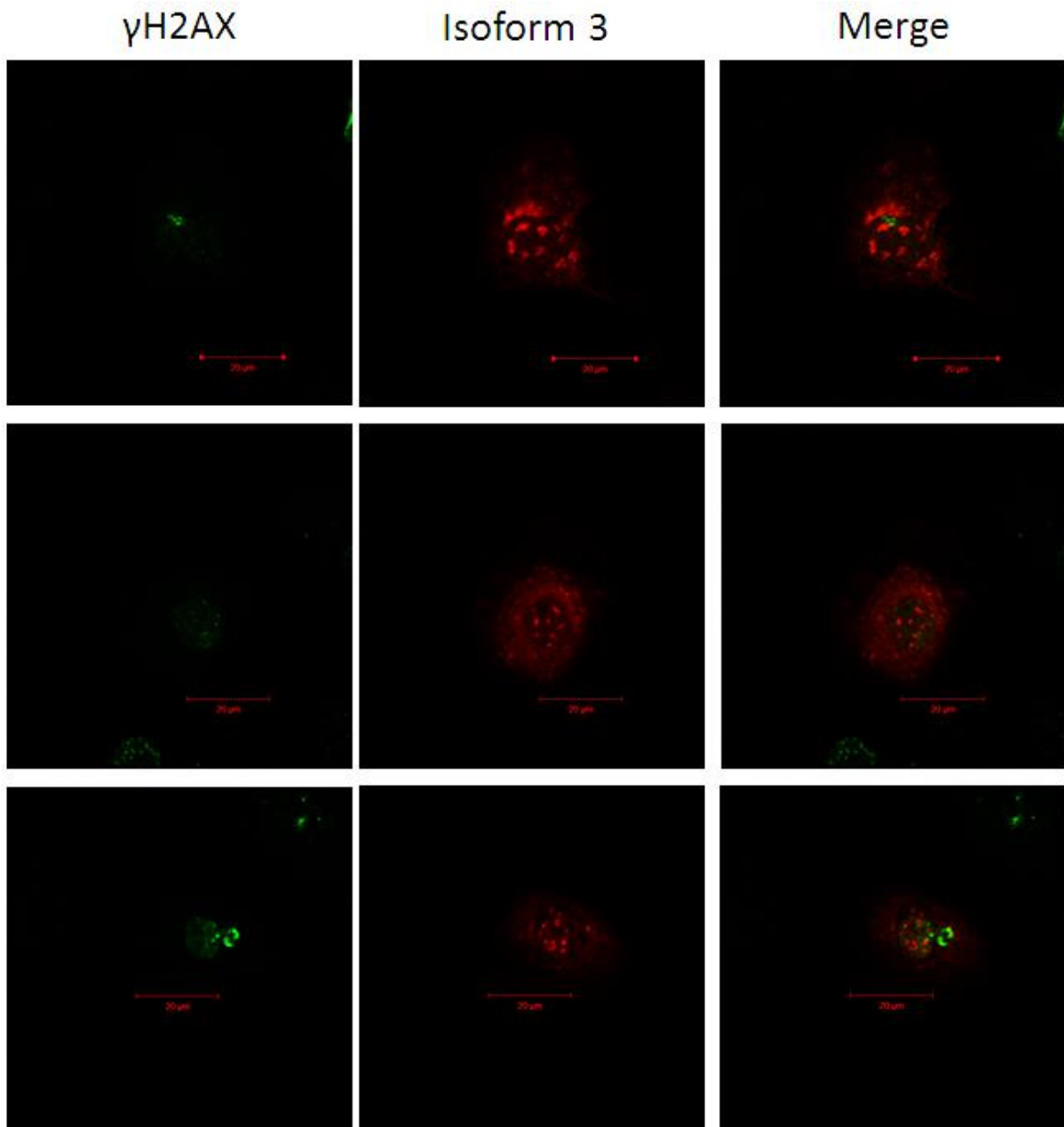


Figure 3.35 Stressed A549 stained with rabbit polyclonal anti- γ H2AX (green) and mouse monoclonal anti-DWNN (red) as well as a merge showing the lack of colocalisation between the two. Cells were stressed using DNA damage caused by 0.6 μ g/ml cisplatin (Sigma) for 1 hour before fixing the cells.

CHAPTER 4 DISCUSSION

RBBP6 is a complex protein that has been implicated in a number of functions in the cell, and has been shown to interact with some of the key players of proliferation, apoptosis and transcriptional control. Unravelling the role of this multifunctional protein in the cell is challenging, made even more so by the fact that the protein is expressed as a number of isoforms that potentially have differing localisations and roles. Knowing where the protein localises, both in unstressed and stressed cells, provides insight into the role of RBBP6. This study provides a sturdy base from which further studies can be derived.

4.1 ISOFORM 3 OF RBBP6 TRANSLOCATES TO NUCLEAR SPECKLES FOLLOWING STRESS

4.1.1 LOCALISATION OF RBBP6 ISOFORMS IN THE CELL, AND THE EFFECT OF CELL STRESS ON THE LOCALISATION OF THESE PROTEINS

A mouse monoclonal antibody and a rabbit polyclonal antibody raised against the N-terminal DWNN domain of RBBP6 were used to investigate the localisation of isoforms 1 and 3 of endogenous RBBP6. The two antibodies were verified using Western blots and peptide blocking to confirm specificity to the DWNN domain. Both antibodies were able to detect a 10 kDa band that disappeared after peptide blocking of the antibodies, suggesting that any signal detected by these antibodies was specific for the DWNN domain of RBBP6. Higher molecular weight bands, such as a 200 kDa band corresponding to isoform 1, have been historically difficult to detect using Western blot using the two antibodies under discussion, particularly when using cell lysates of various cell lines, including HeLa and A549. This may be due to a combination of the low concentration of isoform 1 in the cell and much higher concentration of isoform 3 which may potentially sequester the antibody. These assumptions about the relative concentrations are borne out in the subsequent immunofluorescence experiment where isoform 3 consistently gives a higher signal than isoform 1.

Similar levels of endogenous protein were observed in both the nucleus and the cytoplasm in resting cells with some light speckling in the nucleus, but the nuclear signal increased dramatically and rapidly after the cells were subjected to either heat shock or DNA damage. In particular the intensity of signal increased most dramatically in the punctate bodies in the

nucleus within a short period of time.

The effects of these two types of damage on the cell are known to be very different from each other, and the cellular responses to them are correspondingly different. DNA damage occurs when DNA strands form lesions caused by mismatched nucleotides that inhibit subsequent replication or translation of the strand. The DNA damage repair system targets these lesions and breaks the strands apart, correcting the mismatched nucleotides and restoring replication and transcription activity to the strand. Heat shock, on the other hand, targets proteins and denatures them, resulting in non-functional and misfolded proteins. Heat shock generates a heat shock response, which includes the expression of chaperones known as heat shock proteins which target misfolded proteins and signal their destruction. It is notable that the presence of both these types of damage can trigger the translocation of endogenous RBBP6 from the cytoplasm to the nucleus, and do so despite heat shock and DNA damage having such different repair pathways.

In the initial experiments, a mouse monoclonal antibody targeting the DWNN domain of full-length RBBP6 was used. As this antibody was specific for the DWNN domain and did not target any other part of the protein, it would be expected to detect both isoform 3 - which is the independently expressed DWNN domain - as well as full-length RBBP6. This made it impossible to decide which of the two isoforms (or both) was being shuttled to the nucleus following cell stress. As the two primary isoforms, namely isoform 1 and isoform 3, are very distinct in structure and function, it was important to differentiate between the localisation and cell stress response of these two isoforms.

This differentiation between isoforms 1, 2 and 4 and isoform 3 was performed through the use of an antibody specifically against isoforms 1, 2 and 4 as well as the use of exogenously expressed HA-constructs of the two isoforms. The commercial mouse monoclonal LS-C133084 antibody showed an exclusively nuclear localisation that did not respond or increase in intensity following either DNA damage or heat shock. This antibody detects isoforms 1, 2 and 4 but does not detect isoform 3. From this it can be inferred that isoform 3 is responsible for the cytoplasmic signal seen in the mouse monoclonal anti-DWNN staining and that isoform 3 is responsible for the increase in nuclear intensity following cell stress. These findings were supported by exogenous expression of HA-tagged isoform 1 and isoform 3, where both isoforms 1 and 3 showed punctate nuclear localisation, but only isoform 3 demonstrates a significant increase in nuclear intensity following cell stress.

4.12 CHARACTERISATION OF THE STRESS EFFECT

It was important to distinguish whether the increase of nuclear signal after cell stress was due to *de novo* protein synthesis or whether the proteins were being imported from the cytoplasm into the nucleus. A time course experiment confirmed that the increase in signal occurred rapidly, suggesting that it was not the result of *de novo* protein synthesis, which takes hours to effect significant changes in protein populations (Duncan and Hershey 1984). Cycloheximide, which blocks protein synthesis, was used to confirm this conclusion. As cycloheximide is also a stressor, disrupting the functioning of the cell, we also ensured that there was a negative control in place to ensure that any increase in intensity was not due to cycloheximide acting as a cell stressor but rather due to the heat shock or DNA damage stress to which we intentionally subjected the cells. Cycloheximide treatment did not produce any visible stress effect on the cells and alone did not induce increase of RBBP6 nuclear intensity. Thus, inhibition of protein synthesis showed that the increase in intensity was due to translocation of already existing protein from the cytoplasm to the nucleus, where it then accumulated in punctate structures. Our results using the HA-tagged isoform 3 confirm that the increase in nuclear signal is due to translocation and not an effect of transcriptional control.

The question arises as to whether this translocation of isoform 3 is specific to one type of mammalian cell type or to transformed or otherwise disrupted cells. In order to investigate this question, a panel of cancer cell lines and non-cancerous cell lines was stained with monoclonal mouse anti-DWNN and tested for the translocation effect. All cell lines tested, with the exception of HepG2, displayed significantly increased nuclear signal following cell stress. Our initial experiments regarding the characterization of the cell stress effect on localisation of the various isoforms of RBBP6 were done in HeLa cells, while subsequent experiments were conducted in A549 cells, partially due to the availability of A549 cells and partially due to the fact that A549 cells were more visually defined and striking in appearance, making analysis of images easier and more reliable. As heat shock time and UV exposure were optimised for HeLa cells, we used this as a starting point in the A549 experiments to generate the cell stress phenomenon. After subjecting the A549 cells to the same cell stress parameters, we noted a similar result as in the original HeLa experiments, and thus decided not to optimise these parameters further. At this point it is uncertain whether this lack of translocation in HepG2 cells is due to the protein behaving differently in these cells - HepG2 has been shown to overexpress full-length RBBP6 (Mbita and Dlamini 2006), and this may have some sort of inhibitory role on the translocation of isoform 3 - or the lack of optimisation of UV damage parameters. Further experiments with this cell line would add some needed clarity on the topic. However, all other cell lines examined showed clear signs of the translocation effect, suggesting that this effect is not limited to HeLa

and A549 cells and that in most cases the effect can be induced by the same cell stress parameters.

4.1.3 ISOFORM 3 LOCALISES TO NUCLEAR SPECKLES FOLLOWING CELLSTRESS

A variety of different types of punctate bodies are found in the nucleus, encompassing a wide range of different functions. As isoform 3 occupied punctate bodies within the nucleus, we wished to investigate which type of bodies these were. A large variety of punctate structures are present in the nucleus, including Cajal bodies, paraspeckles, and polycomb bodies, each with a different function. Nuclear speckles, also known as SC35 domains due to the presence of the splicing factor SC35 (Spector, Fu, and Maniatis 1991), are punctate bodies in the nucleus that have been implicated in DNA damage repair as well as in mRNA processing (Sacco-Bubulya and Spector 2002, Campalans *et al.* 2007). Due to their implicated role in mRNA processing it would make sense for isoform 3 to localise to these bodies and they were thus chosen for the first target of colocalisation. It should be noted that the colocalisation study between SC35 (the nuclear speckle marker) and isoform 3 was not intended as an interaction study, but as a study to determine the nuclear localisation of isoform 3. Colocalisation analysis showed that isoform 3 localises in the same bodies as SC35 both before and after cell stress, with more intense isoform 3 signal after cell stress and we can therefore conclude that isoform 3 localises to nuclear speckles in the nucleus.

Since RBBP6 is known to interact with components of the spliceosome and other factors involved in mRNA processing, it is possible that isoform 3 translocates to nuclear speckles as part of the cellular stress response. The question then arises as to which proteins isoform 3 interacts with once in nuclear speckles, which will be further discussed in Section 4.3.

4.2 RBBP6 ISOFORMS DO NOT LOCALISE TO SITES OF DNA DAMAGE

DNA repair protein, hOGG1, is involved in base-excision repair and localises to nuclear speckles in response to UV DNA damage (Campalans *et al.* 2007). Many DNA repair proteins, normally soluble in the nucleoplasm, are reorganised in sub-nuclear foci after induction of DNA damage (Campalans *et al.* 2007). RBBP6 has been implicated in DNA stability and replication through its interaction with ZBTB38, a transcriptional repressor (Miotto *et al.* 2014). RBBP6 ubiquitinates ZBTB38 and promotes its degradation, allowing for replication factor MCM10 to stabilise the genome and promote replication elongation. Cells where RBBP6 was depleted showed increased amounts of DNA damage and slower replication fork progression (Miotto *et al.* 2014).

We wished to examine if, apart from localising to nuclear speckles, it was possible that some portion of isoform 3 localised directly to sites of DNA damage. The colocalisation analysis showed conclusively that γ H2AX does not colocalise with isoform 3, indicating that isoform 3 does not localise directly to sites of double-stranded DNA breaks.

4.3 IMPLICATIONS FOR THE FUNCTION OF RBBP6

This study used immunofluorescence to determine the localisation of both isoform 1 and isoform 3 of RBBP6 and to generate insights into the functional role that the protein plays in the cell. Previous studies have focused on the role of RBBP6 as an E3 ligase, but the functional role of isoform 3 is still a source of conjecture that requires further study.

Recent evidence shows that RBBP6 is involved in 3'-end mRNA processing, associating with CstF factors through the DWNN domain (Di Giammartino *et al.* 2014). A potential model of RBBP6 transcriptional control emerges in which, when isoform 1 levels are normal, 3'-end processing occurs as normal. When levels of isoform 3 increase, they outcompete isoform 1 binding to CstF-64, resulting in reduced mRNA processing efficiency of RBBP6-mediated transcripts. Thus, more conserved and distal poly(A) sites are used in 3'-end processing and if these sites are not available the pre-mRNA is degraded by the exosome, leading to decreased levels of RBBP6-mediated transcripts.

Importantly, CstF-64 and other splicing machinery has been shown to localise to nuclear speckles (Saitoh *et al.* 2004), providing the link between the role of RBBP6 in 3'-end processing and the localisation of RBBP6 to nuclear speckles. This data provides with a model for the function of increased levels of isoform 3 in nuclear speckles during cell stress.

The proteins necessary for the cell during and after cell stress must be given priority, and the expression of other proteins must be reduced. Proliferation factors, such as isoform 1, must be inhibited. It may be possible that isoform 1 reduces the expression of proteins needed for cell proliferation and normal cell function, which is then outcompeted by nuclear isoform 3 during times of cell stress in order to express proteins vital to recovery through the modulation of 3'-end processing.

Saitoh *et al.* also show proteins not linked to mRNA processing are also found in nuclear speckles, including heat shock factor Hsp70. As isoform 3 levels rise in the nucleus following heat shock, another mechanism may be at play in addition to the mRNA 3'-end processing scenario described above. However, we did not have the time to conduct colocalisation experiments of RBBP6 with Hsp70 and we can make no further suppositions based on the data that we currently have.

Another important question that needs to be raised is the mechanism by which isoform 3 moves to the nucleus. Does it covalently attach to a carrier protein or does it form part of a non-covalent complex? The ubiquitin-like structure of the DWNN domain, the presence of the GlyGly motif at its C-terminus and the fact that it is independently expressed in cells suggest that isoform 3 may play the role of a ubiquitin-like modifier (Pugh *et al.* 2006; Mbita *et al.* 2012) in which case a protein that shows stress-related nuclear translocation, such as YB-1 or MDM2 could act as potential carrier protein into the nucleus. It is also possible that isoform 3 itself plays the role of speckle-targeting domain, similar to the ubiquitin-like domain of SAP18 which translocates independently to nuclear speckles without the need for a traditional SR domain (Singh *et al.* 2010).

Regardless of the mechanism for isoform 3 translocation, we have shown that it occurs very rapidly in response to a range of cell stresses, with low levels of stress being sufficient to trigger the response. Only 5 minutes at 42 °C was sufficient to induce the stress response which is considerably less extreme than used in other studies. Taken together the above suggest that translocation of isoform 3 plays a fundamental role in the very earliest response of the cell to stress.

4.4 OUTLOOK

To address and strengthen our current conclusions, there are some potential future experiments that would address the ambiguous nature of the variety of isoforms of RBBP6. While we took on face value the specificity of the commercial mouse monoclonal antibody C133084, the antibody verification described in Section 3.2 would be important to identify precisely which isoforms are targeted by this antibody, as well as ensuring its specificity. The antibody verification of the two anti-DWNN proteins could also be optimised to produce clearer and more convincing results, particularly with regards to the visualization of the larger 200 kDa protein.

As both isoforms 3 and isoforms 1, 2 and 4 show up as punctate bodies in the nucleus, a colocalisation of these isoforms using the anti-DWNN antibodies and the commercial mouse antibody C133084 may provide insight as to whether 1,2 and 4 and isoform 3 share a similar localisation in the cell. By conducting this colocalisation experiment with stressed and unstressed cells, we may also test the validity of our assertion that it is only isoform 3 that is involved in the translocation effect.

We may also use our HA-constructs – which we have shown to behave in a similar manner to the endogenous proteins – to further expand on our initial work on the colocalisation between isoform 3 and SC35. By using either the HA-isoform 1 or HA-isoform 3 construct, we would be able to conclusively determine which of these isoforms localises to nuclear speckles following cell stress.

In addition, while we optimised the heat shock and DNA damage conditions for HeLa cells, these conditions were subsequently not optimised for other cell lines. The reason for this was because through using the optimised parameters for HeLa cells in other cell lines, we were able to generate the same translocation effect in these cell lines and these parameters were deemed sufficient to generate the translocation effect. There may be times when such extrapolation is ineffective, perhaps as in the case of HepG2, and it would be useful to generate such optimised parameters for all cell lines used in subsequent studies.

This study has laid the foundations for understanding the functions of RBBP6 and isoform 3 in the cell, but further investigations are needed to flesh out and expand on our findings.

HSF-1 has been shown to form bodies within the nucleus following cell stress and it would be useful to further investigate the interaction of isoform 3 with heat shock proteins following cell stress through colocalisation or interaction studies such as co-immunoprecipitation. This may provide us with additional information about the role of isoform 3 in the cellular response pathway.

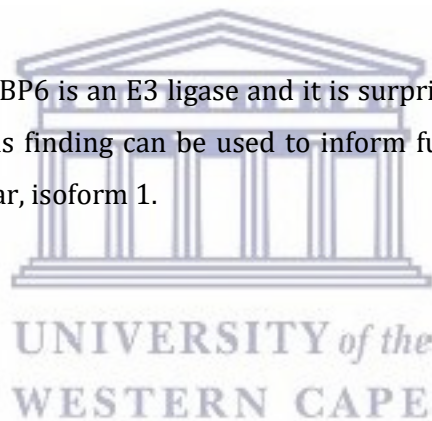
It is clear that isoform 3 plays an important role in cell stress recovery. This could be further investigated by knock-down assays of isoform 3, isoform 1 and both isoform 1 and 3 and the

impact these knock downs have on the ability of cells to recover from heat shock or DNA damage.

Currently we do not have concrete evidence that isoform 1 localises to nuclear speckles. While it appears to share the same localisation as isoform 3, a formal colocalisation study between isoform 1 and nuclear speckles needs to be performed to confirm this speculation. This colocalisation would further strengthen our model of isoform 3 modulating cell stress response through the inhibition of isoform 1-mediated 3'-end processing of proliferation proteins at nuclear speckles.

Our study of RBBP6 focused on the nuclear role of primarily isoform 3. However, isoform 3 is also detected in the cytoplasm of both resting and stressed cells. As isoform 3 has implicated in ubiquitin-like functions, there is plenty of scope into an investigation into its cytoplasmic role.

We know that isoform 1 of RBBP6 is an E3 ligase and it is surprising that this isoform was not detected in the cytoplasm. This finding can be used to inform further studies of the E3 ligase activities of RBBP6, in particular, isoform 1.



CHAPTER 5 REFERENCES

- Aboussekhra A. *et al.*, 1992. Semidominant suppressors of Srs2 helicase mutations of *Saccharomyces cerevisiae* map in the RAD51 gene, whose sequence predicts a protein with similarities to procaryotic RecA proteins. *Molecular and Cellular Biology*, 12(7), pp.3224–3234.
- Akerfelt, M., Morimoto, R.I. & Sistonon, L., 2010. Heat shock factors: integrators of cell stress, development and lifespan. *Nature reviews: Molecular Cell Biology*, 11(8), pp.545–555.
- Alves-Rodrigues, A., Gregori, L. & Figueiredo-Pereira, M.E., 1998. Ubiquitin, cellular inclusions and their role in neurodegeneration. *Trends in Neurosciences*, 21(12), pp.516–520.
- Ashburner, M. & Bonner, J.J., 1979. The induction of gene activity in drosophila by heat shock. *Cell*, 17(2), pp.241–254.
- Bachant, J. *et al.*, 2002. The SUMO-1 isopeptidase Smt4 is linked to centromeric cohesion through SUMO-1 modification of DNA topoisomerase II. *Molecular Cell*, 9(6), pp.1169–82..
- Bai, C. *et al.*, 1996. SKP1 Connects Cell Cycle Regulators to the Ubiquitin Proteolysis Machinery through a Novel Motif, the F-Box. *Cell*, 86(2), pp.263–274.
- Baler, R., Dahl, G. & Voellmy, R., 1993. Activation of human heat shock genes is accompanied by oligomerization, modification, and rapid translocation of heat shock transcription factor HSF1. *Molecular and Cellular Biology*, 13(4), pp.2486–2496.
- Barends, T.R.M., Werbeck, N.D. & Reinstein, J., 2010. Disaggregases in 4 dimensions. *Current Opinion in Structural Biology*, 20(1), pp.46–53.
- Barlow, P.N. *et al.*, 1994. Structure of the C3HC4 domain by 1H-nuclear magnetic resonance spectroscopy. A new structural class of zinc-finger. *Journal of Molecular Biology*, 237(2), pp.201–11.
- Bartek, J. & Lukas, J., 2007. DNA damage checkpoints: from initiation to recovery or adaptation. *Current Opinion in Cell Biology*, 19(2), pp.238–245.
- Basu, A. & Krishnamurthy, S., 2010. Cellular responses to Cisplatin-induced DNA damage. *Journal of Nucleic Acids*, pp. 238-245.
- Bernard, D. *et al.*, 2010. A long nuclear-retained non-coding RNA regulates synaptogenesis by modulating gene expression. *The EMBO Journal*, 29(18), pp.3082–3093.
- de Bie, P. & Ciechanover, A., 2011. Ubiquitination of E3 ligases: self-regulation of the ubiquitin system via proteolytic and non-proteolytic mechanisms. *Cell Death and Differentiation*, 18(9), pp.1393–1402.
- Bolte, S. & Cordelières, F., 2006. A guided tour into subcellular colocalisation analysis in light microscopy. *Journal of Microscopy*, 224(3), pp.213–232.

- Bond, U., 1988. Heat shock but not other stress inducers leads to the disruption of a sub-set of snRNPs and inhibition of in vitro splicing in HeLa cells. *The EMBO Journal*, 7(11), pp.3509–3518.
- Borden, K.L. *et al.*, 1995. The solution structure of the RING finger domain from the acute promyelocytic leukaemia proto-oncoprotein PML. *The EMBO Journal*, 14(7), pp.1532–1541.
- Brede, G., Solheim, J. & Prydz, H., 2002. PSKH1, a novel splice factor compartment-associated serine kinase. *Nucleic Acids Research*, 30(23), pp.5301–5309.
- Bregman, D. *et al.*, 1995. Transcription-dependent redistribution of the large subunit of RNA polymerase II to discrete nuclear domains. *The Journal of Cell Biology*, 129(2), pp.287–98.
- Brown, J. *et al.*, 2008. Association between active genes occurs at nuclear speckles and is modulated by chromatin environment. *The Journal of Cell Biology*, 182(6), pp.1083–1097.
- Bukau, B., Hesterkamp, T. & Luirink, J., 1996. Growing up in a dangerous environment: a network of multiple targeting and folding pathways for nascent polypeptides in the cytosol. *Trends in Cell Biology*, 6(12), pp.480–486.
- Burroughs, M. *et al.*, 2008. Anatomy of the E2 ligase fold: implications for enzymology and evolution of ubiquitin/Ub-like protein conjugation. *Journal of Structural Biology*, 162(2), pp.205–208.
- Cáceres, J. *et al.*, 1997. Role of the modular domains of SR proteins in subnuclear localisation and alternative splicing specificity. *The Journal of Cell Biology*, 138(2), pp.225–38.
- Campalans, A. *et al.*, 2007. UVA irradiation induces relocalisation of the DNA repair protein hOGG1 to nuclear speckles. *Journal of Cell Science*, 120, pp.23–32.
- Campigli di Giammartino, D. *et al.*, 2014. RBBP6 isoforms regulate the human polyadenylation machinery and modulate expression of mRNAs with AU-rich 3' UTRs. *Genes and Development* 28, pp.2248–2260.
- Cashikar, A.G., Duennwald, M. & Lindquist, S.L., 2005. A chaperone pathway in protein disaggregation: HSP26 alters the nature of protein aggregates to facilitate reactivation by HSP104. *Journal of Biological Chemistry*, 280(25), pp.23869–23875.
- Chen, D. *et al.*, 2005. ARF-BP1/Mule is a critical mediator of the ARF tumor suppressor. *Cell*, 121(7), pp.1071–83.
- Chen, J. *et al.*, 2013. Overexpression of RBBP6, alone or combined with mutant TP53, is predictive of poor prognosis in colon cancer. *PLoS One*, 8(6), pp.1–9.
- Chen, P.L. *et al.*, 1998. The BRC repeats in BRCA2 are critical for RAD51 binding and resistance to methyl methanesulfonate treatment. *Proceedings of the National Academy of Sciences*, 95(9), pp.5287–5292.
- Chen, Z. *et al.*, 1990. A 25 kDa, Kilodalton ubiquitin Chain Ubiquitin Synthesis Carrier Protein via

- Lysine 48 of Ubiquitin. *Journal of Biological Chemistry*, 265(35), pp.21835–21842.
- Chen, Z.J., 2005. Ubiquitin signalling in the NF-kappaB pathway. *Nature Cell Biology*, 7(8), pp.758–65.
- Chesnoy, S. & Huang, L., 2000. Structure and function of lipid-DNA complexes for gene delivery. *Annual Review of Biophysics and Biomolecular Structure*, 29, pp.27–47.
- Chibi, M. *et al.*, 2008. RBBP6 interacts with multifunctional protein YB-1 through its RING finger domain, leading to ubiquitination and proteosomal degradation of YB-1. *Journal of Molecular Biology*, 384(4), pp.908–16.
- Christensen, D.E. & Klevit, R.E., 2009. Dynamic interactions of proteins in complex networks: identifying the complete set of interacting E2s for functional investigation of E3-dependent protein ubiquitination. *The FEBS Journal*, 276(19), pp.5381–9.
- Cimprich, K.A. & Cortez, D., 2008. ATR: an essential regulator of genome integrity. *Nature reviews. Molecular cell biology*, 9(8), pp.616–27.
- Cmarko, D. *et al.*, 1999. Ultrastructural analysis of transcription and splicing in the cell nucleus after bromo-UTP microinjection. *Molecular Biology of the Cell*, 10(1), pp.211–23.
- Colwill, K. *et al.*, 1996. The Clk/Sty protein kinase phosphorylates SR splicing factors and regulates their intranuclear distribution. *The EMBO Journal*, 15(2), pp.265–275.
- Conaway, R.C., Brower, C.S. & Conaway, J.W., 2002. Emerging roles of ubiquitin in transcription regulation. *Science* 296(5571), pp.1254–1258.
- Costes, S. V *et al.*, 2004. Automatic and quantitative measurement of protein-protein colocalisation in live cells. *Biophysical Journal*, 86(6), pp.3993–4003.
- Cotto, J., Fox, S. & Morimoto, R., 1997. HSF1 granules: a novel stress-induced nuclear compartment of human cells. *Journal of Cell Science*, 110 (2), pp.2925–2934.
- Coverley, D.A., 1992. A role for the human single-stranded DNA binding protein HSSB/RPA in an early stage of nucleotide excision repair. *Nucleic Acids Research*, 20(15), pp.3873–3880.
- D'Amico, S. *et al.*, 2006. Psychrophilic microorganisms: challenges for life. *EMBO reports*, 7(4), pp.385–9.
- David, Y. *et al.*, 2011. E3 ligases determine ubiquitination site and conjugate type by enforcing specificity on E2 enzymes. *Journal of Biological Chemistry*, 286(51), pp.44104–44115.
- David, Y. *et al.*, 2010. The E2 ubiquitin-conjugating enzymes direct polyubiquitination to preferred lysines. *Journal of Biological Chemistry*, 285(12), pp.8595–8604.
- Demple, B., Herman, T. & Chen, D.S., 1991. Cloning and expression of APE, the cDNA encoding the major human apurinic endonuclease: definition of a family of DNA repair enzymes. *Proceedings of the National Academy of Sciences*, 88(24), pp.11450–11454.
- Deshaies, R., 1999. SCF and Cullin/Ring H2-based ubiquitin ligases. *Annual Review of Cell and Developmental Biology*, 15, pp.435–467.

- Dizdaroglu, M., 1992. Oxidative damage to DNA in mammalian chromatin. *Mutation Research/DNAging*, 275(3-6), pp.331-342.
- Dodson, M.L., Michaels, M.L. & Lloyd, R.S., 1994. Unified catalytic mechanism for DNA glycosylases. *Journal of Biological Chemistry*, 269(52), pp.32709-32712.
- Dostie, J., Lejbkowitz, F. & Sonenberg, N., 2000. Nuclear eukaryotic initiation factor 4E (eIF4E) colocalises with splicing factors in speckles. *The Journal of Cell Biology*, 148(2), pp.239-247.
- Duncan, R. & Hershey, J.W.B., 1984. Heat Shock-induced Translational Alterations in HeLa cells. *The Journal of Biological Chemistry*, 259(19), pp.11882-11889.
- Dunn, K.W., Kamocka, M.M. & McDonald, J.H., 2011. A practical guide to evaluating colocalisation in biological microscopy. *American Journal of Physiology*, 300(4), pp.C723-C742.
- Eilbracht, J. & Schmidt-Zachmann, M., 2001. Identification of a sequence element directing a protein to nuclear speckles. *Proceedings of the National Academy of Sciences*, 98(7), pp.3849-3854.
- Eisen, M.B. *et al.*, 1998. Cluster analysis and display of genome-wide expression patterns. *Proceedings of the National Academy of Sciences*, 95(25), pp.14863-14868.
- Eperon, I.C. *et al.*, 1993. Pathways for selection of 5' splice sites by U1 snRNPs and SF2/ASF. *The EMBO Journal*, 12(9), pp.3607-17.
- Fakan, S., 1994. Perichromatin fibrils are in situ forms of nascent transcripts. *Trends in Cell Biology*, 4(3), pp.86-90.
- Friend, S. *et al.*, 1986. A human DNA segment with properties of the gene that predisposes to retinoblastoma and osteosarcoma. *Letters to Nature*, 323, pp.643-646.
- Frigerio, J.M. *et al.*, 1995. Analysis of 2166 clones from a human colorectal cancer cDNA library by partial sequencing. *Human Molecular Genetics*, 4(1), pp.37-43.
- Frosina, G. *et al.*, 1996. Two pathways for base excision repair in mammalian cells. *The Journal of Biological Chemistry*, 271(16), pp.9573-9578.
- Frydman, J., 1997. Chaperones get in touch: the Hip-Hop connection. *Trends in Biochemical Sciences*, 22(3), pp.87-92.
- Frydman, J. *et al.*, 1994. Folding of nascent polypeptide chains in a high molecular mass assembly with molecular chaperones. *Nature*, 370(6485), pp.111-7.
- Fu, X., 1995. The superfamily of arginine/serine-rich splicing factors. *RNA*, 1, pp.663-680.
- Ganoth, D. *et al.*, 1988. A multicomponent system that degrades proteins conjugated to ubiquitin. Resolution of factors and evidence for ATP-dependent complex formation. *Journal of Biological Chemistry*, 263(25), pp.12412-12419.
- Gao, S. & Scott, R.E., 2002. P2P-R protein overexpression restricts mitotic progression at prometaphase and promotes mitotic apoptosis. *Journal of Cellular Physiology*, 193(2),

pp.199–207.

- Gao, S. & Scott, R.E., 2003. Stable overexpression of specific segments of the P2P-R protein in human MCF-7 cells promotes camptothecin-induced apoptosis. *Journal of Cellular Physiology*, 197(3), pp.445–452.
- Gao, S., Witte, M. & Scott, R., 2002. P2P-R protein localises to the nucleolus of interphase cells and the periphery of chromosomes in mitotic cells which show maximum P2P-R immunoreactivity. *Journal of Cellular Physiology*, 191(2), pp.145–54.
- Gasch, a P. *et al.*, 2000. Genomic expression programs in the response of yeast cells to environmental changes. *Molecular Biology of the Cell*, 11(12), pp.4241–4257.
- Giaever, G. *et al.*, 2002. Functional profiling of the *Saccharomyces cerevisiae* genome. *Nature*, 418(6896), pp.387–91.
- Girard, C. *et al.*, 2012. Post-transcriptional spliceosomes are retained in nuclear speckles until splicing completion. *Nature Communications*, 3, p.994.
- Goloubinoff, P. *et al.*, 1999. Sequential mechanism of solubilization and refolding of stable protein aggregates by a bichaperone network. *Proceedings of the National Academy of Sciences*, 96(24), pp.13732–13737.
- Goodhead, D.T., 1989. The initial physical damage produced by ionizing radiations. *International Journal of Radiation Biology* 56(5) pp. 623-634.
- Gottlieb, T.M. & Jackson, S.P., 1993. The DNA-dependent protein kinase: Requirement for DNA ends and association with Ku antigen. *Cell*, 72(1), pp.131–142.
- Gragerov, a I. *et al.*, 1991. Protein aggregation and inclusion body formation in *Escherichia coli* rpaH mutant defective in heat shock protein induction and inclusion body formation. *FEBS Letters*, 291(2), pp.222–224.
- Grallert, H. & Buchner, J., 2001. Review: a structural view of the GroE chaperone cycle. *Journal of Structural Biology*, 135(2), pp.95–103.
- Grande, M. *et al.*, 1997. Nuclear distribution of transcription factors in relation to sites of transcription and RNA polymerase II. *Journal of Cell Science*, 110, pp.1781–1791.
- Greenblatt, M.S. *et al.*, 1994. Mutations in the p53 Tumor Suppressor Gene : Clues to Cancer Etiology and Molecular Pathogenesis. *Cancer Research*, 54, pp.4855–4878.
- Greinert, R. *et al.*, 2012. UVA-induced DNA double-strand breaks result from the repair of clustered oxidative DNA damages. *Nucleic Acids Research*, 40(20), pp.10263–73.
- Hainaut, P. *et al.*, 1998. IARC Database of p53 gene mutations in human tumors and cell lines: updated compilation, revised formats and new visualisation tools. *Nucleic Acids Research*, 26(1), pp.205–213.
- Hershko, A. *et al.*, 1983. Components of Ubiquitin-Protein Ligase System. *The Journal of Biological Chemistry*, 258(13), pp.8206–8214.

- Hessling, M., Richter, K. & Buchner, J., 2009. Dissection of the ATP-induced conformational cycle of the molecular chaperone Hsp90. *Nature Structural & Molecular Biology*, 16(3), pp.287–93.
- Hochstrasser, M., 2000. Evolution and function of ubiquitin-like protein-conjugation systems. *Nature Cell Biology*, 2(8), pp.153–7.
- Hochstrasser, M., 1996. Ubiquitin-dependent protein degradation. *Annual Review of Genetics*, 30(93), pp.405–39.
- Hock, R. *et al.*, 1998. Dynamic relocation of chromosomal protein HMG-17 in the nucleus is dependent on transcriptional activity. *The EMBO Journal*, 17(23), pp.6992–7001.
- Hoeller, D., Hecker, C.-M. & Dikic, I., 2006. Ubiquitin and ubiquitin-like proteins in cancer pathogenesis. *Nature Reviews. Cancer*, 6(10), pp.776–88.
- Hofmann, R.M. & Pickart, C.M., 1999. Noncanonical MMS2-encoded ubiquitin-conjugating enzyme functions in assembly of novel polyubiquitin chains for DNA repair. *Cell*, 96(5), pp.645–653.
- Honda, R., Tanaka, H. & Yasuda, H., 1997. Oncoprotein MDM2 is a ubiquitin ligase E3 for tumor suppressor p53. *FEBS Letters*, 420(1), pp.25–27.
- Horwich, A.L., Farr, G.W. & Fenton, W.A., 2006. GroEL-GroES-mediated protein folding. *Chemical Reviews*, 106(5), pp.1917–30.
- Hough, R., Pratt, G. & Rechsteiner, M., 1986. Ubiquitin-lysosome conjugates. Identification and characterization of an ATP-dependent protease from rabbit reticulocyte lysates. *Journal of Biological Chemistry*, 261(5), pp.2400–2408.
- Huang, L. *et al.*, 1999. Structure of an E6AP-UbcH7 complex: insights into ubiquitination by the E2-E3 enzyme cascade. *Science* 286(5443), pp.1321–6.
- Huang, S. *et al.*, 1994. In vivo analysis of the stability and transport of nuclear poly(A)⁺ RNA. *The Journal of Cell Biology*, 126(4), pp.877–8799.
- Huang, X. *et al.*, 2004. Assessment of histone H2AX phosphorylation induced by DNA topoisomerase I and II inhibitors topotecan and mitoxantrone and by the DNA cross-linking agent cisplatin. *Cytometry*. 58(2), pp.99–110.
- Huen, M.S.Y. & Chen, J., 2008. The DNA damage response pathways: at the crossroad of protein modifications. *Cell Research*, 18(1), pp.8–16.
- Hutchinson, J. *et al.*, 2007. A screen for nuclear transcripts identifies two linked noncoding RNAs associated with SC35 splicing domains. *BMC Genomics*, 8(39).
- Ischenko, A.A. & Sapparbaev, M.K., 2002. Alternative nucleotide incision repair pathway for oxidative DNA damage. *Nature*, 415(6868), pp.183–7.
- Jackson, S.P. & Bartek, J., 2009. The DNA-damage response in human biology and disease. *Nature*, 461(7267), pp.1071–1078.

- Jagatheesan, G. *et al.*, 1999. Colocalisation of intranuclear lamin foci with RNA splicing factors. *Journal of Cell Science*, 112, pp.4651–4661.
- Jagiello, I. *et al.*, 2000. Nuclear and subnuclear targeting sequences of the protein phosphatase-1 regulator NIPP1. *Journal of Cell Science*, 113, pp.3761–3768.
- Jakob, U. *et al.*, 1993. Small heat shock proteins are molecular chaperones. *The Journal of Biological Chemistry*, 268(3), pp.1517–1520.
- Jakob, U. *et al.*, 1995. Transient interaction of Hsp90 with early unfolding intermediates of citrate synthase: Implications for heat shock in vivo. *Journal of Biological Chemistry*, 270(13), pp.7288–7294.
- Jasin, M., 2002. Homologous repair of DNA damage and tumorigenesis: the BRCA connection. *Oncogene*, 21(58), pp.8981–8993.
- Jin, J. *et al.*, 2007. Dual E1 activation systems for ubiquitin differentially regulate E2 enzyme charging. *Nature*, 447(7148), pp.1135–8.
- Joazeiro, C. & Weissman, A., 2000. RING finger proteins: mediators of ubiquitin ligase activity. *Cell*, 102(5), pp.549–552.
- Johnson, C. *et al.*, 2000. Tracking COL1A1 RNA in osteogenesis imperfecta: splice-defective transcripts initiate transport from the gene but are retained within the SC35 domain. *The Journal of Cell Biology*, 150(3), pp.417–432.
- Jolly, C. *et al.*, 1997. HSF1 transcription factor concentrates in nuclear foci during heat shock: relationship with transcription sites. *Journal of Cell Science*, 110 (2), pp.2935–2941.
- Kappo, M. *et al.*, 2012. Solution structure of RING finger-like domain of retinoblastoma-binding protein-6 (RBBP6) suggests its functions as a U-box. *The Journal of Biological Chemistry*, 287(10), pp.7146–7158.
- Katz, J. & Marin, T., 1991. A Novel Cysteine-Ric sequence motif. *Cell*, 64, pp.483–484.
- Kee, Y. & Huibregtse, J.M., 2007. Regulation of Catalytic Activities of HECT Ubiquitin Ligases. *Biochemical and Biophysical Research Communications*, 354(2), pp.329–333.
- Kerscher, O., Felberbaum, R. & Hochstrasser, M., 2006. Modification of proteins by ubiquitin and ubiquitin-like proteins. *Annual Review of Cell and Developmental Biology*, 22, pp.159–80.
- Kim, H., Chen, J. & Yu, X., 2007. Ubiquitin-Binding Protein RAP80 Mediates BRCA1-Dependent DNA Damage Response. *Science*, 316(5828), pp.1202–1205.
- Kimura, H., Sugaya, K. & Cook, P., 2002. The transcription cycle of RNA polymerase II in living cells. *The Journal of Cell Biology*, 159(5), pp.777–782.
- Koike, K. *et al.*, 1997. Nuclear translocation of the Y-box binding protein by ultraviolet irradiation. *FEBS Letters*, 417(3), pp.390–394.
- Kojima, T. *et al.*, 2001. Cloning of human PRP4 reveals interaction with Clk1. *The Journal of Biological Chemistry*, 276(34), pp.32247–32256.

- Kriehuber, T. *et al.*, 2010. Independent evolution of the core domain and its flanking sequences in small heat shock proteins. *The FASEB Journal* 24(10), pp.3633–3642.
- Krokan, H.E., Standal, R. & Slupphaug, G., 1997. DNA glycosylases in the base excision repair of DNA. *Biochemistry Journal*, 325, pp.1–16.
- Kumar, S., Yoshida, Y. & Noda, M., 1993. Cloning of a cDNA which encodes a novel ubiquitin-like protein. *Biochemical and Biophysical Research Communications*, 195(1), pp.393–9.
- Lambowitz, A.M. *et al.*, 1983. Possible relationship of morphogenesis in pathogenic fungus, *Histoplasma capsulatum*, to heat shock response. *Nature*, 303(5920), pp.806–808.
- Lamond, A. & Earnshaw, W., 1998. Structure and function in the nucleus. *Science*, 280(5363), pp.547–553.
- Lamond, A.I. & Spector, D.L., 2003. Nuclear speckles: a model for nuclear organelles. *Nature Reviews: Molecular Cell Biology*, 4(8), pp.605–12.
- Larsson, S. *et al.*, 1995. Subnuclear localisation of WT1 in splicing or transcription factor domains is regulated by alternative splicing. *Cell*, 81(3), pp.391–401.
- Lavin, M.F., 2007. ATM and the Mre11 complex combine to recognize and signal DNA double-strand breaks. *Oncogene*, 26(56), pp.7749–7758.
- Lawrence, J.B., Carter, K.C. & Xing, X., 1993. Probing Functional Organization within the Nucleus: Is Genome Structure Integrated with RNA Metabolism? *Cold Spring Harbor Symposia on Quantitative Biology*, 58(0), pp.807–818.
- Lehmann, A., 1995. Nucleotide excision repair and the link with transcription. *Trends in Biochemical Sciences*, 20, pp.402–405.
- Li, L. *et al.*, 2007. PACT is a negative regulator of p53 and essential for cell growth and embryonic development. *Proceedings of the National Academy of Sciences of the United States of America*, 104(19), pp.7951–7956.
- Li, Q. *et al.*, 1999. Eukaryotic Translation Initiation Factor 4AIII (eIF4AIII) is functionally distinct from eIF4AI and eIF4AII. *Molecular and Cellular Biology*, 19(11), pp.7336–7346.
- Liakopoulos, D. *et al.*, 1998. A novel protein modification pathway related to the ubiquitin system. *EMBO Journal*, 17(8), pp.2208–2214.
- Lin, S. & Xiang-Dong, F., 2007. SR Proteins and Related Factors in Alternative Splicing. In B. Blencowe & B. Graveley, eds. *Alternative Splicing in the Postgenomic Era*.
- Lindahl, T. & Barnes, D.E., 2000. Repair of endogenous DNA damage. *Cold Spring Harbor Symposia on Quantitative Biology*, 65, pp.127–133.
- Lindquist, S., 1986. The heat-shock response. *Annual Review of Biochemistry*, 55, pp.1151–91.
- Lindquist, S., 1980. Varying patterns of protein synthesis in *Drosophila* during heat shock: Implications for regulation. *Developmental Biology*, 77(2), pp.463–479.
- Liu, J. *et al.*, 2002. NEDD8 Modification of CUL1 Dissociates p120CAND1, an Inhibitor of CUL1-

- SKP1 Binding and SCF Ligases. *Molecular Cell*, 10(6), pp.1511–1518.
- Lowe, J. *et al.*, 1990. Ubiquitin carboxyl-terminal hydrolase (PGP 9.5) is selectively present in ubiquitinated inclusion bodies characteristic of human neurodegenerative diseases. *The Journal of Pathology*, 161(2), pp.153–60.
- Mandel, C.R., Bai, Y. & Tong, L., 2008. Protein factors in pre-mRNA 3'-end processing. *Cellular and Molecular Life Sciences*, 65(7–8), pp.1099–122.
- Manders, E., Verbeek, F. & Aten, J., 1993. Measurement of co-localisation of objects in dual-colour confocal. *Journal of Microscopy*, 169(3), pp.375–382.
- Matsuoka, S. *et al.*, 2007. ATM and ATR substrate analysis reveals extensive protein networks responsive to DNA damage. *Science* 316(5828), pp.1160–1166.
- Matunis, M.J., Coutavas, E. & Blobel, G., 1996. A novel ubiquitin-like modification modulates the partitioning of the Ran-GTPase-activating protein RanGAP1 between the cytosol and the nuclear pore complex. *Journal of Cell Biology*, 135(6), pp.1457–1470.
- Mayer, M.P. & Bukau, B., 2005. Hsp70 chaperones: Cellular functions and molecular mechanism. *Cellular and Molecular Life Sciences*, 62(6), pp.670–684.
- Mbita, Z. *et al.*, 2012. De-regulation of the RBBP6 isoform 3/DWNN in human cancers. *Molecular and Cellular Biochemistry*, 362(1), pp.249–62.
- Mbita, Z. & Dlamini, Z., 2006. Molecular analysis of the RbBP6 in hepatocellular carcinoma. *AACR Meeting Abstracts*.
- McDonald, J.H. & Dunn, K.W., 2013. Statistical tests for measures of colocalisation in biological microscopy. *Journal of Microscopy*, 252(3), pp.295–302.
- Melan, M.A., 1994. Overview of cell fixation and permeabilization. *Methods in Molecular Biology*, 34, pp.55–66.
- Mellon, I. *et al.*, 1986. Preferential DNA repair of an active gene in human cells. *Proceedings of the National Academy of Sciences*, 83(23), pp.8878–8882.
- Miki, Y. *et al.*, 1994. A strong candidate for the breast and ovarian cancer susceptibility gene BRCA1. *Science*, 266(5182), pp.66–71.
- Mintz, P.J. *et al.*, 1999. Purification and biochemical characterization of interchromatin granule clusters. *The EMBO Journal*, 18(15), pp.4308–4320.
- Mintz, P.J. & Spector, D.L., 2000. Compartmentalization of RNA processing factors within nuclear speckles. *Journal of Structural Biology*, 129(2–3), pp.241–51.
- Miotto, B. *et al.*, 2014. The RBBP6/ZBTB38/MCM10 axis regulates DNA replication and common fragile site stability. *Cell Reports*, 7(2), pp.575–87.
- Misteli, T. & Soutoglou, E., 2009. The emerging role of nuclear architecture in DNA repair and genome maintenance. *Nature reviews. Molecular Cell Biology*, 10(4), pp.243–54.
- Misteli, T. & Spector, D., 1997. Protein phosphorylation and the nuclear organization of pre-

- mRNA splicing. *Trends in Cell Biology*, 7(4), pp.135–138.
- Moen, P. *et al.*, 2004. Repositioning of muscle-specific genes relative to the periphery of SC-35 domains during skeletal myogenesis. *Molecular Biology of the Cell*, 15, pp.197–206.
- Mol, C.D. *et al.*, 1999. DNA repair mechanisms for the recognition and removal of damaged DNA bases. *Annual Review of Biophysics and Biomolecular Structure*, 28, pp.101–28.
- van Montfort, R.L. *et al.*, 2001. Crystal structure and assembly of a eukaryotic small heat shock protein. *Nature Structural Biology*, 8(12), pp.1025–1030.
- Morimoto, R.I., 1996. Molecular Aides: The Chaperonins. *Science*, 274(5294), pp.1848–1848.
- Motadi, L., Bhoola, K. & Dlamini, Z., 2011. Expression and function of retinoblastoma binding protein 6 (RBBP6) in human lung cancer. *Immunobiology*, 216(10), pp.1065–1073.
- Moynahan, M.E., 2002. The cancer connection: BRCA1 and BRCA2 tumor suppression in mice and humans. *Oncogene*, 21(58), pp.8994–9007.
- Mu, D. *et al.*, 1997. Characterization of reaction intermediates of human excision repair nuclease. *Journal of Biological Chemistry*, 272(46), pp.28971–28979.
- Müller, S. *et al.*, 2001. SUMO, ubiquitin's mysterious cousin. *Nature reviews. Molecular cell biology*, 2(3), pp.202–10.
- Naganuma, T. *et al.*, 2012. Alternative 3'-end processing of long noncoding RNA initiates construction of nuclear paraspeckles. *The EMBO journal*, 31(20), pp.4020–34.
- Nakagawa, S. & Hirose, T., 2012. Paraspeckle nuclear bodies--useful uselessness? *Cellular and Molecular Life Sciences*, 69(18), pp.3027–36.
- Nakamura, J. *et al.*, 1998. Chemically Induced Depurination under Physiological Conditions. *Cancer Research*, 58(2), pp.222–225.
- Nakawaga, T. & Ogawa, H., 1999. The *Saccharomyces cerevisiae* *MER3* gene, encoding a novel helicase-like protein, is required for crossover control in meiosis. *EMBO Journal*, 18(20), pp.5714–5733.
- Narisawa-Saito, M. & Kiyono, T., 2007. Basic mechanisms of high-risk human papillomavirus-induced carcinogenesis: Roles of E6 and E7 proteins. *Cancer Science*, 98(10), pp.1505–1511.
- Nick McElhinny, S. a *et al.*, 2000. Ku recruits the XRCC4-ligase IV complex to DNA ends. *Molecular and Cellular Biology*, 20(9), pp.2996–3003.
- Nover, L., Scharf, K.D. & Neumann, D., 1989. Cytoplasmic heat shock granules are formed from precursor particles and are associated with a specific set of mRNAs. *Molecular and cellular Biology*, 9(3), pp.1298–1308.
- Ohga, T. *et al.*, 1998. Direct involvement of the Y-box binding protein YB-1 in genotoxic stress-induced activation of the human multidrug resistance 1 gene. *Journal of Biological Chemistry*, 273(11), pp.5997–6000.

- Okamoto, T. *et al.*, 2000. Direct interaction of p53 with the Y-box binding protein, YB-1: a mechanism for regulation of human gene expression. *Oncogene*, 19(54), pp.6194–6202.
- Patriarca, E.J. & Maresca, B., 1990. Acquired thermotolerance following heat shock protein synthesis prevents impairment of mitochondrial ATPase activity at elevated temperatures in *Saccharomyces cerevisiae*. *Experimental Cell Research*, 190(1), pp.57–64.
- Pearson, K., 1896. Mathematical Contributions to the Theory of Evolution.--On a Form of Spurious Correlation Which May Arise When Indices Are Used in the Measurement of Organs. *Proceedings of the Royal Society of London*, 60(1), pp.489–498.
- Pendergrast, P. *et al.*, 2002. FBI-1 Can Stimulate HIV-1 Tat Activity and Is Targeted to a Novel Subnuclear Domain that Includes the Tat-P-TEFb — containing Nuclear Speckles. *Molecular Biology of the Cell*, 13(March), pp.915–929.
- Peterson, N.S., Moller, G. & Mitchell, H.K., 1979. Genetic Mapping of the Coding Regions for Three Heat-Shock Proteins in *Drosophila Melanogaster*. *Genetics*, 92, pp.891–902.
- Petrini, J.H., 1999. The mammalian Mre11-Rad50-nbs1 protein complex: integration of functions in the cellular DNA-damage response. *American Journal of Human Genetics*, 64(5), pp.1264–1269.
- Phair, R. & Misteli, T., 2000. High mobility of proteins in the mammalian cell nucleus. *Nature*, 404(6778), pp.604–609.
- Pickart, C.M. & Eddins, M.J., 2004. Ubiquitin: structures, functions, mechanisms. *Biochimica et Biophysica Acta*, 1695(1–3), pp.55–72.
- Pickart, C.M. & Rose, I.A., 1985. Ubiquitin carboxyl-terminal hydrolase acts on ubiquitin carboxyl-terminal amides. *The Journal of Biological Chemistry*, 260(13), pp.7903–10.
- Polo, S. & Jackson, S., 2011. Dynamics of DNA damage response proteins at DNA breaks: a focus on protein modifications. *Genes and Development*, 25(5), pp.409–33.
- Pratt, W.B. & Toft, D.O., 2003. Regulation of Signaling Protein Function and Trafficking by the hsp90/hsp70-based Chaperone Machinery. *Experimental Biology and Medicine*, 228, pp.111–133.
- Prives, C. & Hall, P., 1999. The p53 pathway. *Journal of Pathology*, 187, pp.112–126.
- Pugh, D. *et al.*, 2006. DWNN, a novel ubiquitin-like domain, implicates RBBP6 in mRNA processing and ubiquitin-like pathways. *BMC Structural Biology*, 6, p.1.
- Raffetseder, U. *et al.*, 2003. Splicing factor SRp30c interaction with Y-box protein-1 confers nuclear YB-1 shuttling and alternative splice site selection. *The Journal of Biological Chemistry*, 278(20), pp.18241–18248.
- Ramsden, D. a. & Geliert, M., 1998. Ku protein stimulates DNA end joining by mammalian DNA ligases: A direct role for Ku in repair of DNA double-strand breaks. *EMBO Journal*, 17(2), pp.609–614.

- Rappsilber, J. *et al.*, 2002. Large-scale proteomic analysis of the human spliceosome. *Genome Research*, 12(8), pp.1231–1245.
- Richter, K. *et al.*, 2003. Sti1 is a non-competitive inhibitor of the Hsp90 ATPase. Binding prevents the N-terminal dimerization reaction during the ATPase cycle. *Journal of Biological Chemistry*, 278(12), pp.10328–10333.
- Richter, K., Haslbeck, M. & Buchner, J., 2010. The heat shock response: life on the verge of death. *Molecular Cell*, 40(2), pp.253–66.
- Riley, T. *et al.*, 2008. Transcriptional control of human p53-regulated genes. *Nature Reviews Molecular Cell Biology*, 9(5), pp.402–12.
- Ritossa, F., 1962. A new puffing pattern induced by temperature shock and DNP in drosophila. *Experientia*, 18(12), pp.571–573.
- Rodrigo-Brenni, M.C., Foster, S.A. & Morgan, D.O., 2010. Catalysis of lysine 48-specific ubiquitin chain assembly by residues in E2 and ubiquitin. *Molecular Cell*, 39(4), pp.548–59.
- Sacco-Bubulya, P. & Spector, D., 2002. Disassembly of interchromatin granule clusters alters the coordination of transcription and pre-mRNA splicing. *The Journal of Cell Biology*, 156(3), pp.425–436.
- Saitoh, N. *et al.*, 2004. Proteomic Analysis of Interchromatin Granule Clusters. *Molecular Biology of the Cell*, 15, pp.3876–3890.
- Sakai, Y. *et al.*, 1995. cDNA Sequence and Chromosomal Localisation of a Novel Human Protein, RBQ-1 (RBBP6), That Binds to the Retinoblastoma Gene Product. *Genomics*, 30(1), pp.98–101.
- Salichs, E. *et al.*, 2009. Genome-wide analysis of histidine repeats reveals their role in the localisation of human proteins to the nuclear speckles compartment. *PLoS Genetics*, 5(3), p.e1000397.
- S Lindquist, and & Craig, E.A., 1988. The Heat-Shock Proteins. *Annual Review of Genetics* 22, pp.631-77.
- Sancar, A. *et al.*, 2004. Molecular mechanisms of mammalian DNA repair and the DNA damage checkpoints. *Annual Review of Biochemistry*, 73, pp.39–85.
- Sanford, J. *et al.*, 2004. A novel role for shuttling SR proteins in mRNA translation. *Genes and Development*, 18(7), pp.755–768.
- Sapetschnig, A. *et al.*, 2002. Transcription factor Sp3 is silenced through SUMO modification by PIAS1. *EMBO Journal*, 21(19), pp.5206–5215.
- Scheffner, M., Nuber, U. & Huibregtse, J.M., 1995. Protein ubiquitination involving an E1-E2-E3 enzyme ubiquitin thioester cascade. *Nature*, 373(6509), pp.81–3.
- Schul, W., van Driel, R. & de Jong, L., 1998. A subset of poly(A) polymerase is concentrated at sites of RNA synthesis and is associated with domains enriched in splicing factors and

- poly(A) RNA. *Experimental Cell Research*, 238(1), pp.1–12.
- Schwartz, D. & Hochstrasser, M., 2003. A superfamily of protein tags: ubiquitin, SUMO and related modifiers. *Trends in Biochemical Sciences*, 28(6), pp.321–328.
- Scott, R. *et al.*, 2003. Functional potential of P2P-R: a role in the cell cycle and cell differentiation related to its interactions with proteins that bind to matrix associated regions of DNA? *Journal of Cellular Biochemistry*, 90(1), pp.6–12.
- Seeler, J.S. & Dejean, A., 2001. SUMO: of branched proteins and nuclear bodies. *Oncogene*, 20(49), pp.7243–9.
- Sellers, W. & Kaelin, W.J., 1997. Role of the retinoblastoma protein in the pathogenesis of human cancer. *Journal of Clinical Oncology*, 15(11), pp.3301–3312.
- Seufert, W., Futcher, B. & Jentsch, S., 1995. Role of a ubiquitin-conjugating enzyme in degradation of S- and M-phase cyclins. *Nature*, 373(6509), pp.78–81.
- Sharan, S.K. *et al.*, 1997. Embryonic lethality and radiation hypersensitivity mediated by Rad51 in mice lacking Brca2. *Nature*, 386(6627), pp.804–810.
- Sharma, A. *et al.*, 2010. Son Is Essential for Nuclear Speckle Organization and Cell Cycle Progression. *Molecular Biology of the Cell*, 21, pp.650–663.
- Shi, Y. *et al.*, 2009. Molecular architecture of the human pre-mRNA 3' processing complex. *Molecular Cell*, 33(3), pp.365–376.
- Shopland, L. *et al.*, 2003. Clustering of multiple specific genes and gene-rich R-bands around SC-35 domains: evidence for local euchromatic neighborhoods. *The Journal of Cell Biology*, 162(6), pp.981–990.
- Simons, A. *et al.*, 1997. PACT: cloning and characterization of a cellular p53 binding protein that interacts with Rb. *Oncogene*, 14(2), pp.145–155.
- Singh, K.K. *et al.*, 2010. Human SAP18 mediates assembly of a splicing regulatory multiprotein complex via its ubiquitin-like fold. *RNA*, 16(12), pp.2442–54.
- Sinha, R.P. & Häder, D.P., 2002. UV-induced DNA damage and repair: a review. *Photochemical and Photobiological Sciences*, 1(4), pp.225–236.
- Smallcombe, A., 2001. Multicolor Imaging: The Important Question of Colocalisation. *Biotechniques*, 30(6), pp.1–5.
- Smith, EM, and Mueller, JD. 2012. "The Statistics of Protein Expression Ratios for Cellular Fluorescence Studies." *European Biophysics Journal* 41 (3): 341–52.
- Sobko, A., Ma, H. & Firtel, R.A., 2002. Regulated SUMOylation and Ubiquitination of DdMEK1 Is Required for Proper Chemotaxis. *Developmental Cell*, 2(6), pp.745–756.
- Spector, D., Fu, X. & Maniatis, T., 1991. Associations between distinct pre-mRNA splicing components and the cell nucleus. *The EMBO Journal*, 10(11), pp.3467–3481.
- Spector, D. & Lamond, A., 2011. Nuclear speckles. *Cold Spring Harbor Perspectives in Biology*,

3(2).

- Spector, D., O'Keefe, R. & Jimenez-Garcia, L., 1993. Dynamics of Transcription and Pre-mRNA Splicing within the Mammalian Cell Nucleus. *Cold Spring Harbor Symposia on Quantitative Biology*, 58(0), pp.799–805.
- Spector, D., Schrier, W. & Busch, H., 1984. Immunoelectron microscopic localisation of snRNPs. *Biology of the Cell*, 49(1), pp.1–10.
- Stein, U. *et al.*, 2001. Hyperthermia-induced nuclear translocation of transcription factor YB-1 leads to enhanced expression of multidrug resistance-related ABC transporters. *The Journal of Biological Chemistry*, 276(30), pp.28562–28569.
- Sung, P. *et al.*, 2003. Rad51 Recombinase and Recombination Mediators. *Journal of Biological Chemistry*, 278(44), pp.42729–42732.
- Sung, P. & Klein, H., 2006. Mechanism of homologous recombination: mediators and helicases take on regulatory functions. *Nature Reviews. Molecular Cell Biology*, 7(10), pp.739–750.
- Takai, K. *et al.*, 1998. Acquired thermotolerance and temperature-induced protein accumulation in the extremely thermophilic bacterium *Rhodothermus obamensis*. *Journal of Bacteriology*, 180(10), pp.2770–2774.
- Tanaka, K. *et al.*, 1990. Analysis of a human DNA excision repair gene involved in group A xeroderma pigmentosum and containing a zinc-finger domain. *Nature*, 348(6296), pp.73–6.
- Tateishi, K. *et al.*, 2001. The NEDD8 system is essential for cell cycle progression and morphogenetic pathway in mice. *Journal of Cell Biology*, 155(3), pp.571–579.
- Thiry, M., 1995. The interchromatin granules. *Histology and Histopathology*, 10(4), pp.1035–1045.
- Todd, M., Viitanen, P. & Lorimer, G., 1994. Dynamics of the chaperonin ATPase cycle: implications for facilitated protein folding. *Science*, 265(5172), pp.659–666.
- Toivola, D.M. *et al.*, 2010. Intermediate filaments take the heat as stress proteins. *Trends in Cell Biology*, 20(2), pp.79–91. 962892409002724 [Accessed June 27, 2015].
- Trinkle-Mulcahy, L., Sleeman, J. & Lamond, A., 2001. Dynamic targeting of protein phosphatase 1 within the nuclei of living mammalian cells. *Journal of Cell Science*, 114, pp.4219–4228.
- Tripathi, V. *et al.*, 2010. The nuclear-retained noncoding RNA MALAT1 regulates alternative splicing by modulating SR splicing factor phosphorylation. *Molecular Cell*, 39(6), pp.925–938.
- Vabulas, R.M. *et al.*, 2010. Heat Shock Response. *Cold Spring Harbour Perspectives in Biology*, pp.1–18.
- Večeřová, J. *et al.*, 2004. Formation of nuclear splicing factor compartments is independent of lamins A/C. *Molecular Biology of the Cell*, 15, pp.4904–4910.

- Verdecia, M.A. *et al.*, 2003. Conformational flexibility underlies ubiquitin ligation mediated by the WWP1 HECT domain E3 ligase. *Molecular Cell*, 11(1), pp.249–59.
- Vergheze, J. *et al.*, 2012. Biology of the Heat Shock Response and Protein Chaperones: Budding Yeast (*Saccharomyces cerevisiae*) as a Model System. *Microbiology and Molecular Biology Reviews*, 76(2), pp.115–158.
- Viitanen, P. V, Gatenby, a a & Lorimer, G.H., 1992. Purified chaperonin 60 (groEL) interacts with the nonnative states of a multitude of *Escherichia coli* proteins. *Protein Science*, 1(3), pp.363–369.
- Vogel, J.L., Parsell, D. a & Lindquist, S., 1995. Heat-shock proteins Hsp104 and Hsp70 reactivate mRNA splicing after heat inactivation. *Curren Biology*, 5(3), pp.306–317.
- Wakasugi, M. & Sancar, A., 1999. Order of assembly of human DNA repair excision nuclease. *Journal of Biological Chemistry*, 274(26), pp.18759–18768.
- Wallace, W., Schaefer, L.H. & Swedlow, J.R., 2001. A working person's guide to deconvolution in light microscopy. *Biotechniques*, 31(5), pp.1076–1097.
- Wandinger, S.K., Richter, K. & Buchner, J., 2008. The Hsp90 chaperone machinery. *Journal of Biological Chemistry*, 283(27), pp.18473–18477.
- Wang, J. & Maldonado, M. a, 2006. The ubiquitin-proteasome system and its role in inflammatory and autoimmune diseases. *Cellular and Molecular Immunology* 3(4), pp.255–261.
- Wansink, D. *et al.*, 1993. Fluorescent labeling of nascent RNA reveals transcription by RNA polymerase II in domains scattered throughout the nucleus. *The Journal of Cell Biology*, 122(2), pp.283–293.
- Weber-Ban, E.U. *et al.*, 1999. Global unfolding of a substrate protein by the Hsp100 chaperone ClpA. *Nature*, 401(6748), pp.90–3.
- Weissman, A.M., 2001. Themes and variations on ubiquitylation. *Nature Reviews. Molecular Cell Biology*, 2(3), pp.169–78.
- Welch, W.J., 1986. Cellular and biochemical events in mammalian cells during and after recovery from physiological stress. *The Journal of Cell Biology*, 103(5), pp.2035–2052.
- Welch, W.J., 1985. Morphological study of the mammalian stress response: characterization of changes in cytoplasmic organelles, cytoskeleton, and nucleoli, and appearance of intranuclear actin filaments in rat fibroblasts after heat-shock treatment. *The Journal of Cell Biology*, 101(4), pp.1198–1211.
- Welch, W.J. & Feramisco, J.R., 1982. Purification of the major mammalian heat shock proteins. *Journal of Biological Chemistry*, 257(24), pp.14949–14959.
- Whitby, F.G. *et al.*, 1998. Crystal structure of the human ubiquitin-like protein NEDD8 and interactions with ubiquitin pathway enzymes. *Journal of Biological Chemistry*, 273(52),

pp.34983–34991.

- van Wijk, S.J.L. & Timmers, H.T.M., 2010. The family of ubiquitin-conjugating enzymes (E2s): deciding between life and death of proteins. *The FASEB Journal*, 24(4), pp.981–993.
- Winn, P.J. *et al.*, 2004. Determinants of functionality in the ubiquitin conjugating enzyme family. *Structure*, 12(9), pp.1563–74.
- Witte, M. & Scott, R., 1997. The proliferation potential protein-related (P2P-R) gene with domains encoding heterogeneous nuclear ribonucleoprotein association and Rb1 binding shows repressed expression during terminal differentiation. *Proceedings of the National Academy of Sciences* 94, pp.1212–1217.
- Wu, L. & Hickson, I.D., 2003. The Bloom's syndrome helicase suppresses crossing over during homologous recombination. *Nature*, 426(6968), pp.870–4.
- Xie, Y. & Varshavsky, A., 1999. The E2-E3 interaction in the N-end rule pathway: the RING-H2 finger of E3 is required for the synthesis of multiubiquitin chain. *The EMBO Journal*, 18(23), pp.6832–6844.
- Xing, Y. *et al.*, 1995. Nonrandom gene organization: structural arrangements of specific pre-mRNA transcription and splicing with SC-35 domains. *The Journal of Cell Biology*, 131, pp.1635–1647.
- Yahara, I., 2013. Introduction. In *Stress-Inducible Cellular Responses*. Birkhäuser, p. 2.
- Yam, A. *et al.*, 2008. Defining the TRiC/CCT interactome links chaperonin function to stabilization of newly-made proteins with complex topologies. *Nature Structure and Molecular Biology*, 15(12), pp.1255–1262.
- Yoshitake, Y. *et al.*, 2004. Proliferation potential-related protein, an ideal esophageal cancer antigen for immunotherapy, identified using complementary DNA microarray analysis. *Clinical Cancer Research*, 10(19), pp.6437–6448.
- Young, P. *et al.*, 1998. Characterization of two polyubiquitin sites in the 26S protease subunit 5a. *J Biol Chem*, 273(10), pp.5461–5467.
- Zahler, A. *et al.*, 1992. SR proteins: a conserved family of pre-mRNA splicing factors. *Genes and Development*, 6(5), pp.837–847.
- Zeng, C. *et al.*, 1997. Dynamic relocation of transcription and splicing factors dependent upon transcriptional activity. *The EMBO Journal*, 16(6), pp.1401–1412.
- Zeuthen, E., 1971. Synchrony in Tetrahymena by heat shocks spaced a normal cell generation apart. *Experimental Cell Research*, 68(1), pp.49–60.
- Zhang, H.-G. *et al.*, 2004. Regulation of apoptosis proteins in cancer cells by ubiquitin. *Oncogene*, 23(11), pp.2009–2015.
- Zhu, X. *et al.*, 1996. Structural Analysis of Substrate Binding by the Molecular Chaperone DnaK. *Science*, 272(5268), pp.1606–1614.

- Zinchuk, V., Zinchuk, O. & Okada, T., 2007. Quantitative colocalisation analysis of multicolor confocal immunofluorescence microscopy images: pushing pixels to explore biological phenomena. *Acta histochemica et cytochemica*, 40(4), pp.101–111.
- Zou, J. *et al.*, 1998. Repression of Heat Shock Transcription Factor HSF1 Activation by HSP90 (HSP90 Complex) that Forms a Stress-Sensitive Complex with HSF1. *Cell*, 94(4), pp.471–480.
- Zuo, P. & Manley, J.L., 1993. Functional domains of the human splicing factor ASF/SF2. *The EMBO Journal*, 12(12), pp.4727–37.



CHAPTER 6 APPENDIX

INTENSITY VALUES FOR HEAT SHOCK EXPERIMENT			
Nuclear Unstressed Samples	Mean Intensity Reading	Cytoplasmic Unstressed	Mean Intensity Reading
N Unstressed 1	39.514	C Unstressed 1	19.251
N Unstressed 2	29.415	C Unstressed 2	13.811
N Unstressed 3	28.903	C Unstressed 3	13.002
N Unstressed 4	33.511	C Unstressed 4	15.227
N Unstressed 5	36.144	C Unstressed 5	15.363
N Unstressed 6	20.534	C Unstressed 6	12.236
N Unstressed 7	20.524	C Unstressed 7	10.189
N Unstressed 8	22.786	C Unstressed 8	12.158
N Unstressed 9	24.927	C Unstressed 9	13.111
N Unstressed 10	23.67	C Unstressed 10	13.255
N Unstressed 11	36.881	C Unstressed 11	17.718
N Unstressed 12	42.607	C Unstressed 12	18.67
N Unstressed 13	39.567	C Unstressed 13	19.734
N Unstressed 14	42.79	C Unstressed 14	17.241
N Unstressed 15	40.896	C Unstressed 15	19.836
N Unstressed 16	42.369	C Unstressed 16	15.951
N Unstressed 17	41.992	C Unstressed 17	20.268
N Unstressed 18	40.996	C Unstressed 18	15.691
N Unstressed 19	35.58	C Unstressed 19	14.702
N Unstressed 20	39.202	C Unstressed 20	17.68
N Unstressed 21	29.08	C Unstressed 21	13.863

N Unstressed 22	29.373	C Unstressed 22	12.464
N Unstressed 23	39.218	C Unstressed 23	17.654
N Unstressed 24	35.235	C Unstressed 24	15.104
N Unstressed 25	36.541	C Unstressed 25	18.311
N Unstressed 26	21.144	C Unstressed 26	10.416
N Unstressed 27	20.603	C Unstressed 27	12.672
N Unstressed 28	25.511	C Unstressed 28	13.207
N Unstressed 29	25.483	C Unstressed 29	14.176
N Unstressed 30	19.969	C Unstressed 30	11.005
Mean for Nuclear Intensity of Unstressed Cells	34.373	Mean for Cytoplasmic Intensity of Unstressed Cells	14.903
Standard Deviation for Nuclear Intensity of Unstressed Cells	6.876881896	Standard Deviation for Cytoplasmic Intensity of Unstressed Cells	2.585621
Nuclear Stressed Samples	Mean Intensity Reading	Cytoplasmic Stressed	Mean Intensity Reading
N Stressed 1	39.969	C Stressed 1	18.078
N Stressed 2	43.555	C Stressed 2	19.632
N Stressed 3	42.723	C Stressed 3	19.043
N Stressed 4	39.045	C Stressed 4	12.901
N Stressed 5	38.649	C Stressed 5	16.732
N Stressed 6	58.804	C Stressed 6	18.418
N Stressed 7	65.631	C Stressed 7	15.277
N Stressed 8	61.926	C Stressed 8	15.71
N Stressed 9	62.577	C Stressed 9	14.56
N Stressed 10	59.47	C Stressed 10	14.572
N Stressed 11	76.546	C Stressed 11	13.416
N Stressed 12	77.159	C Stressed 12	14.023
N Stressed 13	70.278	C Stressed 13	15.202

N Stressed 14	64.35	C Stressed 14	18.16
N Stressed 15	66.62	C Stressed 15	12.377
N Stressed 16	69.484	C Stressed 16	9.08
N Stressed 17	81.627	C Stressed 17	17.182
N Stressed 18	95.242	C Stressed 18	13.327
N Stressed 19	81.768	C Stressed 19	10.963
N Stressed 20	84.313	C Stressed 20	13.384
N Stressed 21	30.561	C Stressed 21	18.081
N Stressed 22	30.655	C Stressed 22	17.798
N Stressed 23	27.054	C Stressed 23	18.324
N Stressed 24	25.175	C Stressed 24	16.881
N Stressed 25	46.55	C Stressed 25	18.815
N Stressed 26	44.562	C Stressed 26	21.268
N Stressed 27	47.977	C Stressed 27	21.238
N Stressed 28	48.392	C Stressed 28	17.794
N Stressed 29	47.248	C Stressed 29	21.535
N Stressed 30	47.927	C Stressed 30	21.219
Mean for Nuclear Intensity of Stressed Cells	53.598	Mean for Cytoplasmic Intensity of Stressed Cells	17.0315
Standard Deviation for Nuclear Intensity of Stressed Cells	2.585621111	Standard Deviation for Cytoplasmic Intensity of Stressed Cells	2.237353
p value for the change in nuclear intensity	2.03111E-08	p value for the change in cytoplasmic intensity	0.073956

INTENSITY VALUES FOR UV EXPERIMENT			
Nuclear Unstressed Samples	Mean Intensity Reading	Cytoplasmic Unstressed	Mean Intensity Reading
N Unstressed 1	108.944	C Unstressed 1	86.76
N Unstressed 2	108.718	C Unstressed 2	72.935
N Unstressed 3	104.695	C Unstressed 3	87.374

N Unstressed 4	109.861	C Unstressed 4	75.047
N Unstressed 5	100.308	C Unstressed 5	72.316
N Unstressed 6	102.182	C Unstressed 6	68.603
N Unstressed 7	99.992	C Unstressed 7	85.723
N Unstressed 8	118.705	C Unstressed 8	93.948
N Unstressed 9	115.108	C Unstressed 9	91.965
N Unstressed 10	116.506	C Unstressed 10	83.006
N Unstressed 11	113.866	C Unstressed 11	104.128
N Unstressed 12	120.714	C Unstressed 12	88.115
N Unstressed 13	133.209	C Unstressed 13	86.313
N Unstressed 14	114.178	C Unstressed 14	74.692
N Unstressed 15	109.072	C Unstressed 15	67.89
N Unstressed 16	110.514	C Unstressed 16	80.172
N Unstressed 17	119.209	C Unstressed 17	95.83
N Unstressed 18	105.047	C Unstressed 18	75.862
N Unstressed 19	254.518	C Unstressed 19	84.211
N Unstressed 20	114.311	C Unstressed 20	89.129
N Unstressed 21	121.216	C Unstressed 21	96.235
N Unstressed 22	116.987	C Unstressed 22	86.581
N Unstressed 23	112.353	C Unstressed 23	81.989
N Unstressed 24	122.807	C Unstressed 24	91.892
N Unstressed 25	121.137	C Unstressed 25	83.815
N Unstressed 26	104.805	C Unstressed 26	72.228
N Unstressed 27	133.159	C Unstressed 27	100.318
N Unstressed 28	114.96	C Unstressed 28	72.89
N Unstressed 29	111.952	C Unstressed 29	77.498
N Unstressed 30	117.57	C Unstressed 30	86.686
Mean for Nuclear Intensity of Unstressed Cells	114.2445	Mean for Cytoplasmic Intensity of Unstressed Cells	84.967

Standard Deviation for Nuclear Intensity of Unstressed Cells	6.487552776	Standard Deviation for Cytoplasmic Intensity of Unstressed Cells	9.420726
Nuclear Stressed Samples	Mean Intensity Reading	Cytoplasmic Stressed	Mean Intensity Reading
N Stressed 1	155.357	C Stressed 1	67.4
N Stressed 2	136.06	C Stressed 2	62.924
N Stressed 3	152.149	C Stressed 3	57.226
N Stressed 4	154.374	C Stressed 4	64.544
N Stressed 5	168.88	C Stressed 5	62.483
N Stressed 6	196.16	C Stressed 6	76.318
N Stressed 7	132.001	C Stressed 7	56.622
N Stressed 8	154.813	C Stressed 8	65.98
N Stressed 9	147.658	C Stressed 9	71.121
N Stressed 10	137.672	C Stressed 10	56.126
N Stressed 11	132.62	C Stressed 11	50.429
N Stressed 12	152.436	C Stressed 12	63.916
N Stressed 13	183.99	C Stressed 13	62.99
N Stressed 14	178.283	C Stressed 14	59.799
N Stressed 15	142.163	C Stressed 15	57.122
N Stressed 16	173.825	C Stressed 16	71.572
N Stressed 17	160.181	C Stressed 17	68.507
N Stressed 18	149.485	C Stressed 18	60.529
N Stressed 19	150.108	C Stressed 19	75.802
N Stressed 20	157.262	C Stressed 20	68.196
N Stressed 21	152.668	C Stressed 21	77.102
N Stressed 22	151.96	C Stressed 22	75.499
N Stressed 23	128.793	C Stressed 23	87.159
N Stressed 24	147.4	C Stressed 24	74.1

N Stressed 25	172.516	C Stressed 25	76.757
N Stressed 26	135.428	C Stressed 26	60.994
N Stressed 27	177.85	C Stressed 27	71.828
N Stressed 28	147.627	C Stressed 28	71.318
N Stressed 29	141.123	C Stressed 29	83.909
N Stressed 30	177.348	C Stressed 30	65.571
Mean for Nuclear Intensity of Stressed Cells	152.2925	Mean for Cytoplasmic Intensity of Stressed Cells	66.69
Standard Deviation for Nuclear Intensity of Stressed Cells	9.420726305	Standard Deviation for Cytoplasmic Intensity of Stressed Cells	6.531493
p value for the change in nuclear intensity	2.99274E-07	p value for the change in cytoplasmic intensity	4.43E-08

INTENSITY VALUES CISPLATIN EXPERIMENT			
Nuclear Unstressed Samples	Mean Intensity Reading	Cytoplasmic Unstressed	Mean Intensity Reading
N Unstressed 1	74.106	C Unstressed 1	72.559
N Unstressed 2	69.204	C Unstressed 2	61.108
N Unstressed 3	74.026	C Unstressed 3	76.824
N Unstressed 4	71.96	C Unstressed 4	79.21
N Unstressed 5	84.622	C Unstressed 5	69.367
N Unstressed 6	89.67	C Unstressed 6	76.085
N Unstressed 7	74.889	C Unstressed 7	69.384
N Unstressed 8	97.501	C Unstressed 8	75.338
N Unstressed 9	90.956	C Unstressed 9	76.988
N Unstressed 10	94.22	C Unstressed 10	83.671

N Unstressed 11	93.525	C Unstressed 11	71.45
N Unstressed 12	92.387	C Unstressed 12	80.447
N Unstressed 13	102.455	C Unstressed 13	78.539
N Unstressed 14	78.796	C Unstressed 14	69.488
N Unstressed 15	93.046	C Unstressed 15	83.574
N Unstressed 16	74.505	C Unstressed 16	72.16
N Unstressed 17	73.91	C Unstressed 17	68.507
N Unstressed 18	70.949	C Unstressed 18	55.802
N Unstressed 19	70.408	C Unstressed 19	76.196
N Unstressed 20	76.254	C Unstressed 20	61.102
N Unstressed 21	87.73	C Unstressed 21	79.498
N Unstressed 22	78.396	C Unstressed 22	75.108
N Unstressed 23	66.505	C Unstressed 23	74.11
N Unstressed 24	78.615	C Unstressed 24	70.966
N Unstressed 25	100.023	C Unstressed 25	76.942
N Unstressed 26	81.947	C Unstressed 26	61.828
N Unstressed 27	99.41	C Unstressed 27	77.884
N Unstressed 28	73.884	C Unstressed 28	73.992
N Unstressed 29	69.8	C Unstressed 29	69.035
N Unstressed 30	97.477	C Unstressed 30	69.99
Mean for Nuclear Intensity of Unstressed Cells	82.70586667	Mean for Cytoplasmic Intensity of Unstressed Cells	72.90506667
Standard Deviation for Nuclear Intensity of Unstressed Cells	11.054229	Standard Deviation for Cytoplasmic Intensity of Unstressed Cells	6.666169582

Nuclear Stressed Samples	Mean Intensity Reading	Cytoplasmic Stressed	Mean Intensity Reading
N Stressed 1	109.685	C Stressed 1	71.88
N Stressed 2	107.693	C Stressed 2	71.556
N Stressed 3	107.422	C Stressed 3	84.975
N Stressed 4	110.409	C Stressed 4	69.487
N Stressed 5	99.775	C Stressed 5	80.029
N Stressed 6	103.569	C Stressed 6	69.22
N Stressed 7	97.501	C Stressed 7	87.693
N Stressed 8	120.745	C Stressed 8	68.338
N Stressed 9	115.994	C Stressed 9	69.256
N Stressed 10	116.506	C Stressed 10	80.426
N Stressed 11	112.69	C Stressed 11	84.128
N Stressed 12	117.714	C Stressed 12	79.395
N Stressed 13	129.26	C Stressed 13	71.997
N Stressed 14	117.881	C Stressed 14	73.258
N Stressed 15	108.348	C Stressed 15	72.482
N Stressed 16	112.004	C Stressed 16	78.466
N Stressed 17	124.209	C Stressed 17	67.003
N Stressed 18	115.047	C Stressed 18	76.39
N Stressed 19	104.518	C Stressed 19	79.128
N Stressed 20	114.311	C Stressed 20	89.36

N Stressed 21	120.756	C Stressed 21	70.311
N Stressed 22	116.987	C Stressed 22	84.581
N Stressed 23	112.353	C Stressed 23	83.989
N Stressed 24	122.807	C Stressed 24	72.991
N Stressed 25	108.33	C Stressed 25	63.815
N Stressed 26	104.805	C Stressed 26	79.689
N Stressed 27	129.66	C Stressed 27	65.89
N Stressed 28	117.221	C Stressed 28	73.104
N Stressed 29	121.964	C Stressed 29	74.982
N Stressed 30	113.369	C Stressed 30	69.065
Mean for Nuclear Intensity of Stressed Cells	113.7844333	Mean for Cytoplasmic Intensity of Stressed Cells	75.09613
Standard Deviation for Nuclear Intensity of Stressed Cells	7.917591395	Standard Deviation for Cytoplasmic Intensity of Stressed Cells	6.766979
p value for the change in nuclear intensity	6.62835E-15	p value for the change in cytoplasmic intensity	0.107709245

INTENSITY VALUES FOR CYCLOHEXIMIDE EXPERIMENT			
Nuclear Unstressed Samples without Cycloheximide	Mean Intensity Reading	Nuclear Unstressed Samples with Cycloheximide	Mean Intensity Reading
N Unstressed - Cyc 1	78.501	N Unstressed + Cyc 1	87.73
N Unstressed - Cyc 2	71.12	N Unstressed + Cyc 2	78.396
N Unstressed - Cyc 3	70.271	N Unstressed + Cyc 3	66.505

N Unstressed - Cyc 4	76.418	N Unstressed + Cyc 4	78.615
N Unstressed - Cyc 5	92.626	N Unstressed + Cyc 5	100.023
N Unstressed - Cyc 6	92.715	N Unstressed + Cyc 6	81.947
N Unstressed - Cyc 7	79.061	N Unstressed + Cyc 7	96.652
N Unstressed - Cyc 8	100.197	N Unstressed + Cyc 8	73.405
N Unstressed - Cyc 9	87.269	N Unstressed + Cyc 9	74.657
N Unstressed - Cyc 10	96.783	N Unstressed + Cyc 10	69.864
N Unstressed - Cyc 11	96.697	N Unstressed + Cyc 11	76.959
N Unstressed - Cyc 12	106.956	N Unstressed + Cyc 12	65.076
N Unstressed - Cyc 13	83.353	N Unstressed + Cyc 13	62.229
N Unstressed - Cyc 14	79.698	N Unstressed + Cyc 14	68.368
N Unstressed - Cyc 15	93.911	N Unstressed + Cyc 15	62.75
N Unstressed - Cyc 16	76.085	N Unstressed + Cyc 16	69.421
N Unstressed - Cyc 17	79.676	N Unstressed + Cyc 17	103.048
N Unstressed - Cyc 18	70.949	N Unstressed + Cyc 18	100.091
N Unstressed - Cyc 19	70.408	N Unstressed + Cyc 19	79.176
N Unstressed - Cyc 20	76.254	N Unstressed + Cyc 20	97.252
Mean for Nuclear Intensity of Unstressed Cells without Cycloheximide	83.9474	Mean for Nuclear Intensity of Unstressed Cells with Cycloheximide	79.6082
Standard Deviation for Nuclear Intensity of Unstressed Cells without Cycloheximide	7.706651	Standard Deviation for Nuclear Intensity of Unstressed Cells with Cycloheximide	2.782337
Nuclear Stressed Samples without Cycloheximide	Mean Intensity Reading	Nuclear Stressed Samples with Cycloheximide	Mean Intensity Reading
N Stressed - Cyc 1	113.761	N Stressed + Cyc 1	131.76
N Stressed - Cyc 2	129.617	N Stressed + Cyc 2	114.901
N Stressed - Cyc 3	146.354	N Stressed + Cyc 3	136.211
N Stressed - Cyc 4	118.112	N Stressed + Cyc 4	133.969
N Stressed - Cyc 5	122.161	N Stressed + Cyc 5	102.192

N Stressed - Cyc 6	119.293	N Stressed + Cyc 6	123.525
N Stressed - Cyc 7	124.712	N Stressed + Cyc 7	77.018
N Stressed - Cyc 8	116.098	N Stressed + Cyc 8	121.4
N Stressed - Cyc 9	94.708	N Stressed + Cyc 9	96.981
N Stressed - Cyc 10	133.152	N Stressed + Cyc 10	108.139
N Stressed - Cyc 11	84.406	N Stressed + Cyc 11	87.128
N Stressed - Cyc 12	90.91	N Stressed + Cyc 12	102.575
N Stressed - Cyc 13	79.636	N Stressed + Cyc 13	100.766
N Stressed - Cyc 14	77.677	N Stressed + Cyc 14	94.332
N Stressed - Cyc 15	125.06	N Stressed + Cyc 15	106.045
N Stressed - Cyc 16	114.577	N Stressed + Cyc 16	154.005
N Stressed - Cyc 17	120.26	N Stressed + Cyc 17	155.072
N Stressed - Cyc 18	142.483	N Stressed + Cyc 18	172.313
N Stressed - Cyc 19	119.08	N Stressed + Cyc 19	159.616
N Stressed - Cyc 20	127.938	N Stressed + Cyc 20	154.44
Mean for Nuclear Intensity of Stressed Cells	114.9998	Mean for Cytoplasmic Intensity of Stressed Cells	121.6194
Standard Deviation for Nuclear Intensity of Stressed Cells	6.90557	Standard Deviation for Cytoplasmic Intensity of Stressed Cells	4.05499
p value for the change in nuclear intensity	1.89987E-05	p value for the change in nuclear intensity with cyclohexemide	3.27964E-07

INTENSITY VALUES FOR TIME COURSE UV AND HEAT SHOCK EXPERIMENTS			
Nuclear Samples from UV Experiment	Mean Intensity Reading	Nuclear Samples from Heat Shock Experiment	Mean Intensity Reading
N Unstressed 1	33.274	N Unstressed 1	23.47
N Unstressed 2	27.632	N Unstressed 2	21.311
N Unstressed 3	24.986	N Unstressed 3	30.345

N Unstressed 4	25.876	N Unstressed 4	24.979
N Unstressed 5	19.844	N Unstressed 5	23.917
N Unstressed 6	38.516	N Unstressed 6	31.04
N Unstressed 7	46.174	N Unstressed 7	30.596
N Unstressed 8	28.435	N Unstressed 8	25.82
N Unstressed 9	28.38	N Unstressed 9	24.898
N Unstressed 10	36.209	N Unstressed 10	22.945
N Unstressed 11	26.4	N Unstressed 11	42.679
N Unstressed 12	23.671	N Unstressed 12	40.262
N Unstressed 13	23.072	N Unstressed 13	42.834
N Unstressed 14	23.811	N Unstressed 14	37.134
N Unstressed 15	28.595	N Unstressed 15	41.49
N Omin 1	42.75	N Omin 1	47.422
N Omin 2	49.804	N Omin 2	46.929
N Omin 3	46.961	N Omin 3	46.78
N Omin 4	47.058	N Omin 4	42.856
N Omin 5	41.992	N Omin 5	47.095
N Omin 6	43.380	N Omin 6	41.098
N Omin 7	44.078	N Omin 7	50.668
N Omin 8	41.685	N Omin 8	52.843
N Omin 9	42.988	N Omin 9	49.87
N Omin 10	47.068	N Omin 10	46.729
N Omin 11	45.821	N Omin 11	51.088
N Omin 12	49.573	N Omin 12	48.371
N Omin 13	40.008	N Omin 13	52.877
N Omin 14	39.684	N Omin 14	48.816
N Omin 15	48.507	N Omin 15	48.227

N 30min 1	56.662	N 30min 1	52.031
N 30min 2	54.889	N 30min 2	48.929
N 30min 3	51.639	N 30min 3	48.894
N 30min 4	52.727	N 30min 4	39.519
N 30min 5	53.948	N 30min 5	51.9
N 30min 6	53.982	N 30min 6	56.186
N 30min 7	58.272	N 30min 7	58.613
N 30min 8	49.147	N 30min 8	57.252
N 30min 9	55.581	N 30min 9	54.633
N 30min 10	62.064	N 30min 10	59.378
N 30min 11	55.494	N 30min 11	52.944
N 30min 12	57.187	N 30min 12	53.66
N 30min 13	55.875	N 30min 13	56.159
N 30min 14	55.65	N 30min 14	58.659
N 30min 15	57.138	N 30min 15	54.975
N 1hour 1	50.246	N 1hour 1	42.006
N 1hour 2	48.788	N 1hour 2	49.087
N 1hour 3	44.698	N 1hour 3	50.912
N 1hour 4	42.677	N 1hour 4	46.515
N 1hour 5	45.909	N 1hour 5	56.059
N 1hour 6	55.49	N 1hour 6	51.98
N 1hour 7	44.174	N 1hour 7	52.613
N 1hour 8	42.593	N 1hour 8	53.735
N 1hour 9	55.408	N 1hour 9	30.685
N 1hour 10	49.333	N 1hour 10	30.435
N 1hour 11	57.358	N 1hour 11	32.363
N 1hour 12	55.51	N 1hour 12	32.387
N 1hour 13	54.617	N 1hour 13	31.748

N 1hour 14	55.28	N 1hour 14	30.209
N 1hour 15	55.281	N 1hour 15	30.631
N 2hour 1	45.108	N 2hour 1	58.033
N 2hour 2	43.496	N 2hour 2	48.285
N 2hour 3	40.792	N 2hour 3	48.969
N 2hour 4	48.57	N 2hour 4	54.873
N 2hour 5	40.552	N 2hour 5	56.441
N 2hour 6	41.381	N 2hour 6	40.211
N 2hour 7	44.668	N 2hour 7	39.686
N 2hour 8	40.218	N 2hour 8	39.825
N 2hour 9	41.874	N 2hour 9	45.013
N 2hour 10	44.439	N 2hour 10	39.598
N 2hour 11	37.812	N 2hour 11	55.233
N 2hour 12	43.842	N 2hour 12	49.242
N 2hour 13	44.828	N 2hour 13	54.065
N 2hour 14	33.873	N 2hour 14	58.331
N 2hour 15	43.611	N 2hour 15	56.311
N 4hour 1	39.33	N 4hour 1	69.426
N 4hour 2	37.362	N 4hour 2	71.068
N 4hour 3	40.544	N 4hour 3	75.611
N 4hour 4	30.958	N 4hour 4	72.065
N 4hour 5	46.995	N 4hour 5	70.549
N 4hour 6	39.421	N 4hour 6	30.294
N 4hour 7	33.584	N 4hour 7	35.035
N 4hour 8	32.055	N 4hour 8	37.756
N 4hour 9	41.861	N 4hour 9	45.082
N 4hour 10	42.907	N 4hour 10	35.854

N 4hour 11	47.187	N 4hour 11	60.431
N 4hour 12	42.688	N 4hour 12	62.651
N 4hour 13	39.761	N 4hour 13	68.975
N 4hour 14	47.453	N 4hour 14	69.92
N 4hour 15	44.814	N 4hour 15	66.532
N 8hour 1	43.927	N 8hour 1	46.371
N 8hour 2	37.354	N 8hour 2	48.924
N 8hour 3	37.112	N 8hour 3	48.811
N 8hour 4	34.765	N 8hour 4	49.836
N 8hour 5	43.64	N 8hour 5	44.975
N 8hour 6	38.474	N 8hour 6	35.584
N 8hour 7	24.84	N 8hour 7	34.48
N 8hour 8	36.33	N 8hour 8	34.721
N 8hour 9	30.829	N 8hour 9	32.53
N 8hour 10	26.992	N 8hour 10	32.344
N 8hour 11	40.699	N 8hour 11	49.786
N 8hour 12	38.345	N 8hour 12	45.273
N 8hour 13	44.561	N 8hour 13	55.323
N 8hour 14	37.539	N 8hour 14	54.761
N 8hour 15	50.317	N 8hour 15	45.676
N 24hour 1	25.797	N 24hour 1	41.574
N 24hour 2	29.613	N 24hour 2	42.825
N 24hour 3	32.214	N 24hour 3	46.099
N 24hour 4	25.814	N 24hour 4	37.557
N 24hour 5	23.877	N 24hour 5	44.567
N 24hour 6	25.987	N 24hour 6	33.943
N 24hour 7	24.875	N 24hour 7	39.124

N 24hour 8		27.791	N 24hour 8		34.296
N 24hour 9		25.617	N 24hour 9		40.381
N 24hour 10		22.961	N 24hour 10		31.305
N 24hour 11		24.395	N 24hour 11		48.496
N 24hour 12		21.288	N 24hour 12		43.679
N 24hour 13		22.5	N 24hour 13		45.083
N 24hour 14		21.647	N 24hour 14		42.991
N 24hour 15		22.213	N 24hour 15		47.936
Time Period After Exposure to UV	Mean Intensity for UV	Standard Deviation for UV	Time Period After Exposure to Heat Shock	Mean Intensity for Heat Shock	Standard Deviation for Heat Shock
No Stress	28.99166667	6.89411952	No Stress	30.91466667	7.911685261
0 minutes	44.75713	3.319197	0 minutes	48.11127	3.246562
30 minutes	55.35033333	2.994362147	30 minutes	53.58213333	5.082601807
1 hour	50.4908	5.389220036	1 hour	41.42433333	10.39612188
2 hour	42.3376	3.496159011	2 hour	45.44635714	9.102293917
4 hour	40.46133333	5.27388291	4 hour	58.08326667	16.23861776
8 hour	37.71493333	6.700537862	8 hour	43.83707143	8.235669731
24 hour	25.10593333	3.028847057	24 hour	41.32373333	5.192137882

INTENSITY VALUES FOR HEAT SHOCK EXPOSURE TIME OPTIMISATION	
Nuclear Samples from Heat Shock Times	Mean Intensity Reading
HeLa unstressed 1	28.435
HeLa unstressed 2	28.38
HeLa unstressed 3	36.209
HeLa unstressed 4	26.4
HeLa unstressed 5	23.671

HeLa unstressed 6	23.072
HeLa unstressed 7	23.811
HeLa unstressed 8	28.595
HeLa unstressed 9	23.47
HeLa unstressed 10	21.311
HeLa unstressed 11	30.345
HeLa unstressed 12	24.979
HeLa unstressed 13	23.917
HeLa unstressed 14	31.04
HeLa unstressed 15	30.596
HeLa unstressed 16	24.986
HeLa unstressed 17	25.876
HeLa unstressed 18	19.844
HeLa unstressed 19	20.669
HeLa unstressed 20	28.904
HeLa 30 seconds 1	43.927
HeLa 30 seconds 2	37.354
HeLa 30 seconds 3	37.112
HeLa 30 seconds 4	34.765
HeLa 30 seconds 5	43.64
HeLa 30 seconds 6	38.474
HeLa 30 seconds 7	24.84
HeLa 30 seconds 8	36.33



HeLa 30 seconds 9	30.829
HeLa 30 seconds 10	26.992
HeLa 30 seconds 11	40.699
HeLa 30 seconds 12	34.48
HeLa 30 seconds 13	34.721
HeLa 30 seconds 14	32.53
HeLa 30 seconds 15	32.344
HeLa 30 seconds 16	49.786
HeLa 30 seconds 17	45.273
HeLa 30 seconds 18	55.323
HeLa 30 seconds 19	54.761
HeLa 30 seconds 20	35.891
	42.907
HeLa 1 minute 1	47.187
HeLa 1 minute 2	42.688
HeLa 1 minute 3	39.761
HeLa 1 minute 4	47.453
HeLa 1 minute 5	44.814
HeLa 1 minute 6	35.035
HeLa 1 minute 7	37.756
HeLa 1 minute 8	45.082
HeLa 1 minute 9	35.854
HeLa 1 minute 10	60.431



HeLa 1 minute 11	40.544
HeLa 1 minute 12	30.958
HeLa 1 minute 13	46.995
HeLa 1 minute 14	39.421
HeLa 1 minute 15	33.584
HeLa 1 minute 16	39.598
HeLa 1 minute 17	55.233
HeLa 1 minute 18	49.242
HeLa 1 minute 19	45.81
HeLa 1 minute 20	42.907
HeLa 2 minutes 1	41.067
HeLa 2 minutes 2	49.741
HeLa 2 minutes 3	40.893
HeLa 2 minutes 4	46.345
HeLa 2 minutes 5	51.462
HeLa 2 minutes 6	53.678
HeLa 2 minutes 7	56.463
HeLa 2 minutes 8	63.032
HeLa 2 minutes 9	51.908
HeLa 2 minutes 10	67.312
HeLa 2 minutes 11	57.98
HeLa 2 minutes 12	51.491
HeLa 2 minutes 13	41.237



HeLa 2 minutes 14	38.958
HeLa 2 minutes 15	42.802
HeLa 2 minutes 16	46.235
HeLa 2 minutes 17	44.695
HeLa 2 minutes 18	47.835
HeLa 2 minutes 19	49.081
HeLa 2 minutes 20	55.641
HeLa 5 minutes 1	65.631
HeLa 5 minutes 2	61.926
HeLa 5 minutes 3	62.577
HeLa 5 minutes 4	59.47
HeLa 5 minutes 5	76.546
HeLa 5 minutes 6	77.159
HeLa 5 minutes 7	70.278
HeLa 5 minutes 8	64.35
HeLa 5 minutes 9	66.62
HeLa 5 minutes 10	69.484
HeLa 5 minutes 11	81.627
HeLa 5 minutes 12	95.242
HeLa 5 minutes 13	44.562
HeLa 5 minutes 14	47.977
HeLa 5 minutes 15	48.392



HeLa 5 minutes 16	67.248
HeLa 5 minutes 17	47.927
HeLa 5 minutes 18	79.676
HeLa 5 minutes 19	70.949
HeLa 5 minutes 20	70.408
HeLa 10 minutes 1	76.254
HeLa 10 minutes 2	83.353
HeLa 10 minutes 3	79.698
HeLa 10 minutes 4	93.911
HeLa 10 minutes 5	76.085
HeLa 10 minutes 6	69.864
HeLa 10 minutes 7	76.959
HeLa 10 minutes 8	65.076
HeLa 10 minutes 9	62.229
HeLa 10 minutes 10	68.368
HeLa 10 minutes 11	62.75
HeLa 10 minutes 12	69.421
HeLa 10 minutes 13	51.9
HeLa 10 minutes 14	56.186
HeLa 10 minutes 15	58.613
HeLa 10 minutes 16	57.252
HeLa 10 minutes 17	54.633
HeLa 10 minutes 18	59.378



HeLa 10 minutes 19	52.944
HeLa 10 minutes 20	53.66
HeLa 30 minutes 1	58.659
HeLa 30 minutes 2	54.975
HeLa 30 minutes 3	56.159
HeLa 30 minutes 4	46.096
HeLa 30 minutes 5	47.108
HeLa 30 minutes 6	40.28
HeLa 30 minutes 7	40.756
HeLa 30 minutes 8	53.805
HeLa 30 minutes 9	56.93
HeLa 30 minutes 10	49.417
HeLa 30 minutes 11	69.1
HeLa 30 minutes 12	79.504
HeLa 30 minutes 13	74.195
HeLa 30 minutes 14	91.493
HeLa 30 minutes 15	90.638
HeLa 30 minutes 16	91.753
HeLa 30 minutes 17	75.346
HeLa 30 minutes 18	81.275
HeLa 30 minutes 19	49.558
HeLa 30 minutes 20	63.466



Heat shock exposure time	Mean Intensity	Standard Deviation
No Stress	26.2255	4.074626
30 seconds	38.50355	8.246042
1 minute	43.01765	7.174417
2 minutes	49.8928	7.618012
5 minutes	66.40245	12.7528
10 minutes	66.4267	11.6325
30 minutes	63.52565	16.98974

NUCLEAR INTENSITY VALUES FOR ISOFORM 1 HEAT SHOCK EXPERIMENT

Nuclear Samples, Unstressed Cells	Mean Intensity Value	Nuclear Samples, Stressed Cells	Mean Intensity Value
Isoform 1 Unstressed 1	9.936	Isoform 1 Stressed 1	12.381
Isoform 1 Unstressed 2	11.486	Isoform 1 Stressed 2	9.85
Isoform 1 Unstressed 3	10.781	Isoform 1 Stressed 3	6.678
Isoform 1 Unstressed 4	12.291	Isoform 1 Stressed 4	10.092
Isoform 1 Unstressed 5	11.148	Isoform 1 Stressed 5	9.719
Isoform 1 Unstressed 6	13.766	Isoform 1 Stressed 6	9.876
Isoform 1 Unstressed 7	10.299	Isoform 1 Stressed 7	11.205
Isoform 1 Unstressed 8	10.594	Isoform 1 Stressed 8	8.562
Isoform 1 Unstressed 9	11.232	Isoform 1 Stressed 9	9.767
Isoform 1 Unstressed 10	13.758	Isoform 1 Stressed 10	8.199
Isoform 1 Unstressed 11	9.827	Isoform 1 Stressed 11	12.877
Isoform 1 Unstressed 12	11.434	Isoform 1 Stressed 12	9.008

Isoform 1 Unstressed 12	10.589	Isoform 1 Stressed 12	10.996
Isoform 1 Unstressed 13	9.955	Isoform 1 Stressed 13	10.193
Isoform 1 Unstressed 14	9.961	Isoform 1 Stressed 14	11.338
Isoform 1 Unstressed 15	10.418	Isoform 1 Stressed 15	12.637
Isoform 1 Unstressed 16	7.65	Isoform 1 Stressed 16	10.406
Isoform 1 Unstressed 17	10.533	Isoform 1 Stressed 17	13.553
Isoform 1 Unstressed 18	8.885	Isoform 1 Stressed 18	10.893
Isoform 1 Unstressed 19	10.253	Isoform 1 Stressed 19	9.435
Isoform 1 Unstressed 20	9.476	Isoform 1 Stressed 20	7.508
Isoform 1 Unstressed 21	9.586	Isoform 1 Stressed 21	12.847
Isoform 1 Unstressed 22	12.07	Isoform 1 Stressed 22	10.364
Isoform 1 Unstressed 23	14.77	Isoform 1 Stressed 23	9.822
Isoform 1 Unstressed 24	11.864	Isoform 1 Stressed 24	9.821
Isoform 1 Unstressed 25	9.936	Isoform 1 Stressed 25	13.041
Isoform 1 Unstressed 26	11.486	Isoform 1 Stressed 26	9.485
Isoform 1 Unstressed 27	10.781	Isoform 1 Stressed 27	12.662
Isoform 1 Unstressed 28	12.291	Isoform 1 Stressed 28	13.255
Isoform 1 Unstressed 29	11.148	Isoform 1 Stressed 29	7.698
Isoform 1 Unstressed 30	13.766	Isoform 1 Stressed 30	10.507
Mean Intensity of HeLa Unstressed	SD of HeLa Unstressed	Mean Intensity of HeLa Stressed	SD of HeLa Stressed
10.79629032	1.673224496	10.4733871	1.79724661
p-value for isoform 1 nuclear intensity change	0.466		

NUCLEAR INTENSITY VALUES FOR ISOFORM 1 DNA DAMAGE EXPERIMENT			
Nuclear Samples, Unstressed Cells	Mean Intensity Value	Nuclear Samples, Stressed Cells	Mean Intensity Value
Isoform 1 Unstressed 1	10.921	Isoform 1 Stressed 1	12.389
Isoform 1 Unstressed 2	12.25	Isoform 1 Stressed 2	9.425
Isoform 1 Unstressed 3	11.135	Isoform 1 Stressed 3	10.844
Isoform 1 Unstressed 4	11.076	Isoform 1 Stressed 4	12.481
Isoform 1 Unstressed 5	15.524	Isoform 1 Stressed 5	11.34
Isoform 1 Unstressed 6	13.14	Isoform 1 Stressed 6	10.373
Isoform 1 Unstressed 7	16.108	Isoform 1 Stressed 7	8.749
Isoform 1 Unstressed 8	13.116	Isoform 1 Stressed 8	8.31
Isoform 1 Unstressed 9	10.765	Isoform 1 Stressed 9	12.215
Isoform 1 Unstressed 10	10.594	Isoform 1 Stressed 10	11.796
Isoform 1 Unstressed 11	13.213	Isoform 1 Stressed 11	10.487
Isoform 1 Unstressed 12	9.073	Isoform 1 Stressed 12	11.794
Isoform 1 Unstressed 12	11.164	Isoform 1 Stressed 12	12.597
Isoform 1 Unstressed 13	9.989	Isoform 1 Stressed 13	11.141
Isoform 1 Unstressed 14	11.57	Isoform 1 Stressed 14	12.095
Isoform 1 Unstressed 15	11.806	Isoform 1 Stressed 15	13.134
Isoform 1 Unstressed 16	13.537	Isoform 1 Stressed 16	11.253
Isoform 1 Unstressed 17	9.629	Isoform 1 Stressed 17	10.193
Isoform 1 Unstressed 18	10.349	Isoform 1 Stressed 18	11.95
Isoform 1 Unstressed 19	7.431	Isoform 1 Stressed 19	12.489
Isoform 1 Unstressed 20	7.889	Isoform 1 Stressed 20	8.599

Isoform 1 Unstressed 21	13.513	Isoform 1 Stressed 21	8.612
Isoform 1 Unstressed 22	11.876	Isoform 1 Stressed 22	10.643
Isoform 1 Unstressed 23	12.459	Isoform 1 Stressed 23	11.804
Isoform 1 Unstressed 24	17.072	Isoform 1 Stressed 24	12.836
Isoform 1 Unstressed 25	12.351	Isoform 1 Stressed 25	10.123
Isoform 1 Unstressed 26	9.591	Isoform 1 Stressed 26	10.606
Isoform 1 Unstressed 27	9.777	Isoform 1 Stressed 27	12.565
Isoform 1 Unstressed 28	9.208	Isoform 1 Stressed 28	9.871
Isoform 1 Unstressed 29	9.244	Isoform 1 Stressed 29	11.364
Isoform 1 Unstressed 30	10.854	Isoform 1 Stressed 30	9.275
Mean Intensity of HeLa Unstressed	SD of HeLa Unstressed	Mean Intensity of HeLa Stressed	SD of HeLa Stressed
11.49109677	2.231923854	11.0113871	1.390030064
p-value for isoform 1 nuclear intensity change	0.157298131		

NUCLEAR INTENSITY VALUES FOR CELL-LINE COMPARISON EXPERIMENT			
H157			
Nuclear Samples, Unstressed Cells	Mean Intensity Value	Nuclear Samples, Stressed Cells	Mean Intensity Value
H157 Unstressed 1	43.499	H157 Stressed 1	82.404
H157 Unstressed 2	62.193	H157 Stressed 2	61.505
H157 Unstressed 3	59.194	H157 Stressed 3	65.556
H157 Unstressed 4	59.027	H157 Stressed 4	83.206
H157 Unstressed 5	47.147	H157 Stressed 5	79.957
H157 Unstressed 6	47.117	H157 Stressed 6	50.714
H157 Unstressed 7	46.815	H157 Stressed 7	66.644
H157 Unstressed 8	48.579	H157 Stressed 8	60.913

H157 Unstressed 9	60.321	H157 Stressed 9	74.232
H157 Unstressed 10	41.055	H157 Stressed 10	68.745
H157 Unstressed 11	37.77	H157 Stressed 11	58.238
H157 Unstressed 12	47.264	H157 Stressed 12	77.781
H157 Unstressed 13	64.545	H157 Stressed 13	67.083
H157 Unstressed 14	53.46	H157 Stressed 14	66.688
H157 Unstressed 15	42.929	H157 Stressed 15	74.371
H157 Unstressed 16	53.81	H157 Stressed 16	72.888
H157 Unstressed 17	50.7	H157 Stressed 17	79.528
H157 Unstressed 18	40.556	H157 Stressed 18	64.423
H157 Unstressed 19	47.778	H157 Stressed 19	78.613
H157 Unstressed 20	35.917	H157 Stressed 20	56.116
H157 Unstressed 21	33.509	H157 Stressed 21	72.026
H157 Unstressed 22	44.546	H157 Stressed 22	85.731
H157 Unstressed 23	32.504	H157 Stressed 23	83.171
H157 Unstressed 24	35.259	H157 Stressed 24	106.7
H157 Unstressed 25	45.56	H157 Stressed 25	89.189
H157 Unstressed 26	42.091	H157 Stressed 26	81.505
H157 Unstressed 27	43.964	H157 Stressed 27	65.916
H157 Unstressed 28	45.121	H157 Stressed 28	87.549
H157 Unstressed 29	27.828	H157 Stressed 29	96.214
H157 Unstressed 30	41.513	H157 Stressed 30	98.712
Mean Intensity of H157 Unstressed	SD of H157 Unstressed	Mean Intensity of H157 Stressed	SD of H157 Stressed
46.05237	9.047521	75.2106	13.04295
<i>p</i> -value for H157	4.53192E-14		
KMST			
Nuclear Samples, Unstressed Cells	Mean Intensity Value	Nuclear Samples, Stressed Cells	Mean Intensity

			Value
KMST Unstressed 1	57.712	KMST Stressed 1	82.446
KMST Unstressed 2	58.401	KMST Stressed 2	65.717
KMST Unstressed 3	64.473	KMST Stressed 3	72.099
KMST Unstressed 4	68.975	KMST Stressed 4	74.886
KMST Unstressed 5	66.367	KMST Stressed 5	78.848
KMST Unstressed 6	50.136	KMST Stressed 6	67.932
KMST Unstressed 7	55.712	KMST Stressed 7	76.867
KMST Unstressed 8	71.441	KMST Stressed 8	115.203
KMST Unstressed 9	66.165	KMST Stressed 9	157.819
KMST Unstressed 10	47.346	KMST Stressed 10	143.694
KMST Unstressed 11	63.232	KMST Stressed 11	145.878
KMST Unstressed 12	59.279	KMST Stressed 12	124.355
KMST Unstressed 13	57.996	KMST Stressed 13	125.479
KMST Unstressed 14	49.762	KMST Stressed 14	147.205
KMST Unstressed 15	45.926	KMST Stressed 15	73.496
KMST Unstressed 16	61.789	KMST Stressed 16	64.599
KMST Unstressed 17	50.307	KMST Stressed 17	76.897
KMST Unstressed 18	69.361	KMST Stressed 18	64.065
KMST Unstressed 19	61.49	KMST Stressed 19	71.243
KMST Unstressed 20	75.74	KMST Stressed 20	66.082
KMST Unstressed 21	62.063	KMST Stressed 21	62.991
KMST Unstressed 22	60.932	KMST Stressed 22	71.316
KMST Unstressed 23	69.622	KMST Stressed 23	80.932
KMST Unstressed 24	65.693	KMST Stressed 24	85.674
KMST Unstressed 25	67.689	KMST Stressed 25	77.294
KMST Unstressed 26	69.008	KMST Stressed 26	73.142
KMST Unstressed 27	53.682	KMST Stressed 27	74.277
KMST Unstressed 28	80.053	KMST Stressed 28	68.877

KMST Unstressed 29	56.285	KMST Stressed 29	84.167
KMST Unstressed 30	54.412	KMST Stressed 30	63.159
Mean Intensity of KMST Unstressed	SD of KMST Unstressed	Mean Intensity of KMST Stressed	SD of KMST Stressed
61.3683	8.402607	87.88797	29.09905
p -value for KMST	1.59729E-05		
HEPG2			
Nuclear Samples, Unstressed Cells	Mean Intensity Value	Nuclear Samples, Stressed Cells	Mean Intensity Value
HEPG2 Unstressed 1	43.565	HEPG2 Stressed 1	107.369
HEPG2 Unstressed 2	50.527	HEPG2 Stressed 2	105.479
HEPG2 Unstressed 3	49.094	HEPG2 Stressed 3	106.147
HEPG2 Unstressed 4	61.472	HEPG2 Stressed 4	95.836
HEPG2 Unstressed 5	56.162	HEPG2 Stressed 5	117.121
HEPG2 Unstressed 6	75.164	HEPG2 Stressed 6	127.479
HEPG2 Unstressed 7	84.601	HEPG2 Stressed 7	100.538
HEPG2 Unstressed 8	93.416	HEPG2 Stressed 8	126.519
HEPG2 Unstressed 9	95.111	HEPG2 Stressed 9	94.879
HEPG2 Unstressed 10	93.952	HEPG2 Stressed 10	85.697
HEPG2 Unstressed 11	86.429	HEPG2 Stressed 11	106.077
HEPG2 Unstressed 12	91.081	HEPG2 Stressed 12	106.776
HEPG2 Unstressed 13	95.953	HEPG2 Stressed 13	129.194
HEPG2 Unstressed 14	132.952	HEPG2 Stressed 14	88.43
HEPG2 Unstressed 15	105.026	HEPG2 Stressed 15	91.37
HEPG2 Unstressed 16	125.374	HEPG2 Stressed 16	98.249
HEPG2 Unstressed 17	122.75	HEPG2 Stressed 17	87.421
HEPG2 Unstressed 18	123.195	HEPG2 Stressed 18	91.944

HEPG2 Unstressed 19	116.149	HEPG2 Stressed 19	92.847
HEPG2 Unstressed 20	95.726	HEPG2 Stressed 20	59.927
HEPG2 Unstressed 21	98.851	HEPG2 Stressed 21	68.926
HEPG2 Unstressed 22	115.464	HEPG2 Stressed 22	55.551
HEPG2 Unstressed 23	111.097	HEPG2 Stressed 23	58.187
HEPG2 Unstressed 24	87.707	HEPG2 Stressed 24	71.094
HEPG2 Unstressed 25	91.862	HEPG2 Stressed 25	78.743
HEPG2 Unstressed 26	79.91	HEPG2 Stressed 26	115.697
HEPG2 Unstressed 27	85.415	HEPG2 Stressed 27	116.87
HEPG2 Unstressed 28	86.239	HEPG2 Stressed 28	97.485
HEPG2 Unstressed 29	77.766	HEPG2 Stressed 29	101.248
HEPG2 Unstressed 30	100.526	HEPG2 Stressed 30	112.234
Mean Intensity of HEPG2 Unstressed	SD of HEPG2 Unstressed	Mean Intensity of HEPG2 Stressed	SD of HEPG2 Stressed
91.08453	23.08473	96.51113	19.86952
p -value for HEPG2	0.166639855		
A549			
Nuclear Samples, Unstressed Cells	Mean Intensity Value	Nuclear Samples, Stressed Cells	Mean Intensity Value
A549 Unstressed 1	78.501	A549 Stressed 1	113.761
A549 Unstressed 2	71.12	A549 Stressed 2	129.617
A549 Unstressed 3	70.271	A549 Stressed 3	146.354
A549 Unstressed 4	76.418	A549 Stressed 4	118.112
A549 Unstressed 5	92.626	A549 Stressed 5	122.161
A549 Unstressed 6	92.715	A549 Stressed 6	119.293
A549 Unstressed 7	79.061	A549 Stressed 7	124.712
A549 Unstressed 8	100.197	A549 Stressed 8	116.098

A549 Unstressed 9	87.269	A549 Stressed 9	94.708
A549 Unstressed 10	96.783	A549 Stressed 10	133.152
A549 Unstressed 11	96.697	A549 Stressed 11	84.406
A549 Unstressed 12	106.956	A549 Stressed 12	90.91
A549 Unstressed 13	83.353	A549 Stressed 13	79.636
A549 Unstressed 14	79.698	A549 Stressed 14	77.677
A549 Unstressed 15	93.911	A549 Stressed 15	125.06
A549 Unstressed 16	76.085	A549 Stressed 16	114.577
A549 Unstressed 17	79.676	A549 Stressed 17	120.26
A549 Unstressed 18	70.949	A549 Stressed 18	142.483
A549 Unstressed 19	70.408	A549 Stressed 19	119.08
A549 Unstressed 20	76.254	A549 Stressed 20	127.938
Mean Intensity of A549 Unstressed	SD of A549 Unstressed	Mean Intensity of A549 Stressed	SD of A549 Stressed
83.9474	7.706651	114.9998	6.90557
<i>p</i> -value for A549	4.59592E-07		
HELA			
Nuclear Samples, Unstressed Cells	Mean Intensity Value	Nuclear Samples, Stressed Cells	Mean Intensity Value
HeLa Unstressed 1	39.514	HeLa Stressed 1	39.969
HeLa Unstressed 2	29.415	HeLa Stressed 2	43.555
HeLa Unstressed 3	28.903	HeLa Stressed 3	42.723
HeLa Unstressed 4	33.511	HeLa Stressed 4	39.045
HeLa Unstressed 5	36.144	HeLa Stressed 5	38.649
HeLa Unstressed 6	20.534	HeLa Stressed 6	58.804
HeLa Unstressed 7	20.524	HeLa Stressed 7	65.631
HeLa Unstressed 8	22.786	HeLa Stressed 8	61.926

HeLa Unstressed 9	24.927	HeLa Stressed 9	62.577
HeLa Unstressed 10	23.67	HeLa Stressed 10	59.47
HeLa Unstressed 11	36.881	HeLa Stressed 11	76.546
HeLa Unstressed 12	42.607	HeLa Stressed 12	77.159
HeLa Unstressed 13	39.567	HeLa Stressed 13	70.278
HeLa Unstressed 14	42.79	HeLa Stressed 14	64.35
HeLa Unstressed 15	40.896	HeLa Stressed 15	66.62
HeLa Unstressed 16	42.369	HeLa Stressed 16	69.484
HeLa Unstressed 17	41.992	HeLa Stressed 17	81.627
HeLa Unstressed 18	40.996	HeLa Stressed 18	95.242
HeLa Unstressed 19	35.58	HeLa Stressed 19	81.768
HeLa Unstressed 20	39.202	HeLa Stressed 20	84.313
HeLa Unstressed 21	29.08	HeLa Stressed 21	30.561
HeLa Unstressed 22	29.373	HeLa Stressed 22	30.655
HeLa Unstressed 23	39.218	HeLa Stressed 23	27.054
HeLa Unstressed 24	35.235	HeLa Stressed 24	25.175
HeLa Unstressed 25	36.541	HeLa Stressed 25	46.55
HeLa Unstressed 26	21.144	HeLa Stressed 26	44.562
HeLa Unstressed 27	20.603	HeLa Stressed 27	47.977
HeLa Unstressed 28	25.511	HeLa Stressed 28	48.392
HeLa Unstressed 29	25.483	HeLa Stressed 29	47.248
HeLa Unstressed 30	19.969	HeLa Stressed 30	47.927
Mean Intensity of HeLa Unstressed	SD of HeLa Unstressed	Mean Intensity of HeLa Stressed	SD of HeLa Stressed
34.373	6.876	53.598	2.58
<i>p</i> -value for HeLa	6.72244E-08		

INTENSITY VALUES FOR HA-ISOFORM 3 EXPERIMENT							
UNSTRESSED CELLS	Nuclear intensity	Cytoplasmic Intensity	Nuc/Cyt	STRESSED CELLS	Nuclear intensity	Cytoplasmic Intensity	Nuc/Cyt
Unstressed Cell 1	19.204	18.337	1.047281	Stressed Cell 1	54.424	44.983	1.209879
Unstressed Cell 2	23.106	18.623	1.240724	Stressed Cell 2	36.097	12.872	2.804304
Unstressed Cell 3	21.524	14.323	1.502758	Stressed Cell 3	35.261	28.569	1.23424
Unstressed Cell 4	19.709	13.608	1.448339	Stressed Cell 4	19.175	18.857	1.016864
Unstressed Cell 5	16.006	26.738	0.598624	Stressed Cell 5	73.719	32.821	2.246092
Unstressed Cell 6	54.159	39.882	1.357981	Stressed Cell 6	29.961	20.979	1.428142
Unstressed Cell 7	2.584	30.062	0.085956	Stressed Cell 7	17.438	25.861	0.674297
Unstressed Cell 8	21.187	22.542	0.93989	Stressed Cell 8	43.362	39.602	1.094945
Unstressed Cell 9	5.261	14.097	0.3732	Stressed Cell 9	30.849	20.697	1.490506
Unstressed Cell 10	38.194	29.604	1.290163	Stressed Cell 10	45.78	36.756	1.245511
Unstressed Cell 11	21.751	22.668	0.959546	Stressed Cell 11	28.693	13.941	2.058174
Unstressed Cell 12	12.971	16.476	0.787266	Stressed Cell 12	32.013	18.423	1.737665
Unstressed Cell 13	53.786	42.645	1.26125	Stressed Cell 13	45.066	38.723	1.163804
Unstressed Cell 14	4.91	11.875	0.413474	Stressed Cell 14	17.487	15.737	1.111203
Unstressed Cell 15	37.108	22.218	1.670177	Stressed Cell 15	28.625	26.732	1.070814
Unstressed Cell 16	5.901	13.39	0.440702	Stressed Cell 16	32.009	20.93	1.529336
Unstressed Cell 17	23.543	26.902	0.875139	Stressed Cell 17	40.939	25.485	1.606396
Unstressed Cell 18	3.854	12.71	0.303226	Stressed Cell 18	36.685	36.55	1.003694
Unstressed Cell 19	26.421	12.09	2.18536	Stressed Cell 19	16.692	20.875	0.799617
Unstressed Cell 20	11.56	24.344	0.47486	Stressed Cell 20	32.579	27.558	1.182198
Mean nuclear/cytoplasm values for unstressed cells			0.962796	Mean nuclear/cytoplasm values for stressed cells			1.385384
Standard deviation			0.23777	Standard deviation			0.211226

MANDER'S COEFFICIENT FOR DWNN/SC35 COLOCALISATION			
Unstressed Cells	M1 Value	Stressed Cells	M1 Value
Mander's Coefficient Unstressed 1	0.168	Mander's Coefficient Stressed 1	0.672
Mander's Coefficient Unstressed 2	0.218	Mander's Coefficient Stressed 2	0.886
Mander's Coefficient Unstressed 3	0.175	Mander's Coefficient Stressed 3	0.777
Mander's Coefficient Unstressed 4	0.149	Mander's Coefficient Stressed 4	0.749
Mander's Coefficient Unstressed 5	0.228	Mander's Coefficient Stressed 5	0.698
Mander's Coefficient Unstressed 6	0.201	Mander's Coefficient Stressed 6	0.816
Mander's Coefficient Unstressed 7	0.173	Mander's Coefficient Stressed 7	0.722
Mander's Coefficient Unstressed 8	0.153	Mander's Coefficient Stressed 8	0.647
Mander's Coefficient Unstressed 9	0.151	Mander's Coefficient Stressed 9	0.751
Mander's Coefficient Unstressed 10	0.187	Mander's Coefficient Stressed 10	0.719
Mander's Coefficient Unstressed 11	0.238	Mander's Coefficient Stressed 11	0.693
Mander's Coefficient Unstressed 12	0.166	Mander's Coefficient Stressed 12	0.847
Mander's Coefficient Unstressed 13	0.142	Mander's Coefficient Stressed 13	0.77
Mander's Coefficient Unstressed 14	0.134	Mander's Coefficient Stressed 14	0.693
Mander's Coefficient Unstressed 15	0.199	Mander's Coefficient Stressed 15	0.801
Mean Intensity of Mander's Coefficient Unstressed	SD of Mander's Coefficient Unstressed	Mean Intensity of Mander's Coefficient Stressed	SD of Mander's Coefficient Stressed
0.1788	0.032123	0.7494	0.067415

MANDER'S COEFFICIENT FOR DWNN/ γ H2AX COLOCALISATION			
Stressed Cells	M1 Value	Stressed Cells	M2 Value
Mander's Coefficient Stressed 1	0.109	Mander's Coefficient Stressed 1	0.148
Mander's Coefficient Stressed 2	0.271	Mander's Coefficient Stressed 2	0.21
Mander's Coefficient Stressed 3	0.11	Mander's Coefficient Stressed 3	0.15

Mander's Coefficient Stressed 4	0.124	Mander's Coefficient Stressed 4	0.245
Mander's Coefficient Stressed 5	0.03	Mander's Coefficient Stressed 5	0.124
Mander's Coefficient Stressed 6	0.373	Mander's Coefficient Stressed 6	0.142
Mander's Coefficient Stressed 7	0.372	Mander's Coefficient Stressed 7	0.17
Mander's Coefficient Stressed 8	0.242	Mander's Coefficient Stressed 8	0.253
Mander's Coefficient Stressed 9	0.047	Mander's Coefficient Stressed 9	0.08
Mander's Coefficient Stressed 10	0.28	Mander's Coefficient Stressed 10	0.051
Mander's Coefficient Stressed 11	0.244	Mander's Coefficient Stressed 11	0.03
Mander's Coefficient Stressed 12	0.042	Mander's Coefficient Stressed 12	0.025
Mander's Coefficient Stressed 13	0.225	Mander's Coefficient Stressed 13	0.049
Mander's Coefficient Stressed 14	0.24	Mander's Coefficient Stressed 14	0.103
Mander's Coefficient Stressed 15	0.354	Mander's Coefficient Stressed 15	0.152
Mean Intensity of Mander's Coefficient M1	SD of Mander's Coefficient M1	Mean Intensity of Mander's Coefficient M2 Unstressed	SD of Mander's Coefficient M2 Unstressed
0.2042	0.061941	0.1288	0.073083